Per Martin Rørvik

Synthesis of ferroelectric nanostructures

Thesis for the degree of Philosophiae Doctor

Trondheim, December 2008

Norwegian University of Science and Technology
Faculty of Natural Sciences and Technology
Department of Materials Science and Engineering

NTNU
Norwegian University of
Science and Technology

NTNU
Norwegian University of Science and Technology

Thesis for the degree of Philosophiae Doctor

Faculty of Natural Sciences and Technology
Department of Materials Science and Engineering

ISBN 978-82-471-1350-9 (printed ver.)
ISBN 978-82-471-1351-6 (electronic ver.)
ISSN 1503-8181

IMT-Report 2008:106

Doctoral theses at NTNU, 2008:321

Printed by NTNU-trykk

Acknowledgements

First of all, I am very grateful to my supervisor, Professor Mari-Ann Einarsrud, for her wide knowledge of materials science, her never-ending support and enthusiasm, her amazingly quick response to drafts of this thesis, and our shared passion for accuracy in the manuscripts. Also, I value her Japanese connections, which made it possible for me to go to Japan. I am also very grateful to my co-supervisor, Professor Tor Grande, for his positive attitude, his interest in this work, his many ideas and his valuable feedback to my research. Additionally, Professor Thomas Tybell has been co-supervisor since November 2006, and his experience and knowledge of ferroelectrics and electronics have been invaluable for the characterization of the ferroelectricity of the nanorods.

During my three months at the Inorganic Chemistry lab at Osaka Prefecture University in Japan, I was received very well and learned a lot about Japanese culture and lab life. My thanks go to the head of the lab, Professor Masahiro Tatsumisago, to my research supervisor, Associate Professor Kiyoharu Tadanaga, and the rest of the members of the lab. I will especially remember the lunches we had at the various restaurants.

I have been fortunate to collaborate with many researchers, both within and outside the ceramics research group. During the first year of my PhD studies, I shared the joys and frustrations of the molten salt synthesis method with Tone Lyngdal, and enjoyed our discussions and cooperation. The work of Dr. Guozhong Wang, who pioneered the use of hydrothermal method for the synthesis of $PbTiO_3$ nanorods, has been very important for the hydrothermal synthesis in this work.

A crucial collaboration has been the characterization work together with the transmission electron microscopy (TEM) group at the Department of Physics. The TEM work that was done by Ragnhild Sæterli and Åsmund Almli has been invaluable to the understanding of both the molten salt synthesis and the hydrothermal synthesis. Their supervisors, Professor Randi Holmestad and Associate Professor Ton van Helvoort, have been very supportive and interested in this work, and their contribution to Paper I and II is highly appreciated.

Chang Chuan You has been very important for the piezoresponse force microscopy study of the nanorods; he has taught me how to use the atomic force microscope and the electron beam lithography equipment, and we have had good discussions about various issues regarding these techniques.

Professor Jarle Hjelen and Engineer Tor Nilsen are appreciated for their help and generosity regarding design of the electron beam induced deposition (EBID) apparatus and use of the JEOL JSM-840 scanning electron microscope. Engineer Ketil Joner rebuilt and modified the EBID apparatus, and his workmanship and positive attitude are highly appreciated.

Financial support from the Strategic Area of Materials at NTNU and the Research Council of Norway is acknowledged. The research stay in Japan was financed by the Scandinavia-Japan Sasakawa Foundation and the International Section at NTNU.

During these four years, the workdays would not have been the same without all the friendly people in Chemistry building II. Thanks to you all for the lunches,

coffee breaks, informal discussions, parties, and the help with lab equipment or software.

And during these years, the leisure time, weekends and holidays would not have been the same without all my good friends and my family. Although you haven't understood the topic of my thesis, I really appreciate your support and encouragement during these years.

Finally, I want to thank Ragnhild a second time, for making me think of other things than nanorods during the last months of the writing of this thesis.

Trondheim, October 16th 2008 Per Martin Rørvik

Summary

The increasing miniaturization of electric and mechanical components makes the synthesis and assembly of nanoscale structures an important step in modern technology. Functional materials, such as the ferroelectric perovskites, are vital to the integration and utility value of nanotechnology in the future. In the present work, chemical methods to synthesize one-dimensional (1D) nanostructures of ferroelectric perovskites have been studied. To successfully and controllably make 1D nanostructures by chemical methods it is very important to understand the growth mechanism of these nanostructures, in order to design the structures for use in various applications. For the integration of 1D nanostructures into devices it is also very important to be able to make arrays and large-area designed structures from the building blocks that single nanostructures constitute. As functional materials, it is of course also vital to study the properties of the nanostructures. The characterization of properties of single nanostructures is challenging, but essential to the use of such structures.

The aim of this work has been to synthesize high quality single-crystalline 1D nanostructures of ferroelectric perovskites with emphasis on $PbTiO_3$, to make arrays or hierarchical nanostructures of 1D nanostructures on substrates, to understand the growth mechanisms of the 1D nanostructures, and to investigate the ferroelectric and piezoelectric properties of the 1D nanostructures.

In Paper I, a molten salt synthesis route, previously reported to yield $BaTiO_3$, $PbTiO_3$ and $Na_2Ti_6O_{13}$ nanorods, was re-examined in order to elucidate the role of volatile chlorides. A precursor mixture containing barium (or lead) and titanium was annealed in the presence of NaCl at 760 °C or 820 °C. The main products were respectively isometric nanocrystalline $BaTiO_3$ and $PbTiO_3$. Nanorods were also detected, but electron diffraction revealed that the composition of the nanorods was respectively $BaTi_2O_5$/$BaTi_5O_{11}$ and $Na_2Ti_6O_{13}$ for the two different systems, in contradiction to the previous studies. It was shown that NaCl reacted with BaO (PbO) resulting in loss of volatile $BaCl_2$ ($PbCl_2$) and formation and preferential growth of titanium oxide-rich nanorods instead of the target phase $BaTiO_3$ (or $PbTiO_3$). The molten salt synthesis route may therefore not necessarily yield nanorods of the target ternary oxide as reported previously. In addition, the importance of NaCl(g) for the growth of nanorods below the melting point of NaCl was demonstrated in a special experimental setup, where NaCl and the precursors were physically separated.

In Paper II and III, a hydrothermal synthesis method to grow arrays and hierarchical nanostructures of $PbTiO_3$ nanorods and platelets on substrates is presented. Hydrothermal treatment of an amorphous $PbTiO_3$ precursor in the presence of a surfactant and $PbTiO_3$ or $SrTiO_3$ substrates resulted in the growth of $PbTiO_3$ nanorods and platelets aligned in the crystallographic <100> orientations of the underlying substrate. The nanorods had a square-shaped cross-section. The growth of nanorods is explained by self-assembly of facetted or cube-shaped nanocrystals. The position of the substrate in the autoclave influenced the length of the nanorods; the longest rods were formed at the lowest position. The growth orientation of the nanorods could be changed by changing the crystal orientation of

the $SrTiO_3$ substrates. $PbTiO_3$ nanorods oriented perpendicular to the substrate surface could also be grown directly on the substrate by a modified synthesis method. The hydrothermal method described in Paper II and III was developed on the basis of the method described in Appendices I and II.

In Paper IV, a template-assisted method to make $PbTiO_3$ nanotubes is presented. An equimolar Pb-Ti sol was dropped onto porous alumina membranes and penetrated into the channels of the template. Single-phase $PbTiO_3$ perovskite nanotubes were obtained by annealing at 700 °C for 6 h. The nanotubes had diameters of 200 - 400 nm with a wall thickness of approximately 20 nm. Excess PbO or annealing in a Pb-containing atmosphere was not necessary in order to achieve single phase $PbTiO_3$ nanotubes. The influence of the heating procedure and the sol concentration is discussed.

In Paper V, a piezoresponse force microscopy study of single $PbTiO_3$ nanorods is presented. The piezoelectric properties were studied in both vertical and lateral mode. Piezoelectric activity and polarization switching was observed in the vertical mode, demonstrating the ferroelectric nature of the nanorods. The nanorods decomposed after repeated cycling of the dc bias at one spot on the nanorod, which resulted in parts of the nanorod disappearing and/or accumulation of particles on the surface of the nanorod.

In Paper VI, a method to contact single nanorods by electron beam induced deposition of platinum is presented. An organometallic compound, (trimethyl)-methylcyclopentadienylplatinum(IV), was used as precursor. A home-made apparatus was constructed for the purpose and was mounted onto a scanning electron microscope. Calculations based on apparatus geometry and molecular flow were used to estimate the deposition time and the height of the deposits. The location and height of the deposits were controlled so that single nanorods could be successfully contacted at the ends of the nanorods.

Fabrication of a sample device for piezoresponse force microscopy studies of single nanorods using an axial dc bias setup is described in Appendix IV. A proposed experimental setup for such studies is also presented.

Table of contents

Papers

Appendices

The author's contribution

The author wrote Papers I - VI and Appendix IV. In Paper I, all the experiments were performed by the author, except the BT-A and BT-B syntheses (and the TGA, XRD and SEM characterization of these) and the TEM investigations of the PT products. In Paper II, all the experiments except the magnetron sputtering, the sample preparation by microtomy, and the TEM investigations, were performed by the author. In Papers III - VI, all the experiments were performed by the author. In Appendices I - III, the author contributed mainly to the development of the synthesis route, the understanding of the growth mechanism, and to the writing. In Appendix IV, all the experiments except the wire bonding were performed by the author.

1. Background

The term nanotechnology is used to refer to a broad field whose unifying theme is the control and fabrication of structures which in at least one dimension are at the nanoscale (1 - 100 nm). With the development of the scanning tunneling microscope in 1981,[1] and the discovery of fullerenes[2] and the detailed description of carbon nanotubes,[3] both new methods to study nanostructures and new nanomaterials with improved properties demonstrated the potential of nano-technology and paved the way for other researchers to follow. The hype of nanotechnology the recent years can be explained by the commercial availability of advanced characterization tools, but also by an increase in funding by governments.

Some believe that nanoscience and nanotechnology have the potential to give changes in the society comparable to the changes induced by the industrial revolution. But then, one may ask; what makes this technology so fantastic? One important aspect is the ability to make existing things smaller, thereby reducing the energy needed, the heat produced, the amount of material needed, and making it possible to integrate advanced technology into everyday objects in order to improve their properties. For instance, in microelectronics, "smaller" has meant greater performance ever since the invention of integrated circuits: more components per chip, faster operation, lower cost, and less power consumption.[4]

Another important aspect is that nanoscale properties of a material often differ from its bulk properties. Quantum confinement of electrons by the potential wells of nanoscale structures may provide one of the most powerful and yet versatile means to control the electrical, optical, magnetic, and thermoelectric properties of a solid-state material.[4] In nanoscale materials, the long-range forces such as gravity and Coulombic (ionic) interaction, become less important, while short-range forces such as covalent interaction and van der Waals forces dominate. The crystal structure of nanoscale materials will therefore often deviate from the bulk crystal structure, usually toward a structure with higher symmetry (a high-temperature phase). Another important aspect is the surface/volume ratio, which increases with decreasing particle size. The relative number of surface atoms in a nanoparticle is far greater than in a larger particle, so the surface atoms will in a much greater degree control the properties of the nanoparticle than in a larger particle, in which mainly the interior atoms control the properties. In addition, the surface diffusion of atoms across the surface of a nanoparticle is rapid compared to a large particle. This has profound implications for particle sintering and coalescence, diffusion-determined deformations, chemical reactions, and other changes in nanoparticle assemblies.[5]

Nanoscale structures consist of one or several of the three basic nanoshapes: zero-dimensional (0D) quantum dots and nanoparticles, one-dimensional (1D) nanorods and nanotubes, and two-dimensional (2D) thin films and nanoplatelets. These nanoshapes will of course have a certain extension, so they are strictly speaking quasi-0D, quasi-1D and quasi-2D structures. The focus of this work is on 1D nanostructures.

The increasing miniaturization of electric and mechanical components makes the synthesis and assembly of nanoscale structures an important step in modern technology. Functional materials, such as the ferroelectric perovskites, are vital to

the integration and utility value of nanotechnology in the future. The recent years have seen a bloom in the synthesis of 1D nanostructures of ferroelectric perovskites. To successfully and controllably make 1D nanostructures by chemical methods it is important to understand the growth mechanism of these nanostructures, in order to design the structures for use in various applications. The integration of 1D nanostructures into devices requires routes to make arrays and large-area designed structures from the building blocks that single nanostructures constitute. As functional materials, it is of course also vital to study the properties of the 1D nanostructures. The characterization of properties of single nanowires and nanorods is challenging, but essential for future applications.

2. Aim of work

The choice of research topics for this work has been based on the following overall goals. First, we wanted to synthesize high quality single-crystalline 1D nanostructures of ferroelectric perovskites with a high yield. Second, we were interested in making arrays or hierarchical nanostructures of 1D nanostructures on substrates, since the assembly of 1D nanostructures into larger structures is vital to the use in applications. Third, we wanted to understand the growth mechanisms of the 1D nanostructures, since such an understanding is necessary for the development and advance of the syntheses. Fourth, we wanted to investigate ferroelectricity in 1D nanostructures.

To reach these goals, several synthesis methods were used to fabricate nanorods and nanotubes: molten salt synthesis (Paper I), hydrothermal synthesis (Paper II and III), and template-assisted synthesis (Paper IV). The molten salt synthesis was used to try to reproduce previously reported syntheses of $BaTiO_3$ and $PbTiO_3$ nanorods. The hydrothermal synthesis of $PbTiO_3$ nanorods had been developed in our laboratory (Appendices I and II), and in this work we wanted to refine the synthesis to grow nanorod arrays on substrates. Template-assisted methods have been reported to be well suited for the synthesis of nanotubes, so for the synthesis of $PbTiO_3$ nanotubes, a template-assisted synthesis was examined.

Finally, to study the ferroelectric and piezoelectric properties of single nanorods, we chose to use piezoresponse force microscopy (PFM) (Paper V). As we were interested in using an axial dc bias setup for the PFM study, methods to contact single nanorods (Paper VI) and to make a sample device with an electrode pattern (Appendix IV), were necessary steps and constitute the last part of the thesis.

3. Introduction

3.1. Synthesis of one-dimensional nanostructures

3.1.1. One-dimensional nanostructures

1D nanostructures such as nanorods and nanotubes are the smallest dimension structures that can be used for efficient transport of electrons and optical excitations, and are thus expected to be critical to the function and integration of components at nanoscale.[6] The use of 1D nanostructures in applied technology devices is currently still in the initial phase, but they are expected to play an important role as both interconnects and functional units in fabricating electronic, optoelectronic, electrochemical, and electromechanical devices with nanoscale dimensions.[4] The novelty of these 1D nanostructures makes them interesting for such varied fields as electronics, photonics, sensors, catalysts, energy harvesting, information storage and mechanical strength enhancement. Most of the potential applications for 1D nanostructures take use of the inherent properties of a certain material (electrical, optical, magnetic or thermoelectric properties), so any general applications for such nanostructures are few. However, the large surface area generally makes them interesting for catalysis and sensors, and the anisometric shape can be used in composites for improving the mechanical strength.

The synthesis of 1D nanostructures has mainly been directed towards metals, semiconductors, binary oxides, and carbonaceous materials,[4,6-12] but syntheses of complex ternary oxide materials have been rapidly emerging the last 3 - 4 years.[13] A number of reviews of the literature have been published,[4,6-13] which give an overview of the field. The last years have seen a steadily increase in the literature on 1D nanostructures, showing the widespread and growing research field that these structures represent. While much of the literature so far has been focused on the synthesis and basic properties of 1D nanostructures, demonstrations of more advanced applications and controlled assembly are now emerging.

1D nanostructures have been produced in several morphologies. While hollow 1D nanostructures are all called nanotubes, a variety of names is used for dense 1D nanostructures: nanorod, nanowire, nanobelt, nanofiber and nanowhisker (figure 1). A nanorod and a nanowire can be differentiated by the aspect ratio (length/diameter). For instance, Murphy and Jana[14] defined nanorods as nanostructures with a width of ~1 - 100 nm and aspect ratios greater than 1 but less than 20; and nanowires analogous nanostructures that have aspect ratios greater than 20. However, as no standard is given, these two terms are widely mixed. Nanobelts are 1D nanostructures with a rectangular cross-section, with a width markedly different from the height. Nanofiber is often used to name 1D nanostructures made by electrospinning and in addition sometimes used to describe clearly polycrystalline 1D nanostructures. Nanowhisker is seldom used.

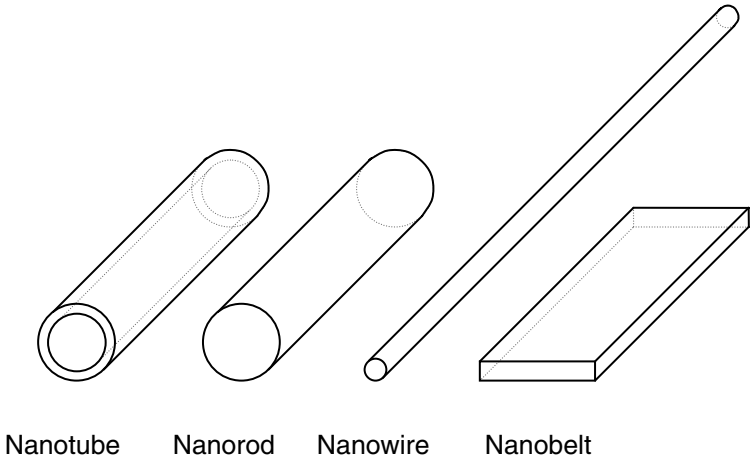

Figure 1. Schematic illustration of the most important 1D nanostructures.

3.1.2. Synthesis methods

The production of nanostructures can generally be divided into two approaches: "top-down" and "bottom-up". The top-down approach employs physical methods such as lithography, etching, milling and probe-based methods to downsize larger structures, while the bottom-up approach typically employs chemical methods to assemble nanostructures from individual atoms and molecules. Physical top-down methods can be used to fabricate a wide variety of 1D nanostructures of various materials. These methods include advanced nanolithographic techniques such as electron-beam or focused-ion-beam writing. However, great ingenuity is required to rapidly fabricate large quantities of 1D nanostructures by these techniques from a diversified range of materials at reasonable low costs. In contrast, unconventional methods based on chemical synthesis might provide an alternative and intriguing strategy for generating 1D nanostructures in terms of material diversity, cost, throughput, and the potential for high-volume production.[4]

Many standard chemical methods to fabricate and shape bulk materials use high temperature as the driving force for reaction or diffusion of species. However, the diffusion processes that are central at high temperature such as sintering, Ostwald ripening and grain growth are often detrimental in the making of nanostructures, and must be avoided or carefully controlled, in order to retain separate nanoparticles and the small size of the particles. Chemical methods to prepare nanostructures therefore often involve synthesis at lower temperatures than in synthesis of bulk materials. For chemical reaction to occur, diffusion of the reacting species is always necessary. A sufficient diffusion rate at lower temperature can be accomplished by using smaller sized precursors (single molecules and atoms, instead of agglomerates or bulk particles) and a solvent in which the precursors can dissolve and easily diffuse. Many of the chemical methods are therefore called "wet chemistry" methods, implying the use of a

solvent, in contrast to solid state reactions. The main advantage of the wet chemistry methods is the homogeneous mixing of the precursors, which reduces the necessary diffusion distance. However, many nanoparticle syntheses take place at high temperatures, but then excessive diffusion is hindered by a low and controllable concentration of reactant species.

To synthesize 1D nanostructures by chemical methods it is necessary to induce anisometric growth of the material. Figure 2 shows some methods to accomplish such growth. The probably most studied and best controlled method to prepare 1D nanostructures (excluding carbon nanotubes), is the vapour-liquid-solid (VLS) or solution-liquid-solid (SLS) method (figures 2b and 3). This method has especially been used to prepare nanowires of semiconductors such as Si, GaAs and ZnO.[4,8,16] A liquid droplet is used as catalyst seed. Each liquid droplet serves as a soft template to strictly limit the lateral growth of an individual wire. The precursor is introduced as a vapour or in a solution, and dissolves into the catalyst droplet. When the droplet is supersaturated with the dissolved species, the nanowire starts to grow. The diameter of the nanowire is governed by the size of the catalyst droplet.

The VLS and SLS methods are better suited to produce binary semiconductors and oxides, than more complex materials such as ternary oxides, because of the need of more complex precursors for the ternary oxides, and the corresponding difficulty in controlling the growth conditions. For complex materials such as perovskites and spinels other methods are used instead. Many of these other methods are specific for the material; however, some general synthesis methods are widely used and will be described briefly here.

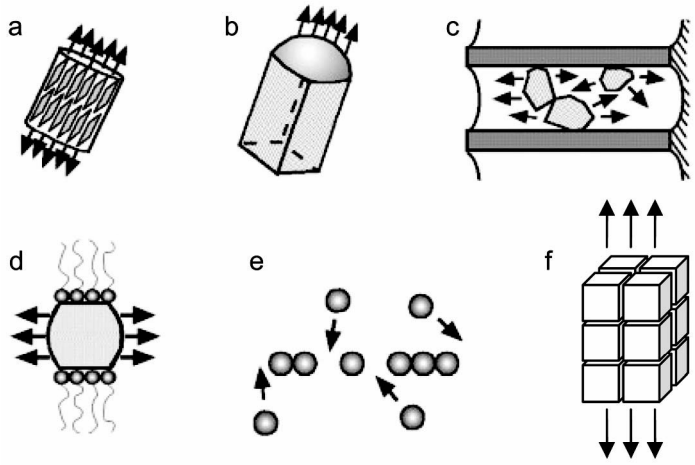

Figure 2. Schematic illustration of various methods to induce 1D growth in order to obtain 1D nanostructures: (a) use of the anisometric crystallographic structure of a solid, (b) introduction of a liquid-solid interface to reduce the symmetry of a seed, (c) use of various templates with 1D morphologies to direct the formation of 1D nanostructures, (d) use of appropriate capping reagent(s) to kinetically control the growth rates of various facets of a seed, (e) self-assembly of spherical 0D nanostructures, and (f) self-assembly of non-spherical 0D nanostructures into mesocrystals.[4,15] The figure is partly adapted from Xia *et al*.[4]

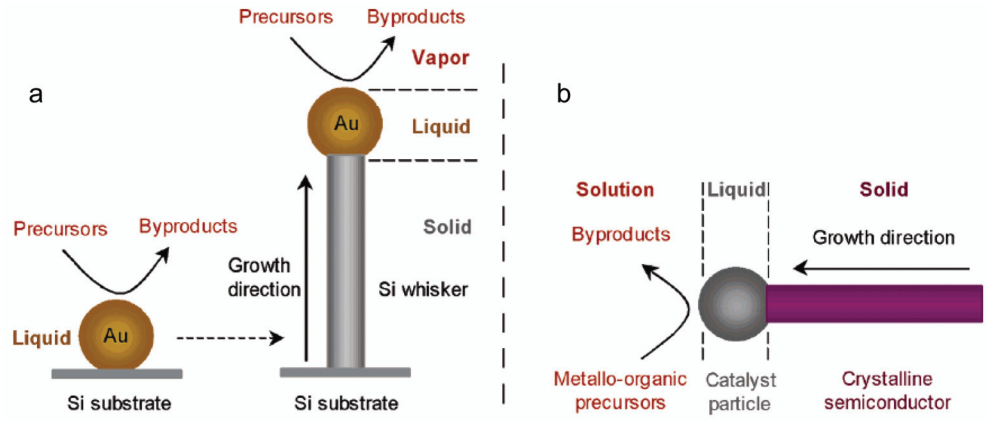

Figure 3. Schematic illustration of the VLS and SLS mechanisms for nanowire growth. (a) VLS mechanism for growth under chemical vapour deposition conditions. (b) SLS mechanism for analogous growth from solution. The figure is adapted from Wang *et al*.[16]

The easiest method to produce 1D nanostructures is to use a negative template such as porous alumina (also named anodic aluminium oxide, AAO) or track-etched polymer (mostly polycarbonate), which has 1D pores or channels in which a sol or an aqueous solution can penetrate (figure 2c).[11,12] By a following heat treatment, the solvent evaporates, and the material starts to crystallize on the surfaces of the channels of the template. Nanotubes are most frequently produced by this method, but by increasing the immersion time or employing a particle-directing force such as electrophoresis,[17] nanowires have also been reported. AAO templates can be purchased commercially; however, better control of the pore diameter and pore distribution is obtained if the AAO templates are produced in the lab.[18]

In addition to the negative templates, positive templates such as nanowires, nanorods, and carbon nanotubes can also be used to make 1D nanostructures, by coating the outer surface of the template with the desired material.[11] Subsequently, the positive templates can either be removed by chemical etching and/or pyrolysis to make nanotubes, or remain as the core in core-shell nanowires.

Electrospinning is another method that can be used to produce a wide variety of materials as nanowires or nanofibers. The formation of a thin fiber via electrospinning is based on the uniaxial stretching (or elongation) of an electrified jet derived from a highly viscous polymer solution. A solid fiber is produced due to the evaporation of solvent.[19]

Other methods to prepare complex materials as 1D nanostructures include molten salt synthesis, hydrothermal synthesis and thermolysis. Common for all these methods is that the 1D growth takes place in a solution, and one or several of the mechanisms in figure 2 (a, d, e, or f) are responsible for the growth. These methods are more trial-and-error approaches than the previously described template methods, because it can be difficult to determine the correct set of

synthesis parameters that can induce 1D crystal growth in a system without any inherent driving forces for such growth.

In molten salt synthesis a variety of salts can be used, such as chlorides, nitrates and hydroxides. The features of this synthesis method are related to the surface energies and the interface energies between the constituents and the salt, resulting in a tendency to minimize the energies by forming a specific morphology. The size, shape and crystallinity of the products as well as the growth rate are affected by the preparation conditions, the type of salt or salt mixture, the precursor composition and morphology, the initial particle size and the solubilities of the precursor constituents in the salt.[20]

In hydrothermal synthesis the precursor(s), the solvent, and in some cases the surfactant(s) or other additives, are mixed and heated in a closed container. The elevated temperature increases the pressure inside the container, so that the synthesis conditions approach the critical point of the solvent. This increases the solubility and the reactivity of reactants, and makes it possible to crystallize 0D and 1D nanoparticles at a significantly lower temperature than other methods.[4]

Thermolysis (thermal decomposition) has been used to prepare many different materials as 0D, 1D and 2D nanostructures, mostly binary compounds,[21] but also ternary compounds.[22] Typically, molecular precursors are injected into a hot (~100 - 350 °C) organic solvent containing capping molecules (surfactants), inducing a rapid increase of the monomer concentration, followed by nanocrystal growth through aggregation of the monomers, and surface passivation of the resulting nanocrystals with capping molecules.[23] An important aspect of this method is the facile separation between the nucleation and growth stages, so that the nanocrystal growth can be more easily controlled than in other methods.

Several of the reported syntheses of 1D nanostructures only describe the synthesis of individual particles. However, from a practical point of view, methods to fabricate arrays of 1D nanostructures are more attractive than syntheses of randomly oriented individual particles. Future applications and nanomanufacturing will strongly rely on large-scale patterned and designed growth, and on self-assembly technology. Therefore, an essential step in integrating nanostructures with existing technologies will be to be able to control the number, location and orientation of the 1D nanostructures.[10] In the VLS synthesis of semiconductor nanowires, this is now possible for many materials, but for other materials and methods this is a subject of intense study.

3.1.3. Growth mechanisms for template-free syntheses

For template-free synthesis routes such as molten salt and hydrothermal synthesis, the 1D growth is induced by one of the mechanisms depicted in figure 2. The more important mechanisms for this work are further described here.

For materials with an anisometric crystal lattice, 1D growth is more easily obtained due to the energy difference between different crystal faces (figure 2a). Simply put, when the number of atoms per surface area is high, then the surface energy is high, because many bonds have to be broken if two such surfaces are formed by cleaving the material. Although the crystal faces of materials with isometric crystal lattice also have different surface energies, the difference is not

directed in 1D or 2D direction(s). Wulff's rule defines the equilibrium morphology of a crystal as being given by the minimum surface energy of all exposed crystal faces. Crystal faces with high surface energies exhibit the fastest growth rate and are minimized or even disappear in the final morphology.[24] However, growth of 1D nanostructures is in general a thermodynamically non-equilibrium process which is controlled by kinetics. As growth kinetics is a rather complex process, a solid understanding of the growth kinetics is essential for controlling the growth process.[10]

The surface energy of the nanocrystals can be modulated by introducing surfactants that adsorb onto surfaces of growing crystallites (figure 2d). When surfactants stabilize a certain surface by selective adhesion, the growth rate difference between different crystallographic directions can be accentuated.[21] The choice of a surfactant in a synthesis is often more or less arbitrary, or done on a trial-and-error approach, as knowledge of how strongly or if at all specific surfactants adsorb on specific crystal faces is scarce. When choosing surfactant several factors should be considered: the type (anionic, cationic or non-ionic), the size (length of alkyl chain, polymeric or non-polymeric), the head size (size of polar end) and the shape of the nonpolar end (single/double alkyl chain, straight or branched alkyl chain, benzene rings) are all factors that influence the interaction of the surfactant with the material and the solvent. By appropriately choosing surfactant(s), the crystallization and growth can be controlled and directed to obtain the desired nanostructure.

The two growth mechanisms described above (anisometric growth because of anisometric crystal lattice or the use of a capping reagent) are both examples of classic crystallization, that is, ion-by-ion growth on a primary nanoparticle by amplification. Contrary to the classic crystallization, the recent decade has seen many examples of an alternative crystallization mechanism based on self-assembly, named oriented attachment or mesocrystal formation.[15,24] Figure 4 shows the steps in this particular mechanism. Primary nanoparticles can arrange into an iso-oriented crystal via oriented attachment (path b), and form a single crystal upon fusion of the nanoparticles. If the nanoparticles are coated by adsorbed surfactants, they can form a mesocrystal via mesoscale assembly (path c), possibly followed by fusion to an iso-oriented crystal and finally to a single crystal.[15,24] Fusion is accomplished by desorption of surfactant molecules and formation of chemical bonds at the interface between primary particles. The total energy is decreased as a result of the elimination of solid-liquid or solid-gas interface and an increase in entropy because of surfactant desorption.[25] Due to the anisometric shape of the building blocks, anisometric shapes are frequently formed as a result of the self-assembly. 1D growth can be enhanced by electric or magnetic polarization inherent in the nanoscale building blocks.

It must be emphasized that much of the literature on 1D nanostructures is purely descriptions of the synthesis, without any study or discussion of the growth mechanism behind the 1D growth. In order to develop the field further and be able to design syntheses of new materials without extensive trial and error, the underlying mechanisms for 1D growth are important to unveil.

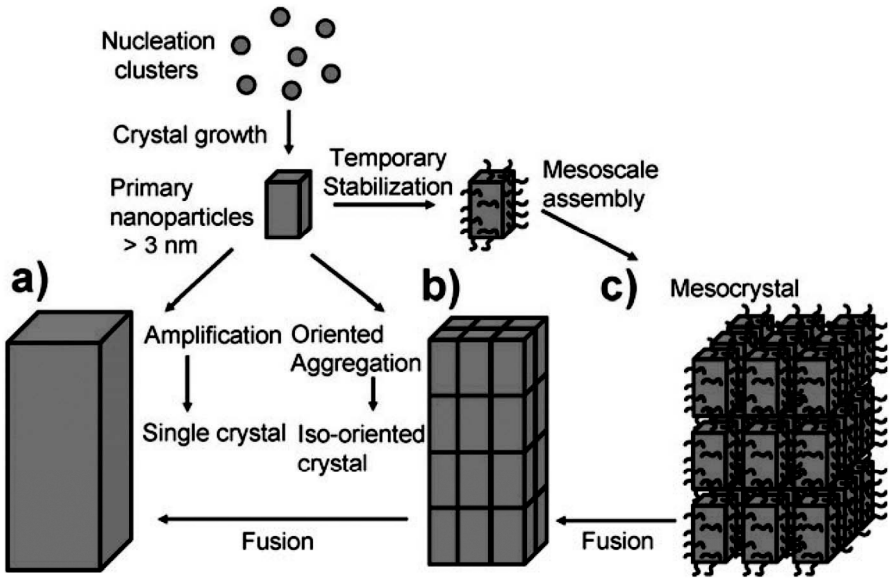

Figure 4. Schematic illustration of classical and non-classical crystallization. (a) Classical crystallization pathway. (b) Oriented attachment of primary nanoparticles forming an iso-oriented crystal upon fusing. (c) Mesocrystal formation via self-assembly of primary nanoparticles covered with organics. The figure is adapted from Niederberger *et al*.[24]

3.1.4. Syntheses of one-dimensional nanostructures of ferroelectric perovskites

The main topic of this work has been the synthesis of 1D nanostructures of ferroelectric perovskites, especially $PbTiO_3$. Until recently, few 1D nanostructures of ferroelectric perovskites had been synthesized, only sub-micron- or micron-sized structures had been made.[26-30] One exception is the hydrothermal synthesis of so-called PX-phase $PbTiO_3$ (with a tetragonal bcc structure), which was transformed into the tetragonal $PbTiO_3$ perovskite structure after heat treatment at ~605 °C.[31] Then in 2001, Cho *et al.*[32] reported a hydrothermal synthesis of $PbZr_{1-x}Ti_xO_3$ (PZT) nanowires, while Limmer *et al.*[33] described an electrophoretic sol-gel template synthesis of PZT nanorods. Urban *et al.*[22] reported synthesis of $BaTiO_3$ and $SrTiO_3$ nanowires in 2002. The same year Hernandez *et al.*[34] reported a template-assisted synthesis of $BaTiO_3$ and $PbTiO_3$ nanotubes, and Liu *et al.*[35] reported a hydrothermal synthesis of $KNbO_3$ nanorods. From 2003 and forwards, many other groups have reported the synthesis and studied the properties of 1D nanostructures of ferroelectric perovskites, especially the last three years. A summary of the available literature on 1D nanostructures of ferroelectric perovskites and closely related compounds, made mainly by chemical methods, is given in table 1.

Table 1. A summary of synthesis studies of 1D nanostructures of ferroelectric perovskites and closely related compounds.

Material	Synthesis method	Reference(s)
$BaTiO_3$	Thermolysis	22, 36
	Sol-gel deposition in AAO template	34, 37
	Sol-gel electrophoretic deposition in polycarbonate template	38
	Sol-gel deposition in electron beam resist mold	39,40
	Molten salt	41
	Hydrothermal	42,43
	Hydrothermal conversion of TiO_2 nanotubes	44-47
	Hydrothermal conversion of sodium titanate nanowires and nanotubes	48
	Hydrothermal conversion of sodium hydrogen titanate nanotubes	49
	Hydrothermal conversion of potassium titanate nanowires	50,51
	Calcination of gel	52
	Electrospinning	53-56
	Low-temperature crystallization in ethanol solution	57
	Magnetron sputtering onto Si or ZnO nanowires as positive templates	58
$PbTiO_3$	Sol-gel deposition in AAO template	18,34,59-61
	Sol-gel deposition in polycarbonate template	59
	Aqueous salt solution deposition in AAO template	62
	Molten salt	63,64
	Hydrothermal	31,65-71
	Microwave-hydrothermal	72
	Hydrothermal conversion of TiO_2 nanotubes	73,74
	Hydrothermal formation of stripes in grooves on $SrTiO_3$ substrates	75
	Electrospinning	76

continues on next page

Table 1 continues

Material	Synthesis method	Reference(s)
$PbZr_{1-x}Ti_xO_3$ (PZT)	Sol-gel deposition in AAO template	37,77-82
	Sol-gel electrophoretic deposition in AAO template	83,84
	Sol-gel electrophoretic deposition in polycarbonate template	33,38
	Centrifugation-assisted sol-gel deposition in polycarbonate template	85
	Sol-gel deposition in porous silicon	77,86
	Hydrothermal	32,87-90
	Electrospinning	91-94
	Thermal evaporation formation of stripes on $SrTiO_3$ substrates controlled by gold particles	95
	Pulsed laser deposition onto Si, ZnO or MgO nanowires as positive templates	58,96,97
	Liquid source misted chemical deposition onto carbon nanotubes as positive templates	98
	Liquid source misted chemical deposition onto ZnO nanowires as positive templates	99
$PbZrO_3$	Pulsed laser deposition in AAO template	100
$SrTiO_3$	Thermolysis	22
	Hydrothermal	42,101
	Hydrothermal conversion of TiO_2 nanotubes	44
	Hydrothermal conversion of hydrogen titanate nanotubes	102
	Hydrothermal conversion of potassium titanate nanotubes	103
	Hydrothermal conversion of layered titanate nanowires	104
	Self-propagating high-temperature combustion	105

continues on next page

Table 1 continues

Material	Synthesis method	Reference(s)
$Ba_{1-x}Sr_xTiO_3$	Sol-gel deposition in AAO template	106
	Hydrothermal conversion of TiO_2 nanotubes	46,107
	Hydrothermal conversion of sodium titanate nanowires and nanotubes	48
	Electrospinning	108
	Ultrasonic irradiation of sol followed by calcination of gel	109
	Room-temperature microemulsion	110
$Pb_{0.25}Ba_{0.15}Sr_{0.6}TiO_3$	Sol-gel deposition in AAO template	111
$LiNbO_3$	Thermolysis of bimetallic precursor in AAO template	112
$NaNbO_3$	Hydrothermal	113
	Molten salt conversion of $K_2Nb_8O_{12}$ nanowires	114
$KNbO_3$	Hydrothermal	35,115-122
	Calcination of polymeric gel	123
$KNb_{1-x}Ta_xO_3$	Hydrothermal	116,124
$NaTaO_3$	Alkalide reduction	125
$BiFeO_3$	Sol-gel deposition in AAO template	126-130
$Na_{0.5}Bi_{0.5}TiO_3$	Hydrothermal treatment of dry gel	131
$K_{0.5}Bi_{0.5}TiO_3$	Molten salt	132
	Hydrothermal treatment of dry gel	133,134
$(Na_{0.8}K_{0.2})_{0.5}Bi_{0.5}TiO_3$	Hydrothermal treatment of dry gel	135
$(K_{0.5}Bi_{0.5})_{0.4}Ba_{0.6}TiO_3$	Hydrothermal treatment of dry gel	136
$Bi_{3.15}Nd_{0.85}Ti_3O_{12}$	Electrospinning	137
$Bi_{3.25}La_{0.75}Ti_3O_{12}$	Precursor solution deposition in AAO template	138,139
$Sr_{0.8}Bi_{2.2}Ta_2O_9$	Liquid source misted chemical deposition in porous silicon templates	77,140
Multiferroic $CoFe_2O_4$-PZT composite	Sol-gel deposition in AAO template	141
	Electrospinning	142
Multiferroic $NiFe_2O_4$-PZT composite	Electrospinning	143

Several of the syntheses in table 1 include advanced chemistry and detailed procedures. Often, the necessary information to precisely duplicate the experimental procedure is not described in detail, and therefore it may be problematic to reproduce the synthesis. For instance, although the paper by Urban *et al.*[22] reporting synthesis of $BaTiO_3$ and $SrTiO_3$ nanowires is highly cited, no follow-up studies using the same method by other research groups have been published. Our preliminary efforts to synthesize $BaTiO_3$ nanowires by the method published by Urban *et al.* gave very low yields of nanorods.[144,145] In Paper I in this work, we describe our study to reproduce the molten salt synthesis of $BaTiO_3$ and $PbTiO_3$ nanorods reported in the literature,[41,63,64] but we were unsuccessful in producing perovskite nanorods. Instead, nanorods of titanium-oxide rich compounds were formed,[146] which has also been confirmed by others.[147,148] In general, most of the non-template methods have been used only by one research group. In comparison, the template-assisted methods are the simplest and most studied methods, and they are also more easily reproduced due to the simplicity of the method. The template method can be used for all ternary oxides, as long as a suitable precursor solution can be made. However, the template methods generally produce polycrystalline nanotubes or nanowires, which presents a serious problem in terms of controlling the uniformity of their ferroelectric properties.[149] In addition, the removal of the template often cause the 1D nanostructures to bundle together, especially when the template is etched in a solution, because of capillary stress created during evaporation of liquids. Such bundling can however be avoided by supercritical CO_2 drying which gives negligible surface tension.[150]

Since the ferroelectric perovskites in general have a pseudo-cubic unit cell, with c/a ratios of 1.01 for $BaTiO_3$ and 1.06 for $PbTiO_3$ (where a and c are the lattice constants in the tetragonal structure),[151,152] the surface energies of closely related crystal faces (such as (100) and (001)) will be almost equal. Hence, the products will most often have an isometric morphology unless some structure-directing agent is present in the synthesis. In the syntheses listed in table 1, the 1D structure is in most cases controlled by the template, the surfactant(s), the precursor morphology, or the synthesis method (for electrospinning). However, several of the syntheses in table 1 contain none of these structure-directing means, especially some of the hydrothermal syntheses.[35,42,43,65-67,72,101,113,115-119] The morphology may then be controlled by differences in surface energy. In the hydrothermal synthesis, the effect of the difference in surface energy may be enhanced because of the high solubility of reactants in the solution leading to kinetic growth control and a high growth rate in one direction. Regrettably, many authors do not comment on the anisometric growth mechanism, although it is very important in order to improve the syntheses. For the $KNbO_3$ nanowires synthesized by hydrothermal method, Goh *et al.*[118] have proposed a spiral growth mechanism because of screw dislocations parallel to the axial direction, while Vasco *et al.*[153] have proposed a cube-based growth mechanism. In the syntheses with calcination of a polymeric gel, the morphology may be controlled by an intermediate phase with anisometric crystal structure, such as the layer-structured compound $K_4Nb_6O_{17}$ in the synthesis of $KNbO_3$.[123]

Although none have studied the inclusion of foreign cations in the perovskite lattice of 1D nanostructures, it can be of importance for the application of 1D

nanostructures of ferroelectric perovskites. Both alkali metal and proton substitution adversely affect the dielectric properties of the perovskites.[154,155] In both the molten salt and hydrothermal syntheses, alkali cations such as Na^+ and K^+ are usually present in significant amounts. Na^+ and K^+ may substitute the Ba^{2+} or Pb^{2+} ions in the lattice, creating oxygen vacancies to maintain charge neutrality.[154] In addition, OH^- may substitute O^{2-}, creating cation vacancies.[155] The protons can be removed from the structure by annealing. Heat treatment up to 600 °C may be necessary to remove all the protons from the lattice; however, a significant amount of protons is removed at lower temperatures.[156] So although the hydrothermal synthesis route is a low-temperature synthesis route, subsequent high-temperature annealing to annihilate defects in the structure may be necessary.

3.2. Ferroelectricity

3.2.1. Ferroelectric materials

Ferroelectric materials (named "ferroelectrics") have a spontaneous electric polarization which can be switched by an external electric field. In all known ferroelectric crystals, the spontaneous polarization is produced by the arrangement of ions in the crystal structure, depending on their positions, as in conventional ferroelectrics, or on charge ordering of multiple valences, as in electronic ferroelectrics.[157,158] Only materials with a non-centrosymmetric point group which contains alternate atom positions or molecular orientations to permit the reversal of the dipole and the retention of polarization after voltage removal are ferroelectric. Ferroelectricity is closely related to piezoelectricity and pyroelectricity; all ferroelectric materials are also piezoelectric and pyroelectric, but not all piezoelectrics are pyroelectric, and not all pyroelectrics are ferroelectric.[157]

Among the ferroelectric materials, the technologically most important ones are the perovskite-type compounds. The perovskite structure (ABX_3) is the most multifunctional among the ternary crystal structures, as it can produce an incredibly wide array of phases with totally different properties for advanced technological applications. The oxide structure (ABO_3) is by far the most studied, and has been used to make materials with unique electronic, magnetic and optical properties, including ferroelectricity, high-temperature superconductivity, and colossal magnetoresistance.[159] The ideal (cubic) perovskite structure consists of corner-sharing oxygen-octahedra with the B cation in the middle of the octahedra, and with the A cation in the 12-coordinated hole between 8 octahedra (figure 5a). The three main classes of perovskites are $A^{I}B^{V}O_3$, $A^{II}B^{IV}O_3$, and $A^{III}B^{III}O_3$, with the Roman numerals depicting the valence state of the cations. In this work the ferroelectric perovskites $BaTiO_3$ and especially $PbTiO_3$ have been central.

The prototype ferroelectric perovskite is $BaTiO_3$, in which ferroelectricity was discovered in the 1940s.[159] The ferroelectricity in $BaTiO_3$ arises from a displacement of the titanium ion in the [001] direction of the tetragonal perovskite structure, and $BaTiO_3$ is therefore labelled a displacive ferroelectric. At high temperature, $BaTiO_3$ has a paraelectric cubic perovskite structure (*Pm*-3*m*, figure 5a). At 120 °C, it transforms from the cubic phase to a ferroelectric tetragonal

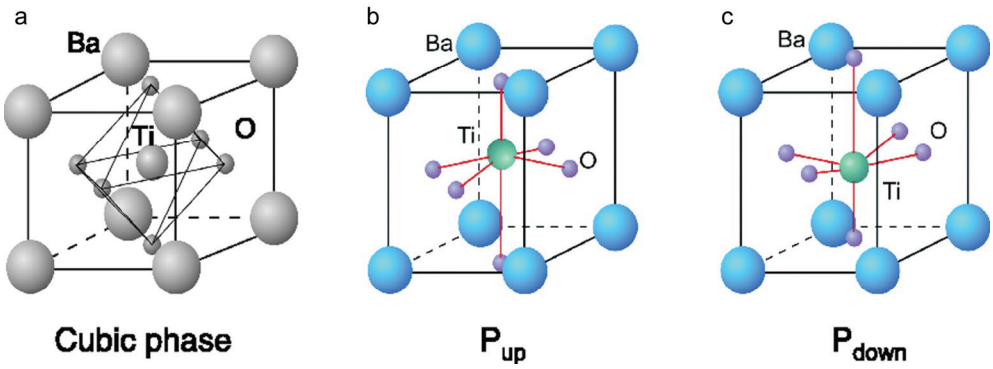

Figure 5. Crystal structure of the ferroelectric perovskite $BaTiO_3$. (a) High-temperature paraelectric cubic phase. (b)-(c) Room-temperature ferroelectric tetragonal phases, showing up and down polarization variants. The atomic displacements are scaled to be clearly visible. The figure is adapted from Ahn *et al*.[160]

phase (*P*4*mm*, figures 5b and c). This phase remains stable until 5 °C, where there is a second transformation to a ferroelectric orthorhombic phase (*Amm*2). The last transition occurs at -90 °C, where $BaTiO_3$ transforms to a ferroelectric rhombohedral phase (*R*3*m*). Each transition is accompanied by small atomic displacements, dominated by displacement of the Ti ion relative to the oxygen octahedron network, and a macroscopic strain. In the successive ferroelectric phases, the polar axis is aligned respectively along the <100>, <110> and <111> directions corresponding to the direction of the atomic displacements with respect to their position in the cubic reference structure.[157,158]

Compared to $BaTiO_3$, $PbTiO_3$ has a higher spontaneous polarization at room temperature (75 μC/cm^2 versus 26 μC/cm^2)[157,158] and a higher *c*/*a* ratio (1.06 versus 1.01).[151,152] The transition from the high-temperature cubic phase to the ferroelectric tetragonal phase occurs at ~490 °C, which is much higher than for $BaTiO_3$ (120 °C).[152,157,158] First-principles calculations[151] and experimental verification[152] have shown that the hybridization between the Ti 3*d* states and the O 2*p* states is essential to the ferroelectric instability in both $PbTiO_3$ and $BaTiO_3$. The orbital hybridization existing between the Pb 6*s* state and O 2*p* states plays a crucial role for the larger ferroelectricity in tetragonal $PbTiO_3$, whereas the interaction between Ba and O is almost ionic in tetragonal $BaTiO_3$ (figure 6). The Pb-O hybridization leads to a large strain that stabilizes the tetragonal phase via strain-polarization coupling. Another difference is that displacement of the Pb ion, in addition to that of Ti, is substantial and contributes significantly to the spontaneous polarization.[151,152,158]

When a crystal is cooled from a paraelectric phase to a ferroelectric phase in the absence of an electric field, different regions of the crystal will polarize in different directions. These regions are referred to as domains. Domains form to minimize the energy associated with the depolarization field. The depolarization fields which appear on cooling are usually sufficient to prevent any net polarization in a virgin crystal. The boundaries separating domains are referred to as domain walls. Domain walls are characterized by the angle between the polarization

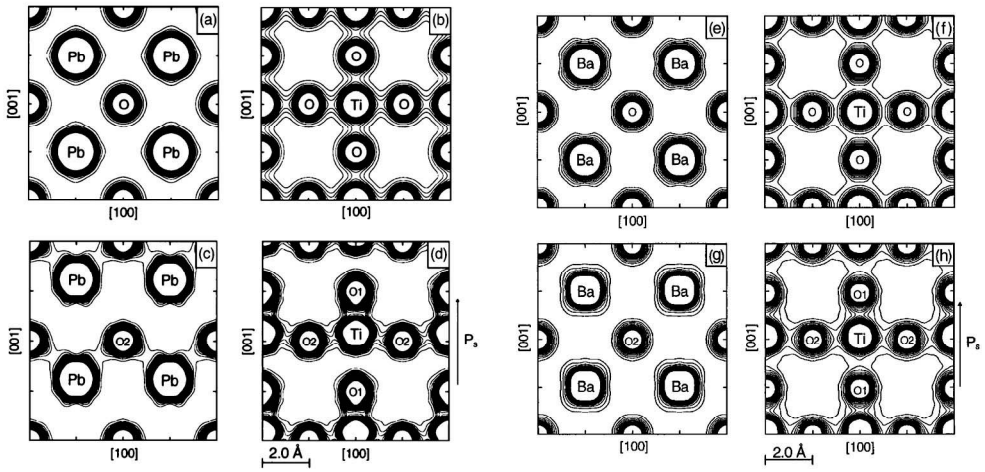

Figure 6. Maximum entropy method charge-density distributions of $PbTiO_3$ (a-d) and $BaTiO_3$ (e-h): (a)-(b) cubic $PbTiO_3$ phase at 527 °C, (c)-(d) tetragonal $PbTiO_3$ phase at 27 °C, (e)-(f) cubic $BaTiO_3$ phase at 300 °C, and (g)-(h) tetragonal $BaTiO_3$ phase at 27 °C. The columns show the Pb-O plane, Ba-O plane and Ti-O planes. The figure is adapted from Kuroiwa *et al*.[152]

directions on either side of the wall. The allowed angles for domain walls depend on the orientations of the polarization allowed by symmetry. In tetragonal perovskites such as $BaTiO_3$ and $PbTiO_3$, the domains align with 180° and 90° domain walls (figure 7), while in rhombohedrally distorted perovskites, there are no 90° domain walls, but instead 71° and 109° walls. The domain pattern in a crystal depends on many factors including the crystal symmetry, the electrical conductivity, the defect structure, the magnitudes of the spontaneous polarization and elastic and dielectric compliances, as well as the history of the crystal preparation and sample geometry.[157,161,162]

A defining property of ferroelectricity is the switching between different metastable states by the application and removal of an electric field. The domains are highly active in the switching process, through the motion of domain walls. Ferroelectricity is typically demonstrated by a hysteresis loop between the applied electric field (E) and the polarization (P) (figure 8). The ideal ferroelectric P-E hysteresis loop is symmetric and the remanent polarization (P_r) and coercive fields (E_c) are easily defined and extracted. For an initially non-polarized crystal the ferroelectric domains are randomly oriented prior to application of the electric field, with a zero net polarization. As the electric field is increased, the domains begin to reorient in the crystal and align parallel to the applied field. The polarization reaches a saturation value (B) when all the domains are aligned in the direction of the field. If the electric field then is reduced to zero, many of the domains will remain aligned such that a remanent polarization (P_r) exists. If the electric field is reversed, the domains are forced to switch direction. When the domains in one direction balance the domains in the opposite direction, the result is zero net polarization, which occurs at $-E_c$, called the coercive field. Continued increase in the negative electric field causes net polarization in the opposite direction.[157,158,163]

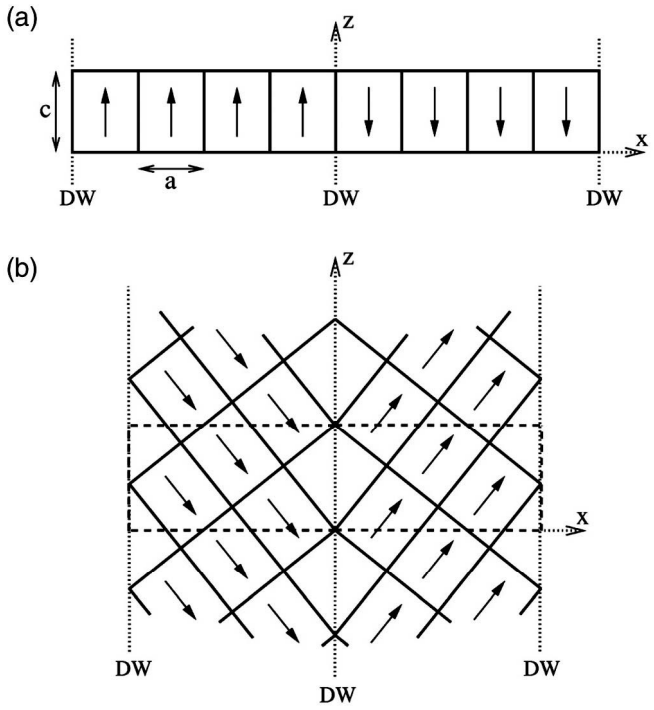

Figure 7. Schematic illustration of domain walls in $PbTiO_3$. Supercell geometries containing eight perovskite primitive cells for (a) 180° and (b) 90° domain walls (DW). Atoms are omitted and only solid lines connecting the Pb atoms are drawn. Supercell boundaries are indicated by dashed lines. The figure is adapted from Weber and Vanderbilt.[161]

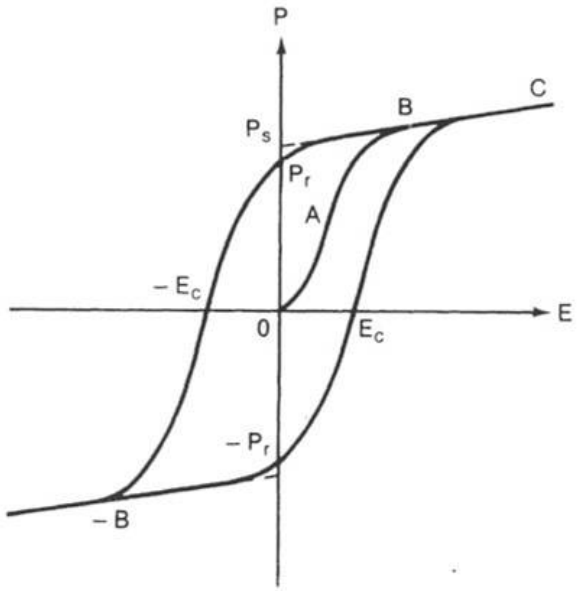

Figure 8. Ferroelectric hysteresis loop between applied electric field (E) and polarization (P). The figure is adapted from Richerson.[163]

3.2.2. Nanoscale ferroelectricity

Recent advances in science and technology of ferroelectrics have resulted in the development of ferroelectric structures and devices with length scales of several hundred nanometres and less. Scaling of the device dimensions to the range where ferroelectric materials start to show a pronounced size effect has emphasized the importance of nanoscale studies of ferroelectric properties. When the physical dimensions of ferroelectric structures are reduced, the size effect is observed by a decrease in the remanent polarization, dielectric permittivity and phase transition temperature, increase in the coercive field, changes in the domain structure, etc.[149]

Ferroelectricity at the nanoscale is limited by the relevant electrical and mechanical boundary conditions, but also by the practical issues involved in producing high-quality samples on the extreme nanoscale.[164] Size effects can be of intrinsic nature (related to the changes in atomic polarization at small scales) or extrinsic nature. Extrinsic effects are caused by the patterning and processing of materials, or more complicated effects which include the influence of inhomogeneous strain, incomplete polarization screening at the surface and defect microstructure. Most of the early studies of the size effects refer to the extrinsic ones; therefore, information is rather contradictory and scattered even for the same materials prepared with different processing routes.[149]

Current opinion is that, once the processing effects are eliminated, the critical dimensions in nanoparticles of ferroelectric oxides lie in the range 5 - 15 nm.[149,165] The size-driven phase transition in $PbTiO_3$ from the ferroelectric tetragonal phase to the paraelectric cubic phase has for instance recently been determined at 6 nm by Erdem *et al.*[166] and ~15 nm by Akdogan *et al.*[167] Nuraje *et al.*[168] and Spanier *et al.*[169] have demonstrated ferroelectric properties of 6 - 12 nm $BaTiO_3$ nanoparticles and $BaTiO_3$ nanowires with diameter down to 3 nm, respectively, using electrostatic force microscopy (EFM).

Epitaxial thin films of perovskite oxides can be made with thicknesses down to a single unit cell.[160] For instance, Fong *et al.*[170] have made ultrathin $PbTiO_3$ films on $SrTiO_3$ substrates with thicknesses from one to four unit cells. With X-ray synchrotron diffraction the ferroelectric phase was shown to be stable down to three unit cells (~1.2 nm) in these films.[170] First-principles calculations on $BaTiO_3$ thin films between $SrRuO_3$ electrodes in short circuit have demonstrated that the ferroelectric properties are lost below a critical thickness of about six unit cells (~2.4 nm).[171] In addition to the critical size for ferroelectricity, many researchers have studied how strain from the crystal lattice of the substrate can affect the ferroelectric properties of the films. In $BaTiO_3$ thin films on $DyScO_3$ and $GdScO_3$ substrates, Choi *et al.*[172] have demonstrated an up to 500 °C increase of the ferroelectric transition temperature, and a remanent polarization up to 250 % higher than for bulk $BaTiO_3$ single crystals. A 50 % increase in the polarization compared to bulk $BaTiO_3$ has also been shown in asymmetric superlattices consisting of alternate layers of $BaTiO_3$, $SrTiO_3$ and $CaTiO_3$, even though both $SrTiO_3$ and $CaTiO_3$ are paraelectric.[173]

Compared to nanoparticles and thin films, the ferroelectric size effect in 1D nanostructures has been much less studied. This is largely because of the difficulty of producing ferroelectric 1D nanostructures with controllable dimensions. The

only experimental study is the EFM study of $BaTiO_3$ nanowires by Spanier *et al.*[169] Their measurements show that the ferroelectric phase transition temperature (T_C) is depressed as the nanowire diameter (d_{nw}) decreases, following a $1/d_{nw}$ scaling (figure 9). The diameter at which T_C falls below room temperature was determined to be ~3 nm, and extrapolation of the data indicated that nanowires with d_{nw} as small as 0.8 nm can support ferroelectricity at lower temperatures.[169] However, the observation of the ferroelectric behaviour in these nanowires is not without controversy. One of the possibilities is that the applied field resulted in the depletion of or accumulation of charge underneath the tip without actual ferroelectric switching.[149]

In the lack of experimental evidence, various theoretical calculations on ferroelectric nanodots, nanowires and nanotubes have shed light on the ferroelectricity in these structures. From these studies, ferroelectricity is generally conserved down to nanowire diameters of only a few unit cells.[174-178] A few studies have shown that surface tension can increase the transition temperature and polarization above bulk values in nanorods[178,179] and nanotubes[180] of a certain diameter. In very small nanoparticles of $BaTiO_3$,[181] $PbTiO_3$,[182] and PZT,[183,184] a vortex phase with toroidicity of dipoles has been demonstrated (see for instance the recent review by Prosandeev *et al.*[185]). Simulations show that the toroidicity in nanoparticles transforms to a directed polarization when one of the dimensions of the nanoparticle is increased to change it into a nanowire.[186]

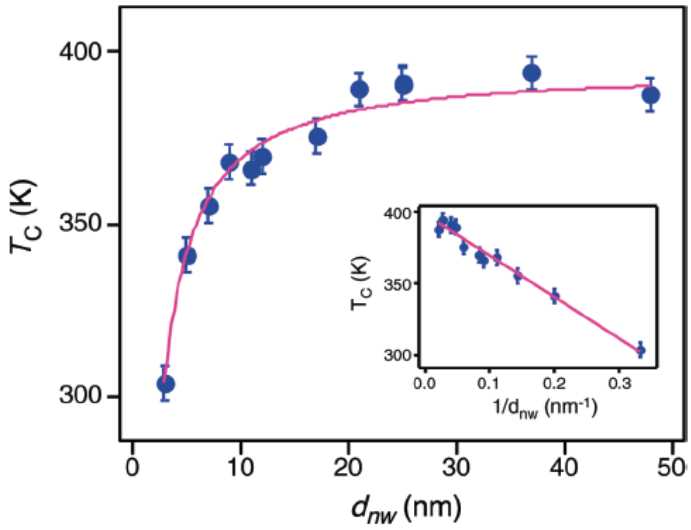

Figure 9. Ferroelectric phase transition temperature (T_C) as a function of $BaTiO_3$ nanowire diameter (d_{nw}). The solid circles are the experimentally determined T_C, and the error bars are uncertainties. The solid line is the result of the fit to the data using the $1/d_{nw}$ scaling relation. The inset plots T_C as a function of $1/d_{nw}$ and illustrates the inverse diameter dependence. The figure is adapted from Spanier *et al.*[169]

3.2.3. Characterization of ferroelectrics at the nanoscale

Until recently, high-resolution studies of ferroelectrics were limited to electron microscopy methods. Scanning probe microscopy (SPM) techniques have emerged as a powerful tool for high-resolution characterization of ferroelectrics, providing an opportunity for non-destructive visualization of ferroelectric domain structures. SPM has made it possible to map the surface potential at the nanoscale, to evaluate local electromechanical properties, and to measure non-linear optical and dielectric constants. Among the SPM techniques for the nanoscale characterization of ferroelectrics, the most popular one is piezoresponse force microscopy (PFM). The high spatial resolution, easy implementation, effective manipulation and control of nanoscale domains, and local spectroscopy capabilities make PFM a well-suited tool for nanoscale ferroelectric studies. PFM is used both for imaging and for non-imaging spectroscopy studies.[149]

In PFM, a conductive AFM probe tip is brought into contact with the sample top surface in contact mode. An ac bias is applied between the probe and the conductive sample back surface, which induces local oscillatory structural deformation due to the converse piezoelectric effect. This deformation is measured through a lock-in amplifier. PFM can be operated in two modes, vertical and lateral (figure 10). In the vertical PFM mode, the induced local vertical deformation is measured through the vertical deflection of the AFM cantilever and the out-of-plane polarization is studied, while in the lateral PFM mode, the local shear deformation of the sample is measured through the torsional twisting of the AFM cantilever and the in-plane polarization is studied. The conventional PFM technique for studying 1D nanostructures is shown in figure 11a, where both the ac bias and the dc bias are applied between the AFM tip and the sample back electrode.[187]

Response mechanisms in PFM are complex and include electrostatic, electromechanical and non-local contributions. Quantitative spectroscopic piezoresponse measurements require that the electrostatic and non-local components of the response should be minimized. Relatively stiff cantilevers with

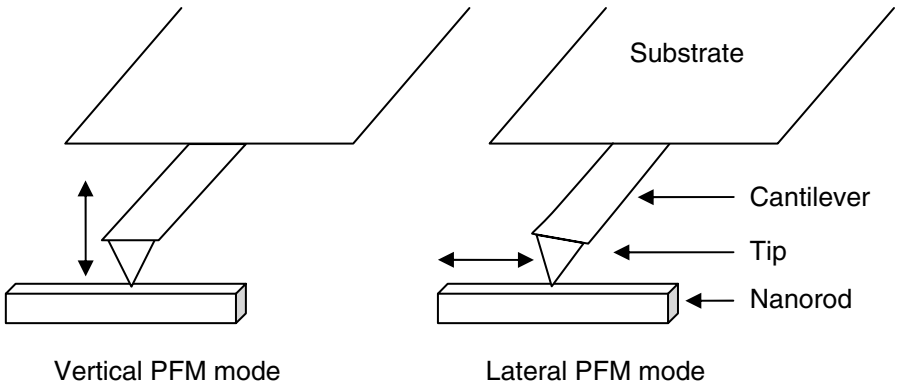

Figure 10. Schematic illustration of the vertical and lateral modes of PFM in the study of a single nanorod, with the three major components of the AFM probe.

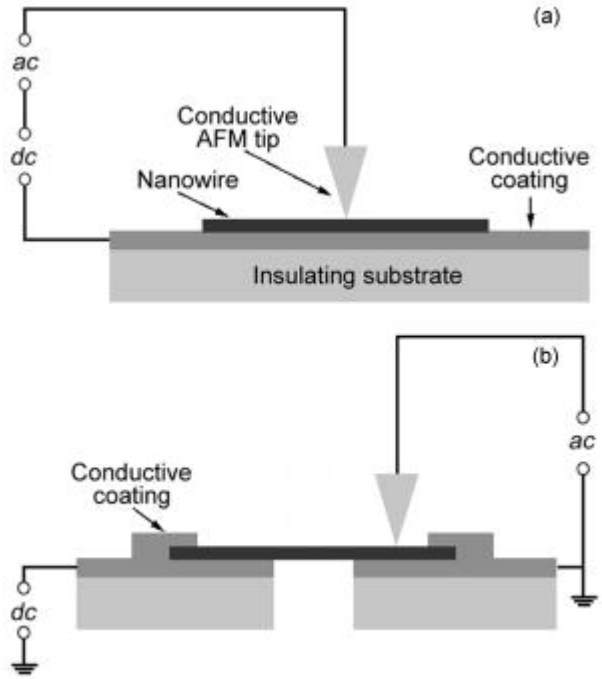

Figure 11. Schematic illustration of (a) the biasing condition in conventional PFM of nanowires, and (b) the axial biasing setup in the study of Wang *et al.*[187] The figure is adapted from Wang *et al.*[187]

spring constants of $k_{eff} > 1$ N/m will reduce these non-local electrostatic interactions.[188] However, Wang *et al.*[189] have claimed that for lateral PFM the effect of electrostatic interaction between the sample and the cantilever is negligible when using a cantilever with spring constant of only 0.15 N/m, as the signal is detected through the twisting of the AFM cantilever.

The use of SPM methods to demonstrate ferroelectric and piezoelectric properties of single 1D nanostructures of ferroelectric perovskites have been reported by several groups. Park and co-workers[35,169,190] and Bao *et al.*[48] have studied the radial ferroelectric response in $BaTiO_3$ nanowires using EFM as described above (figure 9). Conventional PFM studies have been reported on a variety of 1D nanostructures, such as $BaTiO_3$ nanowires,[189] PZT nanowires[78,89,94] and nanotubes,[37,58] $CoFe_2O_4$-PZT nanofibers,[142] $KNbO_3$ and $KNb_{1-x}Ta_xO_3$ nanorods,[116] $NaNbO_3$ nanorods,[113] and $BiFeO_3$ nanotubes,[127] while the present study[191] (Paper V) is the first PFM study of single $PbTiO_3$ nanorods. For instance, by comparing the amplitude and phase loops obtained by lateral and vertical PFM, Wang *et al.*[189] observed that the polarization of $BaTiO_3$ nanowires was oriented in the length direction of the nanowires, as hysteresis loops were obtained by lateral PFM (figure 12).

However, there exist some limitations in the conventional PFM setup for in-plane polarization study. Because of the concern of electric breakdown, and the localized nature of the electric field, whenever a high bias is needed for in-plane polarization switching or a sample segment needs to be uniformly polarized, the

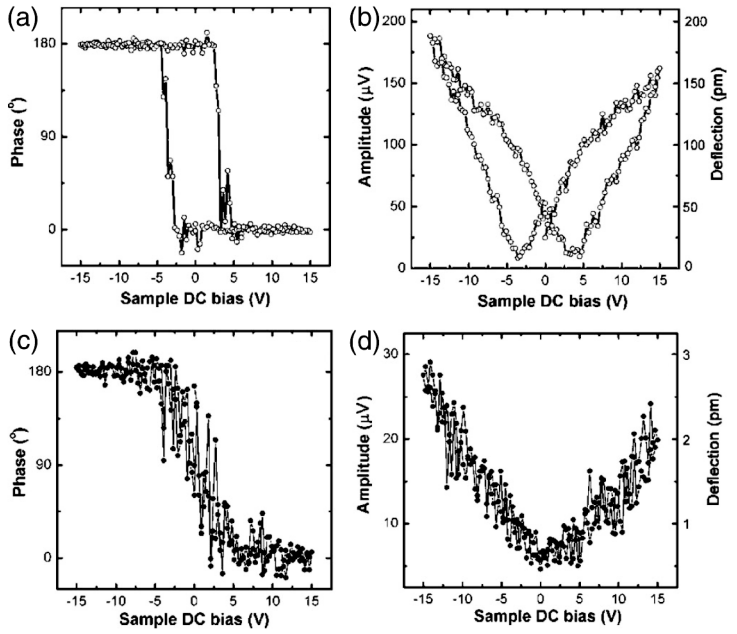

Figure 12. PFM study of a $BaTiO_3$ nanowire lying on a Au/Pd-coated substrate. (a)-(b) Lateral PFM in-field hysteresis phase loop (a) and amplitude loop (b). (c)-(d) Vertical PFM phase loop (c) and amplitude loop (d). All loops were obtained from the same spot on the nanowire. The figure is adapted from Wang *et al.*[189]

conventional lateral PFM setup is incapable. Wang *et al.*[187] have reported a setup where the dc bias is applied along the length direction of a nanowire (figure 11b). The ac bias is still applied through the AFM tip, but the dc bias used to switch the in-plane polarization of the nanowire is applied directly between the two ends of the nanowire. This provides in-plane polarization control while simultaneously allowing the study of ferroelectric hysteresis and shear piezoresponse of a nanowire with PFM. This technique facilitated the study of polarization formation and switching in a $BaTiO_3$ nanowire.[187,192] The polarization switching was shown to be non-remanent, because of an unswitchable shell of ~10 nm thickness, which made the switched core polarizations spontaneously switch back to conform to the surface polarizations.[192]

3.3. Potential use of one-dimensional nanostructures of ferroelectric perovskites

Ferroelectrics find three main technological applications based on three related physical characteristics. First, as a result of their spontaneous electric polarization, they can be used as binary data storage media in which opposite directions of polarization represent the 1 or 0 data bits. Second, because the electric polarization is coupled to the structure of the material, ferroelectrics can convert mechanical energy to electrical energy and vice versa. This leads to their widespread use in transducer applications such as piezoelectric actuators and sonar detectors. Finally,

they have very large dielectric permittivities leading to applications in capacitors.[193] Ferroelectric nanostructures will be important within all these applications. Here, some of the ideas that have been proposed for the use of ferroelectric 1D nanostructures are presented.

The present roadmap for ferroelectric random access memory (FeRAM) development[194] calls for fully 3D devices by 2016. The drive for implementation of more complex 3D structures into FeRAM, instead of the conventional 2D plate capacitor arrangements, is caused by the requirement that FeRAM capacitors must have large enough electrode surfaces to generate sufficient switched charge for the sense amplifiers to reliably discriminate between the "1" and "0" states in the memory.[195] The down-sizing of the current 2D arrangements will result in too small electrode surfaces to accomplish the necessary charge. Schemes for 3D development include both free-standing nanotubes and nanowires,[77,82] and maybe more importantly ferroelectric nanotubes made by coating electronically conducting positive templates (such as carbon nanotubes[98] or Pt-covered Si or ZnO nanowires[58,99]) with a ferroelectric material, as this results in a large electrode surface. Such metal-ferroelectric-metal composite nanotubes are good candidates for 3D capacitors for non-volatile FeRAMs approaching Tb/in^2 storage density.

Nanowires and nanotubes are of course also very important in fundamental experimental studies of nanoscale ferroelectricity, as described in chapter 3.2.2. and 3.2.3. Most other possible applications of 1D nanostructures of ferroelectric perovskites do not make use of the ferroelectricity itself, but of the related properties of piezoelectricity, pyroelectricity and dielectricity. Pyroelectrics are useful in a variety of imaging and detection applications, and pyroelectric 1D nanostructures could be well suited for sensors. Piezoelectrics find a host of uses in electromechanical devices. Piezoelectric nanotubes have for instance been presented as candidates for microfluidic delivery systems, making ultra-small ink-jet printers possible.[77] An interesting energy-harvesting concept using piezoelectric nanowires has been developed by Wang *et al.*[196,197] They have shown that ZnO nanowire arrays can generate electrical energy when the nanowires are deflected, thus enabling a self-powering nanosystem that harvests its operating energy from the mechanical and vibrational energy of the environment. However, this energy-harvesting concept have recently been questioned by Alexe *et al.*,[198] who demonstrated that the measured signals might have different sources than the piezoelectric effect. Nevertheless, considering the relatively low charge constants (piezoelectric constant) of ZnO (~12 pC/N), it would be desirable to use nanowires made of piezoelectric perovskite materials with high charge constants such as $BaTiO_3$ (up to 85 pC/N) and PZT (up to 268 pC/N), instead of ZnO nanowires.[199] Wang *et al.*[199] have demonstrated periodic voltage generation from a single $BaTiO_3$ nanowire by applying a periodically varying tensile mechanical strain using a precision mechanical testing stage. Recently, Zheng *et al.*[178] simulated the behaviour of an uniaxially pulse-loaded $PbTiO_3$ nanowire using a thermodynamic model, and showed that under a suitable load, an appropriately dimensioned ferroelectric nanowire can produce a sizable alternating current voltage, sufficient for applications as a nanopower source for energy harvesting, or as an effective nanomechanical sensor. These demonstrations of the direct piezoelectric effect in a

single nanowire show the possibility of using such piezoelectric perovskite nanowires for energy-harvesting applications.

The optical properties of 1D perovskite nanostructures are useful in applications such as photonic crystals and subwavelength optics. The important fundamental property of photonic crystals lies in the photonic band gaps that emerge in periodic dielectric structures having refractive index contrast. The photonic band gaps result from the diffraction of electromagnetic waves generated in the periodic dielectric structures, creating standing wave conditions. Periodic dielectric structures with a large refractive index contrast produce photonic band gaps at limited frequencies, where light of the same frequencies is forbidden to exist inside the perfect photonic crystals.[200] This enables control of photons in a wide range of possible applications in wave-guiding devices. Photonic crystals of $BaTiO_3$ with regular hexagonal arrays of $BaTiO_3$ nanorods have been made by templating, and have been shown to exhibit photonic band gaps in good agreement with calculations.[39] These photonic crystals require perfect periodicity of the dielectric structures, and the template methods are therefore the most likely candidates for the synthesis of such structures.

Another novel optical application has been described by Nakayama *et al.*[119] They used an optically trapped single $KNbO_3$ nanowire as a tuneable nonlinear optical probe in a scanning light microscopy setup. The $KNbO_3$ nanowire exhibit efficient second harmonic generation, doubling the frequency of the trapping light and then waveguiding this locally generated light to its ends. The large second-order susceptibility $\chi^{(2)}$ of $KNbO_3$ nanowires facilitates the generation of tuneable, coherent visible radiation that is sufficient for *in situ* scanning and fluorescence microscopy.

Because of the high surface/volume ratio of 1D nanostructures, they should also be attractive for catalytic devices. Miyauchi[102] has for instance shown the strong photocatalytic oxidative activity of $SrTiO_3$ nanorod films. Other applications include templates for textured ceramics[201] and composites. As is evident from this overview, application studies and practical use of 1D perovskite nanostructures lie far behind the synthesis studies of these structures; however, the coming years will certainly see a flourish also on the application side.

4. Conclusions and outlook

In this work we have investigated several synthesis methods to produce nanorods, nanotubes, and nanostructures of ferroelectric perovskites. The use of different methods has given insight into many techniques, and has shown the advantages and disadvantages of various methods. Generally, the synthesis of 1D nanostructures of ternary oxides by chemical methods is challenging, but compared to physical methods, chemical methods are cost-effective and offer the possibility of high-volume production of a variety of materials if a suitable method is used.

The molten salt method described in Paper I was shown to produce isometric nano-crystalline $BaTiO_3$ and $PbTiO_3$ particles as the main products, but nanorods were also detected. It was demonstrated that the stochiometry of the nanorods was difficult to control due to formation and volatility of $BaCl_2$ and $PbCl_2$, which resulted in formation of nanorods of titanium oxide-rich compounds rather than the desired perovskites $BaTiO_3$ and $PbTiO_3$. By a salt-assisted method conducted below the melting point of the salt, volatile NaCl was shown to be vital for the growth of nanorods. The experimental results suggest that the molten salt synthesis is best suited for the synthesis of nanorods of compounds with highly anisometric crystal structures, because the difference in surface energy of different crystal faces can enhance the anisometric growth. After Paper I was published, Yu *et al.*[148] have reported the synthesis of $BaTi_2O_5$ nanobelts by reacting $BaTiO_3$ powder in a NaCl/KCl mixture at 950 °C for 5 h, supporting our results. In addition, Xu[202] has made $BaTi_5O_{11}$ microrods by reacting TiO_2 with $BaCl_2$ at 800 °C.

In order to prepare nanorods of compounds with cubic or pseudo-cubic crystal structure by molten salt synthesis, a more promising method is probably to use a rod-shaped precursor which has a low solubility in the salt for a topotactic reaction or transformation into the desired material, keeping the shape of the precursor. For the $BaTiO_3$ and $PbTiO_3$ systems, a rod-shaped titanium-containing precursor can be used, as TiO_2 has very low solubility in alkali chlorides.[203] Then the more soluble precursor, such as BaO or PbO,[204,205] can dissolve into the salt and diffuse onto the surface of the less soluble precursor and react there to form the product phase. This principle has been demonstrated by Hayashi *et al.*[27] using rod-shaped $TiO_2{\cdot}nH_2O$ to produce submicron $BaTiO_3$ rods, by Cai *et al.*[64] using rod-shaped TiO_2 to produce microrods of $PbTiO_3$, and by Xu *et al.*[114] to produce $NaNbO_3$ nanorods from $K_2Nb_8O_{12}$ nanowires. This method is therefore a more general approach, which can be used to make nanorods of other ternary oxides, if the appropriate rod-shaped precursor with low solubility in the salt is used, combined with a precursor with a higher solubility. In hydrothermal syntheses of 1D nanostructures of ferroelectric perovskites, the use of an anisometric precursor have been employed by many researchers (see table 1 in chapter 3.1.4.).

In Paper II and III we describe a surfactant-assisted hydrothermal synthesis method to produce arrays and hierarchical structures of nanorod and platelets of $PbTiO_3$. An amorphous $PbTiO_3$ precursor was hydrothermally treated at 180 °C in the presence of $SrTiO_3$ or $PbTiO_3$ substrates. The main advantages of this method are the absence of a template-removing step in the synthesis and the production of single-crystalline nanorods. The nanorods had a square cross-section of 35 - 400 nm and were up to 5 μm long. Homogeneous growth across the substrate

and increased control of the morphology were enabled by changing the orientation of the exposed side of the substrates from being faced upwards (Paper II) to facing downwards (Paper III), because sedimentation of particles was hindered. In Paper III, it was shown that, initially, platelets grew oriented in the crystallographic <100> orientations of the underlying $SrTiO_3$ substrate. Nanorods with a square-shaped cross-section then grew from the platelet surfaces. The morphology of the $PbTiO_3$ micro/nanostructures was varied by controlling the height of the substrate in the autoclave, the synthesis time, and the crystallographic orientation of the $SrTiO_3$ substrates. $PbTiO_3$ nanorods oriented perpendicular to the substrate surface could also be grown directly on the substrate by a modified synthesis method.

A growth model, based on initial growth of platelets and/or an epitaxial layer by ions, followed by self-assembly of cube-shaped or facetted nanocrystals into nanorods, was proposed for the hydrothermal growth. The basis of this growth model is a dissolution-reprecipitation mechanism: dissolution of the amorphous precursor into ions, followed by nucleation of crystalline nanoparticles which grow into cube-shaped or facetted nanocrystals. We can not exclude the possibility that also the nanorods grew by a classic nucleation and growth mechanism based on Ostwald ripening, aided by surfactant adsorption; however, the transition of growth from platelets to nanorods indicates two different growth mechanisms for the platelets and the nanorods. A two-stage growth mechanism was also observed in the growth of burr-like nanostructures described in Appendices I and II. To gain further insight into the growth mechanism of the platelets and the nanorods, detailed transmission electron microscopy (TEM) should be performed. For instance, cross-sections of nanorods cut along the length direction would be interesting to study, to investigate if grooves or irregularities in the structure could be found also in the radial direction of the nanorods, similar to the ones found in the longitudinal direction (Appendices I - III).

An optimized synthesis procedure may give even more interesting structures, such as $PbTiO_3$ nanorods growing directly on conducting substrates in large areas, not just in small areas as demonstrated in Paper III. The principle of $PbTiO_3$ nanorods grown directly on substrates is interesting for applications such as energy-harvesting devices[199] or ferroelectric random access memory.[195] For the optimization, several synthesis parameters can be varied. For instance, stirring of the dispersion, intermediate washing of the dispersion to remove organics, varying the concentration of KOH, precursor, or surfactant, or changing the OH^--source, are all variations that will influence the growth and final morphology of the products.[69,206,207]

An interesting question is if this hydrothermal method can be used for the growth of nanorods and hierarchical nanostructures of other materials? A preliminary experiment with barium acetate instead of lead acetate as precursor in order to make $BaTiO_3$ did however not produce nanorods of $BaTiO_3$. If the ferroelectric polarization of the nanocrystals is important for the self-assembly into nanorods, nanorod growth will be prevented at temperatures above the tetragonal to cubic phase transition. For $BaTiO_3$, with T_C = 120 °C,[157] a synthesis temperature of 180 °C may thus inhibit nanorod growth. In addition, the precursor chemistry is different, and other complexing agents or surfactants may be necessary. A systematic study to grow PZT, $BaTiO_3$ and $SrTiO_3$ by the present hydrothermal

method would be interesting for the further understanding of the growth mechanism. Other materials such as $KNbO_3$ may be too different for the exact same growth mechanism to take place; however, oriented attachment of nanocrystals into $KNb_{0.75}Ta_{0.25}O_3$ tower-like nanostructures was recently reported by Hu *et al.*[124], using Nb_2O_5 and Ta_2O_5 as precursors in a KOH solution with polyethylene glycol as surfactant. In our laboratory, $KNbO_3$ nanorods have been made by a hydrothermal method, using Nb_2O_5 as precursor in a KOH solution with sodium dodecylsulfonate as surfactant.[121,122] Both the $KNb_{0.75}Ta_{0.25}O_3$ tower-like nanostructures and the $KNbO_3$ nanorods grow in the [001] direction,[121,122,124] while the polar direction of these materials (with an orthorhombic crystal structure) is the [011] direction,[157] so the ferroelectric polarization is probably not important for the anisometric growth of these materials. For the epitaxial growth of nanostructures on substrates, the crystal lattice match or mismatch between the material and the substrate is of course vital, so an other substrate than $SrTiO_3$ may have to be used if other materials are synthesized.

In Paper IV, a template-assisted method to produce $PbTiO_3$ nanotubes is described. A Pb-Ti sol was dropped onto porous alumina membranes and penetrated into the channels of the template. Direct heating at 700 °C for 6 h was shown to be sufficient to obtain single-phase perovskite nanotubes from an equimolar precursor solution, avoiding the addition of excess lead or annealing in a Pb-rich atmosphere. The nanotubes had diameters of 200 - 400 nm. Variation of the sol concentration did not significantly affect the wall thickness of the nanotubes. Large internal pores in the membranes with nominal pore diameters of 20 nm and 100 nm prevented the formation of nanotubes with smaller diameters.

The template-assisted method is an easy route to obtain polycrystalline nanotubes of complex materials, and it has therefore been studied by many researchers. However, the control of wall thickness is rarely reported and should be an interesting issue for future studies. The template-assisted method is best suited for production of nanotubes, but nanowires or nanorods can also be obtained if a particle-directing method such as electrophoresis is used.

In addition to the syntheses reported in the thesis, a few other synthesis methods have also been investigated. Our preliminary efforts to synthesize $BaTiO_3$ nanowires by the inverse micelle method reported by Urban *et al.*[22] gave very low yields of nanowires.[144,145] We have also tried to reproduce the hydrothermal synthesis of $BaTiO_3$ nanowires reported by Joshi *et al.*,[42,43] but only produced $BaCO_3$ nanowires.[208] Finally, we tried to reproduce a composite-hydroxide-mediated approach[209,210] for the synthesis of $BaMnO_3$ and $BaCeO_3$ nanorods, but only produced $BaCO_3$ and/or $K_{0.5}Mn_2O_4$ nanorods and $BaCO_3$ and/or CeO_2 nanorods, respectively.[211] A closer inspection of the X-ray diffractogram of the $BaCeO_3$ product in Liu *et al.*[210] also revealed that their synthesis product was CeO_2, not $BaCeO_3$ as reported. In general, in any low-temperature synthesis of Ba-containing perovskites, the high stability of $BaCO_3$ is a challenge for the production of single-phase perovskite.

These attempts to reproduce other syntheses (including Paper I), show that the synthesis procedures are delicate, and small variations in the procedure may yield a different product. Often, the necessary synthesis parameters to precisely reproduce the experimental procedure are not described in detail. In general, most of the non-

template methods have been used by only one research group. It must also be mentioned that some of the literature are of questionable quality, especially regarding the determination of the phase composition of the 1D nanostructures by selected area electron diffraction and X-ray diffraction. During the initial phase of our molten salt synthesis study, we were fooled by the results of the X-ray diffraction. The psychological fact that one wants to succeed with the project and to obtain the desired phase, can result in being less critical than one should be. So to conclude, although many reports of synthesis of 1D nanostructures of ferroelectric perovskites have been published the recent years, the research field is still in its childhood.

For the future work on the synthesis of 1D nanostructures of ferroelectric perovskites, the experience gained by the author over these years justify some thoughts about the future direction and possibilities of the field. The simplest method to obtain 1D nanostructures of ternary oxides is the template-assisted method using a template with channels, such as porous alumina. For the fabrication of polycrystalline nanotubes this method should be the preferred one for most materials. An advantage is also that arrays of nanotubes can be obtained. For the production of nanowires or nanofibers instead of nanotubes, electrospinning is probably the most versatile method. However, polycrystalline 1D nanostructures are produced also with electrospinning. To produce single-crystalline 1D nanostructures, synthesis by thermolysis, molten salt method or hydrothermal method should be used. A 1D-shaped precursor can be used to direct the morphology; however, the obtained 1D nanostructures are typically polycrystalline if a polycrystalline precursor is used, such as nanotube arrays. But if a single-crystalline 1D-shaped precursor is used, single-crystalline perovskite nanorods and nanowires can be (and have been) obtained. Taken all the synthesis methods into account, the most interesting synthesis method appears to be the hydrothermal method. This method typically yields single-crystalline materials and can be used to obtain hierarchical structures and arrays of nanorods on substrates. However, in order to obtain advanced single-crystalline nanostructures on substrates, 1D-shaped precursors cannot be used, if not already patterned into the desired nanostructures. The chemistry involved to obtain anisometric growth can therefore be quite complex, but in order to develop and control the synthesis routes it is therefore important to understand the growth mechanism(s). We hope that in the coming years it will be an increased focus on the structured growth of 1D nanostructures into more complex structures, and that the growth mechanism of such structures will be thoroughly addressed.

In addition to investigating synthesis methods, the ferroelectric and piezoelectric properties of single $PbTiO_3$ nanorods were studied by piezoresponse force microscopy (PFM) (Paper V). Piezoelectric activity was observed perpendicular to the length direction of the nanorods that had been annealed at 600 °C, and it was shown that the polarization could be switched. The ferroelectric nature of the nanorods was thus demonstrated. The nanorods decomposed after repeated cycling of the dc bias at one spot on the nanorod, which resulted in disintegration of parts of the nanorod and/or accumulation of particles at the top of the nanorod.

We were interested in using an axial dc bias setup to uniformly polarize the nanorods, obtaining a much better control of the polarization in the nanorod. The disintegration of the nanorod that was observed when using the conventional PFM setup could be a result of the localized electric field, so an axial dc bias setup would then reduce or eliminate any disintegration. However, because of experimental challenges and insufficient time, a sample device was not completed within the time limit for this thesis, so the PFM studies using an axial bias setup will be a topic for future work. In Appendix IV, the efforts to fabricate a sample device and the ideas for the setup that were developed are described. For the axial dc bias setup, it was necessary to contact the ends of single nanorods onto gold electrodes. As no suitable method to make such contacts, such as focused ion beam microscopy, existed at NTNU at the time, we built an apparatus ourselves. It was chosen to use electron beam induced deposition (EBID) of a platinum-carbon composite from an organometallic platinum precursor. A home-made EBID apparatus was constructed for the deposition and is described in detail in Paper VI. The height and the position of the deposits could be controlled and the ends of single nanorods were successfully contacted. Geometry-based calculations that were helpful to design the EBID apparatus and to estimate the deposition time and the deposit height are described.

In order to understand the ferroelectric and piezoelectric properties of the $PbTiO_3$ nanorods, it will be important to study the domain structure of the nanorods and how or if the domain structure change with annealing temperature. Although challenging, various TEM techniques in combination with PFM could reveal much that is hitherto unknown and unstudied.

Several steps are still to be climbed before the 1D nanostructures reported in this thesis can be applied in future electronic and electromechanical devices. First, one must be able to control the morphology of the structures over large areas with reproducible synthesis conditions. Second, a detailed characterization of the properties and the long-term stability of these nanostructures must be carried out. Third, the use of the structures in applications must be tested.

Other challenges also remain for the $PbTiO_3$ nanostructures reported here. Concerns regarding the toxicity of Pb have made governments planning a reduction in the use of Pb in electronic equipment and other applications. While the problem in electronics mainly is the Pb solder, in the recent years it has also been a move to replace the Pb-based piezoceramics with Pb-free piezoceramics, such as $KNbO_3$ and related materials ($K_xNa_{1-x}Nb_yTa_{1-y}O_3$).[212] However, the useful properties of the Pb-based piezoceramics that have made these materials widely used in various technological applications for decades will probably make the materials also important in the future, but in lower quantities than they are used today, and for use in special applications. Another aspect is the possible toxicological properties of nanoparticles, Pb-based or not, which has not been studied much yet, but which will be necessary to address before any large-scale implementation of nanoparticles into everyday applications.

5. References

1. G. Binnig and H. Rohrer, “Scanning Tunneling Microscopy”, *Helv. Phys. Acta*, 1982, 55, 726-735.
2. H. W. Kroto, J. R. Heath, S. C. O'Brien, R. F. Curl, and R. E. Smalley, “C_{60}: Buckminsterfullerene”, *Nature*, 1985, 318, 162–163.
3. S. Iijima, “Helical microtubules of graphitic carbon”, *Nature*, 1991, 354, 56-58.
4. Y. Xia, P. Yang, Y. Sun, Y. Wu, B. Mayers, B. Gates, Y. Yin, F. Kim, and H. Yan, “One-Dimensional Nanostructures: Synthesis, Characterization, and Applications”, *Adv. Mater.*, 2003, 15, 353-389.
5. Y. Min, M. Akbulut, K. Kristiansen, Y. Golan, and J. Israelachvili, “The role of interparticle and external forces in nanoparticle assembly”, *Nat. Mater.*, 2008, 7, 527-538.
6. J. Hu, T. W. Odom, and C. M. Lieber, “Chemistry and Physics in One Dimension: Synthesis and Properties of Nanowires and Nanotubes”, *Acc. Chem. Res.*, 1999, 32, 435-445.
7. C. N. R. Rao, F. L. Deepak, G. Gundiah, and A. Govindaraj, “Inorganic Nanowires”, *Prog. Solid State Chem.*, 2003, 31, 5-147.
8. M. Law, J. Goldberger, and P. Yang, “Semiconductor nanowires and nanotubes”, *Annu. Rev. Mater. Res.*, 2004, 34, 83-122.
9. C. M. Lieber and Z. L. Wang, “Functional Nanowires”, *MRS Bulletin*, 2007, 32, 99-104.
10. Z. L. Wang, “Oxide Nanobelts and Nanowires – Growth, Properties and Applications”, *J. Nanosci. Nanotechnol.*, 2008, 8, 27-55.
11. C. Bae, H. Yoo, S. Kim, K. Lee, J. Kim, M. M. Sung, and H. Shin, “Template-Directed Synthesis of Oxide Nanotubes: Fabrication, Characterization, and Applications”, *Chem. Mater.*, 2008, 20, 756-767.
12. G. Cao and D. Liu, “Template-based synthesis of nanorod, nanowire, and nanotube arrays”, *Adv. Colloid Interfac.*, 2008, 136, 45-64.
13. Y. Mao, T.-J. Park, and S. S. Wong, “Synthesis of classes of ternary metal oxide nanostructures”, *Chem. Commun.*, 2005, 5721-5735.
14. C. J. Murphy and N. R. Jana, “Controlling the Aspect Ratio of Inorganic Nanorods and Nanowires”, *Adv. Mater.*, 2002, 14, 80-82.
15. H. Cölfen and M. Antonietti, “Mesocrystals: Inorganic Superstructures Made by Highly Parallel Crystallization and Controlled Alignment”, *Angew. Chem. Int. Ed.*, 2005, 44, 5576-5591.
16. F. Wang, A. Dong, J. Sun, R. Tang, H. Yu, and W. E. Buhro, “Solution-Liquid-Solid Growth of Semiconductor Nanowires”, *Inorg. Chem.*, 2006, 45, 7511-7521.
17. G. Cao, “Growth of Oxide Nanorod Arrays through Sol Electrophoretic Deposition”, *J. Phys. Chem. B*, 2004, 108, 19921-19931.
18. P. M. Rørvik, K. Tadanaga, M. Tatsumisago, T. Grande, and M.-A. Einarsrud, “Template-assisted synthesis of $PbTiO_3$ nanotubes”, to be submitted. (Paper IV)
19. D. Li and Y. Xia, “Electrospinning of Nanofibres: Reinventing the Wheel?”, *Adv. Mater.*, 2004, 16, 1151-1170.

20. K. H. Yoon, Y. S. Cho, and D. H. Kang, "Molten salt synthesis of lead-based relaxors", *J. Mater. Sci.*, 1998, 33, 2977-2984.
21. Y.-W. Jun, J.-S. Choi, and J. Cheon, "Shape Control of Semiconductor and Metal Oxide Nanocrystals through Nonhydrolytic Colloidal Routes", *Angew. Chem. Int. Ed.*, 2006, 45, 3414-3439.
22. J. J. Urban, W. S. Yun, Q. Gu, and H. Park, "Synthesis of Single-Crystalline Perovskite Nanorods Composed of Barium Titanate and Strontium Titanate", *J. Am. Chem. Soc.*, 2002, 124, 1186-1187.
23. Y.-W. Jun, J.-H. Lee, J.-S. Choi, and J. Cheon, "Symmetry-Controlled Colloidal Nanocrystals: Nonhydrolytic Chemical Synthesis and Shape Determining Parameters", *J. Phys. Chem. B.*, 2005, 109, 14795-14806.
24. M. Niederberger and H. Cölfen, "Oriented attachment and mesocrystals: Non-classical crystallization mechanisms based on nanoparticle assembly", *Phys. Chem. Chem. Phys.*, 2006, 8, 3271-3287.
25. R. L. Penn, "Kinetics of Oriented Aggregation", *J. Phys. Chem. B*, 2004, 108, 12707-12712.
26. Y. Ohara, K. Koumoto, and H. Yanagida, "Barium Titanate Ceramics with High Piezoelectricity Fabricated from Fibrous Particles", *J. Am. Ceram. Soc.*, 1985, 68, C-108-C-109.
27. Y. Hayashi, T. Kimura, and T. Yamaguchi, "Preparation of rod-shaped $BaTiO_3$ powder", *J. Mater. Sci.*, 1986, 21, 757-762.
28. T. Kimura, A. Takenaka, T. Mifune, Y. Hayashi, and T. Yamaguchi, "Preparation of needle-like $TiZrO_4$ and PZT powders", *J. Mater. Sci.*, 1992, 27, 1479-1483.
29. Y. Ohara, K. Koumoto, T. Shimizu, and H. Yanagida, "Hydrothermal synthesis of fibrous lead titanate powders", *J. Mater. Sci.*, 1995, 30, 263-266.
30. B. Brahmaroutu, G. L. Messing, and S. Trolier-McKinstry, "Molten Salt Synthesis of Anisotropic $Sr_2Nb_2O_7$ Particles", *J. Am. Ceram. Soc.*, 1999, 82, 1565-1568.
31. H. Cheng, J. Ma, Z. Zhao, D. Qiang, Y. Li, and X. Yao, "Hydrothermal Synthesis of Acicular Lead Titanate Fine Powders", *J. Am. Ceram. Soc.*, 1992, 75, 1123-1128.
32. S.-B. Cho, M. Oledzka, and R. E. Riman, "Hydrothermal synthesis of acicular lead zirconate titanate (PZT)", *J. Cryst. Growth*, 2001, 226, 313-326.
33. S. J. Limmer, S. Seraji, M. J. Forbess, Y. Wu, T. P. Chou, C. Nguyen, and G. Cao, "Electrophoretic Growth of Lead Zirconate Titanate Nanorods", *Adv. Mater.*, 2001, 13, 1269-1272.
34. B. A. Hernandez, K.-S. Chang, E. R. Fischer, and P. K. Dorhout, "Sol-Gel Template Synthesis and Characterization of $BaTiO_3$ and $PbTiO_3$ Nanotubes", *Chem. Mater.*, 2002, 14, 480-482.
35. J.-F. Liu, X.-L. Li, and Y.-D. Li, "Novel Synthesis of Polymorphous Nanocrystalline $KNbO_3$ by a Low Temperature Solution Method", *J. Nanosci. Nanotechnol.*, 2002, 2, 617-619.
36. J. J. Urban, J. E. Spanier, L. Ouyang, W. S. Yun, and H. Park, "Single-Crystalline Barium Titanate Nanowires", *Adv. Mater.*, 2003, 15, 423-426.

37. Y. Luo, I. Szafraniak, N. D. Zakharov, V. Nagarajan, M. Steinhart, R. B. Wehrspohn, J. H. Wendorff, R. Ramesh, and M. Alexe, “Nanoshell tubes of ferroelectric lead zirconate titanate and barium titanate”, *Appl. Phys. Lett.*, 2003, 83, 440-442.
38. S. J. Limmer, S. Seraji, Y. Wu, T. P. Chou, C. Nguyen, and G. Cao, “Template-Based Growth of Various Oxide Nanorods by Sol-Gel Electrophoresis”, *Adv. Funct. Mater.*, 2002, 12, 59-64.
39. S. Hirano, S. Shimada, and M. Kuwabara, “Fabrication and optical reflection behavior of a two-dimensional barium titanate ceramic photonic crystal”, *Appl. Phys. A*, 2005, 80, 783-786.
40. T. Hosukura, Y. Sakabe, and M. Kuwabara, “Preparation of Barium Titanate with Patterned Microstructure by a Novel Electrophoretic Deposition Method”, *J. Sol-Gel Sci. Techn.*, 2005, 33, 221-228.
41. Y. Mao, S. Banerjee, and S. S. Wong, “Large-Scale Synthesis of Single-Crystalline Perovskite Nanostructures”, *J. Am. Chem. Soc.*, 2003, 125, 15718-15719.
42. U. A. Joshi and J. S. Lee, “Template-Free Hydrothermal Synthesis of Single-Crystalline Barium Titanate and Strontium Titanate Nanowires”, *Small*, 2005, 1 , 1172-1176.
43. U. A. Joshi, S. Yoon, S. Baik, and J. S. Lee, “Surfactant-Free Hydrothermal Synthesis of Highly Tetragonal Barium Titanate Nanowires: A Structural Investigation”, *J. Phys. Chem. B*, 2006, 110, 12249-12256.
44. Y. Mao, S. Banerjee, and S. S. Wong, “Hydrothermal synthesis of perovskite nanotubes”, *Chem. Commun.*, 2003, 408-409.
45. N. P. Padture and X. Wei, “Hydrothermal Synthesis of Thin Films of Barium Titanate Ceramic Nano-Tubes at 200 ºC”, *J. Am. Ceram. Soc.*, 2003, 86, 2215-2217.
46. J. Zhao, X. Wang, R. Chen, and L. Li, “Synthesis of thin films of barium titanate and barium strontium titanate nanotubes on titanium substrates”, *Mater. Lett.*, 2005, 59, 2329-2332.
47. X. Wang, L. Chen, J. Zhao, L. Jin, and L. Li, “Hydrothermal Synthesis of Thin Films of Barium Titanate Nanotube Arrays”, *Integr. Ferroelectr.*, 2008, 99, 125-131.
48. N. Bao, L. Shen, G. Srinivasan, K. Yanagisawa, and A. Gupta, “Shape-Controlled Monocrystalline Ferroelectric Barium Titanate Nanostructures: From Nanotubes and Nanowires to Ordered Nanostructures”, *J. Phys. Chem. C*, 2008, 112, 8634-8642.
49. F. Maxim, P. Ferreira, P. M. Vilarinho, and I. Reaney, “Hydrothermal Synthesis and Crystal Growth Studies of $BaTiO_3$ Using Ti Nanotube Precursors”, *Cryst. Growth Des.*, 2008, 8, 3309-3315.
50. S.-O. Kang, H.-S. Jang, K.-B. Kim, B. H. Park, M.-J. Jung, and Y.-I. Kim, “Synthesis of single-crystal barium titanate nanorods transformed from potassium titanate nanostructures“, *Mater. Res. Bull.*, 2008, 43, 996-1003.
51. S.-O. Kang, B. H. Park, and Y.-I. Kim, “Growth Mechanism of Shape-Controlled Barium Titanate Nanostructures through Soft Chemical Reaction”, *Cryst. Growth Des.*, 2008, 8, 3180-3186.

52. S. Zhang, F. Jiang, G. Qu, and C. Lin, “Synthesis of single-crystalline perovskite barium titanate nanorods by a combined route based on sol-gel and surfactant-templated methods”, *Mater. Lett.*, 2008, 62, 2225-2228.
53. J. Yuh, J. C. Nino, and W. M. Sigmund, “Synthesis of barium titanate ($BaTiO_3$) nanofibers via electrospinning”, *Mater. Lett.*, 2005, 59, 3645-3647.
54. J. Yuh, L. Perez, W. M. Sigmund, and J. C. Nino, “Electrospinning of complex oxide nanofibers”, *Physica E*, 2007, 37, 254-259
55. J. Yuh, L. Perez, W. M. Sigmund, and J. C. Nino, ”Sol-gel based synthesis of complex oxide nanofibers”, *J. Sol-Gel Sci. Techn.*, 2007, 42, 323-329.
56. J. T. McCann, J. I. L. Chen, D. Li, Z.-G. Ye, and Y. Xia, “Electrospinning of polycrystalline barium titanate nanofibers with controllable morphology and alignment”, *Chem. Phys. Lett.*, 2006, 424, 162-166.
57. C. Jiang, K. Kiyofumi, Y. Wang, and K. Koumoto, “Synthesis of $BaTiO_3$ Nanowires at Low Temperature”, *Cryst. Growth Des.*, 2007, 7, 2713-2715.
58. M. Alexe, D. Hesse, V. Schmidt, S. Senz, H. J. Fan, M. Zacharias, and U. Gösele, “Ferroelectric nanotubes fabricated using nanowires as positive templates”, *Appl. Phys. Lett.*, 2006, 89, 172907.
59. B. A. Hernandez-Sanchez, K.-S. Chang, M. T. Scancella, J. L. Burris, S. Kohli, E. R. Fischer, and P. K. Dorhout, “Examination of Size-Induced Ferroelectric Phase Transitions in Template Synthesized $PbTiO_3$ Nanotubes and Nanofibers”, *Chem. Mater.*, 2005, 17, 5909-5919.
60. L. Zhao, M. Steinhart, J. Yu, and U. Gösele, “Lead titanate nano- and microtubes”, *J. Mater. Res.*, 2006, 21, 685-690.
61. L. Liu, T. Ning, Y. Ren, Z. Sun, F. Wang, W. Zhou, S. Xie, L. Song, S. Luo, D. Liu, J. Shen, W. Ma, and Y. Zhou, “Synthesis, characterization, photoluminescence and ferroelectric properties of $PbTiO_3$ nanotube arrays”, *Mat. Sci. Eng. B*, 2008, 149, 41-46.
62. M. C. Hsu, I. C. Leu, Y. M. Sun, and M. H. Hon, “Template synthesis and characterization of $PbTiO_3$ nanowire arrays from aqueous solution”, *J. Solid State Chem.*, 2006, 179, 1421-1425.
63. Y. Deng, J. L. Wang, K. R. Zhu, M. S. Zhang, J. M. Hong, Q. R. Gu, and Z. Yin, “Synthesis and characterization of single-crystal $PbTiO_3$ nanorods”, *Mater. Lett.*, 2005, 59, 3272-3275.
64. Z. Cai, X. Xing, R. Yu, X. Sun, and G. Liu, “Morphology-Controlled Synthesis of Lead Titanate Powders”, *Inorg. Chem.*, 2007, 46, 7423-7427.
65. Y. Hu, H. Gu, X. Sun, J. You, and J. Wang, “Photoluminescence and Raman scattering studies on $PbTiO_3$ nanowires fabricated by hydrothermal method at low temperature”, *Appl. Phys. Lett.*, 2006, 88, 193120.
66. H. Gu, Y. Hu, J. You, Z. Hu, Y. Yuan, and T. Zhang, “Characterization of single-crystalline $PbTiO_3$ nanowire growth via surfactant-free hydrothermal method”, *J. Appl. Phys.*, 2007, 101, 024319.
67. H. Gu, Y. Hu, H. Wang, X. Yang, Z. Hu, Y. Yuan, and J. You, “Fabrication of lead titanate single crystalline nanowires by hydrothermal method and their characterization”, *J. Sol-Gel Sci. Techn.*, 2007, 42, 293-297.

68. G. Wang, R. Sæterli, P. M. Rørvik, A. van Helvoort, R. Holmestad, T. Grande, and M.-A. Einarsrud, "Hierarchical Nanostructures of $PbTiO_3$ Through Mesocrystal Formation", *J. Nanosci. Nanotechnol.*, 2007, 7, 2538-2541. (Appendix I)
69. G. Wang, R. Sæterli, P. M. Rørvik, A. T. J. van Helvoort, R. Holmestad, T. Grande, and M.-A. Einarsrud, "Self-Assembled Growth of $PbTiO_3$ Nanoparticles into Microspheres and Bur-like Structures", *Chem. Mater.*, 2007, 19, 2213-2221. (Appendix II)
70. P. M. Rørvik, Å. Almli, A. T. J. van Helvoort, R. Holmestad, T. Tybell, T. Grande, and M.-A. Einarsrud, "$PbTiO_3$ nanorod arrays grown by self-assembly of nanocrystals", *Nanotechnology*, 2008, 19, 225605. (Paper II)
71. P. M. Rørvik, T. Grande, and M.-A. Einarsrud, "Controlling the morphology of hierarchical $PbTiO_3$ nanostructures on $SrTiO_3$ substrates", to be submitted. (Paper III)
72. X. Zhu, J. Wang, Z. Zhang, J. Zhu, S. Zhou, Z. Liu, and N. Ming, "Perovskite Nanoparticles and Nanowires: Microwave-Hydrothermal Synthesis and Structural Characterization by High-Resolution Transmission Electron Microscopy", *J. Am. Ceram. Soc.*, 2008, 2683-2689.
73. Y. Yang, X. Wang, C. Zhong, C. Sun, and L. Li, "Ferroelectric $PbTiO_3$ nanotube arrays synthesized by hydrothermal method", *Appl. Phys. Lett.*, 2008, 92, 122907.
74. Y. Yang, X. Wang, C. Zhong, C. Sun, G. Yao, and L. Li, "Synthesis and Growth Mechanism of Lead Titanate Nanotube Arrays by Hydrothermal Method", *J. Am. Ceram. Soc.*, 2008, 91, 3388-3390.
75. R. H. Kim, W. S. Ahn, S. H. Han, and S. K. Choi, "Two-dimensional self-patterning of $PbTiO_3$ on a Nb-$SrTiO_3$ (001) surface using atomic force microscope lithography and hydrothermal epitaxy", *Appl. Phys. Lett.*, 2007, 90, 172907.
76. X. Lu, D. Zhang, Q. Zhao, C. Wang, W. Zhang, and Y. Wei, "Large-Scale Synthesis of Necklace-Like Single-Crystalline $PbTiO_3$ Nanowires", *Macromol. Rapid Commun.*, 2006, 27, 76-80.
77. F. D. Morrison, Y. Luo, I. Szafraniak, V. Nagarajan, R. B. Wehrspohn, M. Steinhart, J. H. Wendorff, N. D. Zakharov, E. D. Mishina, K. A. Vorotilov, A. S. Sigov, S. Nakabayashi, M. Alexe, R. Ramesh, and J. F. Scott, "Ferroelectric nanotubes", *Rev. Adv. Mater. Sci.*, 2003, 4, 114-122.
78. X. Y. Zhang, X. Zhao, C. W. Lai, J. Wang, X. G. Tang, and J. Y. Dai, "Synthesis and piezoresponse of highly ordered $Pb(Zr_{0.53}Ti_{0.47})O_3$ nanowire arrays", *Appl. Phys. Lett.*, 2004, 85, 4190-4192.
79. O. M. Zhigalina, E. D. Mishina, N. E. Sherstyuk, K. A. Vorotilov, V. A. Vasiljev, A. S. Sigov, O. I. Lebedev, Yu. V. Grigoriev, M. P. De Santo, R. Barberi, and Th. Rasing, "Crystallization of PZT in Porous Alumina Membrane Channels", *Ferroelectrics*, 2006, 336, 247-254.
80. M. Liu, X. Li, H. Imrane, Y. Chen, T. Goodrich, Z. Cai, K. S. Ziemer, J. Y. Huang, and N. X. Sun, "Synthesis of ordered arrays of multiferroic $NiFe_2O_4$-$Pb(Zr_{0.52}Ti_{0.48})O_3$ core-shell nanowires", *Appl. Phys. Lett.*, 2007, 90, 152501.

81. S. A. Yang, K. O. Jeong, J. Kim, Y. C. Choi, J. K. Han, and S. D. Bu, "Synthesis of PZT Nanotubes and Its Nanometer-Scale Shape Modification with an Electron-Beam Irradiation", *J. Korean Phys. Soc.*, 2007, 51, S174-S177.
82. J. Kim, S. A. Yang, Y. C. Choi, J. K. Han, K. O. Jeong, Y. J. Yun, D. J. Kim, S. M. Yang, D. Yoon, H. Cheong, K.-S. Chang, T. W. Noh, and S. D. Bu, "Ferroelectricity in Highly Ordered Arrays of Ultra-Thin-Walled $Pb(Zr,Ti)O_3$ Nanotubes Composed of Nanometer-Sized Perovskite Crystallites", *Nano Lett.*, 2008, 8, 1813-1818.
83. A. Nourmohammadi, M. A. Bahrevar, S. Schulze, and M. Hietschold, "Electrodeposition of lead zirconate titanate nanotubes", *J. Mater. Sci.*, 2008, 43, 4753-4759.
84. A. Nourmohammadi, M. A. Bahrevar, and M. Hietschold, "Sol-gel electrophoretic deposition of PZT nanotubes", *Mater. Lett.*, 2008, 62, 3349-3351.
85. T. Wen, J. Zhang, T. P. Chou, S. J. Limmer, and G. Cao, "Template-Based Growth of Oxide Nanorod Arrays by Centrifugation", *J. Sol-Gel. Sci. Techn.*, 2005, 33, 193-200.
86. E. D. Mishina, K. A. Vorotilov, V. A. Vasil'ev, A. S. Sigov, N. Ohta and S. Nakabayashi, "Porous Silicon-Based Ferroelectric Nanostructures", *J. Exp. Theor. Phys.*+, 2002, 95, 502-504.
87. G. Xu, Z. Ren, P. Du, W. Wang, G. Shen, and G. Han, "Polymer-Assisted Hydrothermal Synthesis of Single-Crystalline Tetragonal Perovskite $PbZr_{0.52}Ti_{0.48}O_3$ Nanowires", *Adv. Mater.*, 2005, 17, 907-910.
88. Z. Ren, G. Xu, X. Wei, Y. Liu, G. Shen, and G. Han, "Shape Evolution of $Pb(Zr,Ti)O_3$ Nanocrystals Under Hydrothermal Conditions", *J. Am. Ceram. Soc.*, 2007, 90, 2645-2648.
89. J. Wang, C. S. Sandu, E. Colla, Y. Wang, W. Ma, R. Gysel, H. J. Trodahl, N. Setter, and M. Kuball, "Ferroelectric domains and piezoelectricity in monocrystalline $Pb(Zr,Ti)O_3$ nanowires", *Appl. Phys. Lett.*, 2007, 90, 133107.
90. X. Yang, Y. Zhao, Y. Yang, and Z. Dong, "Facile hydrothermal preparation of furcated PZT nanowhiskers", *Mater. Lett.*, 2007, 61, 3462-3465.
91. Y. Wang and J. J. Santiago-Avilés, "Synthesis of lead zirconate titanate nanofibres and the Fourier-transform infrared characterization of their metallo-organic decomposition process", *Nanotechnology*, 2004, 15, 32-36.
92. N. Dharmaraj, C. H. Kim, and H. Y. Kim, "$Pb(Zr_{0.5}, Ti_{0.5})O_3$ nanofibres by electrospinning", *Mater. Lett.*, 2005, 59, 3085-3089.
93. S. Xu, Y. Shi, and S.-G. Kim, "Fabrication and mechanical property of nano piezoelectric fibres", *Nanotechnology*, 2006, 17, 4497-4501.
94. Z. H. Zhou, X. S. Gao, J. Wang, K. Fujihara, S. Ramakrishna, and V. Nagarajan, "Giant strain in $PbZr_{0.2}Ti_{0.8}O_3$ nanowires", *Appl. Phys. Lett.*, 2007, 90, 052902.
95. W. Gong, J.-F. Li, C.-E Peng, Z. L. Gui, and L. T. Li, "In-Plane Aligned $Pb(Zr_xTi_{1-x})O_3$ Microbelts Fabricated by Near Migration and Resctricted Growth", *Adv. Mater.*, 2005, 17, 1952-1956.

96. S. Han, C. Li, Z. Liu, B. Lei, D. Zhang, W. Jin, X. Liu, T. Tang, and C. Zhou, "Transition Metal Oxide Core-Shell Nanowires: Generic Synthesis and Transport Studies", *Nano. Lett.*, 2004, 4, 1241-1246.
97. B. Lei, S. Han, C. Li, D. Zhang, Z. Liu, and C. Zhou, "Synthesis and electronic properties of transition metal oxide core-shell nanowires", *Nanotechnology*, 2007, 18, 044019.
98. S. Kawasaki, G. Catalan, H. J. Fan, M. M. Saad, J. M. Gregg, M. A. Correa-Duarte, J. Rybczynski, F. D. Morrison, T. Tatsuta, O. Tsuji, and J. F. Scott, "Conformal oxide coating of carbon nanotubes", *Appl. Phys. Lett.*, 2008, 92, 053109.
99. S. Kawasaki, H. J. Fan, G. Catalan, F. D. Morrison, T. Tatsuta, O. Tsuji, and J. F. Scott, "Solution-process coating of vertical ZnO nanowires with ferroelectrics", *Nanotechnology*, 2008, 19, 375302.
100. S. Singh and S. B. Krupanidhi, "Synthesis and structural characterization of the antiferroelectric lead zirconate nanotubes by pulsed laser deposition", *Appl. Phys. A*, 2007, 87, 27-31.
101. Y. Jing, S. Jin, Y. Jia, J. Han, and J. Sun, "Preparation of $SrTiO_3$ nanofibres by hydrothermal method", *J. Mater. Sci.*, 2005, 40, 6315-6317.
102. M. Miyauchi, "Thin Films of Single-Crystalline $SrTiO_3$ Nanorod Arrays and Their Surface Wettability Conversion", *J. Phys. Chem. C*, 2007, 111, 12440-12445.
103. S.-O. Kang, J. Choi, I. Hwang, S. Hong, B. H. Park, Y.-I. Kim, S.-J. Ahn, and K.-S. Yun, "Shape-Control of Strontium Titanate Nanostructures by a Surface-Capping Soft Chemical Process", *J. Kor. Phys. Soc.*, 2008, 52, 466-470.
104. J. Xie, T. Ji, X. Ou-Yang, Z. Xiao, and H. Shi, "Preparation of $SrTiO_3$ nanomaterial from layered titanate nanotubes or nanowires", *Solid State Commun.*, 2008, 147, 226-229.
105. T. Toshima, H. Ishikawa, S. Tanda, and T. Akiyama, "Multipod Crystals of Perovskite $SrTiO_3$", *Cryst. Growth Des.*, 2008, 8, 2066-2069.
106. S. Singh and S. B. Krupanidhi, "Synthesis and structural characterization of $Ba_{0.6}Sr_{0.4}TiO_3$ nanotubes", *Phys. Lett. A*, 2007, 367, 356-359.
107. X. Wei, A. L. Vasiliev, and N. P. Padture, "Nanotubes patterned thin films of barium-strontium titanate", *J. Mater. Res.*, 2005, 20, 2140-2147.
108. S. Maensiri, W. Nuansing, J. Klinkaewnarong, P. Laokul, and J. Khemprasit, "Nanofibers of barium strontium titanate (BST) by sol-gel processing and electrospinning", *J. Coll. Int. Sci.*, 2006, 297, 578-583.
109. W. Jiang, X. Gong, Z. Chen, Y. Hu, X. Zhang, and X. Gong, "Preparation of barium strontium titanate $Ba_{1-x}Sr_xTiO_3$ ($0 \leq x \leq 0.2$) single-crystal nanorods by a novel combined method", *Ultrason. Sonochem.*, 2007, 14, 208-212.
110. W. Chen and Q. Zhu, "Synthesis of barium strontium titanate nanorods in reverse microemulsion", *Mater. Lett.*, 2007, 61, 3378-3380.
111. W. Liu, X. Sun, H. Han, M. Li, and X.-Z. Zhao, "Surface polarization enhancement in $(Pb_{0.25}Ba_{0.15}Sr_{0.6})TiO_3$ nanotubes", *Appl. Phys. Lett.*, 2006, 89, 163122.

112. L. Zhao, M. Steinhart, M. Yosef, S. K. Lee, and S. Schlecht, “Large-scale template-assisted growth of $LiNbO_3$ one-dimensional nanostructures for nano-sensors”, *Sensor. Actuat. B – Chem.*, 2005, 109, 86-90.
113. T.-Y. Ke, H.-A. Chen, H.-S. Sheu, J.-W. Yeh, H.-N. Lin, C.-Y. Lee, and H.-T. Chiu, “Sodium Niobate Nanowire and Its Piezoelectricity”, *J. Phys. Chem. C*, 2008, 112, 8827-8831.
114. C.-Y. Xu, L. Zhen, R. Yang, and Z. L. Wang, “Synthesis of Single-Crystalline Niobate Nanorods via Ion-Exchange Based on Molten-Salt Reaction”, *J. Am. Chem. Soc.*, 2007, 129, 15444-15445.
115. J.-F. Liu, X.-L. Li, and Y.-D. Li, “Synthesis and characterization of nanocrystalline niobates”, *J. Cryst. Growth*, 2003, 247, 419-424.
116. G. Suyal, E. Colla, R. Gysel, M. Cantoni, and N. Setter, “Piezoelectric Response and Polarization Switching in Small Anisotropic Perovskite Particles”, *Nano. Lett.*, 2004, 4, 1339-1342.
117. A. Magrez, E. Vasco, J. W. Seo, C. Dieker, N. Setter, and L. Forró, “Growth of Single-Crystalline $KNbO_3$ Nanostructures”, *J. Phys. Chem. B*, 2006, 110, 58-61.
118. G. K. L. Goh, C. G. Levi, J. H. Choi, and F. F. Lange, “Hydrothermal epitaxy of $KNbO_3$ thin films and nanostructures”, *J. Cryst. Growth*, 2006, 286, 457-464.
119. Y. Nakayama, P. J. Pauzauskie, A. Radenovic, R. M. Onorato, R. J. Saykally, J. Liphardt, and P. Yang, “Tunable nanowire nonlinear optical probe”, *Nature*, 2007, 447, 1098-1102.
120. A. J. Paula, R. Parra, M. A. Zaghete, and J. A. Varela, “Synthesis of $KNbO_3$ nanostructures by a microwave assisted hydrothermal method”, *Mater. Lett.*, 2008, 62, 2581-2584.
121. G. Wang, Y. Yu, T. Grande, and M.-A. Einarsrud, “Synthesis of $KNbO_3$ nanorods by hydrothermal method”, *J. Nanosci. Nanotechnol.*, in print.
122. G. Wang, S. M. Selbach, Y. Yu, X. Zhang, T. Grande, and M.-A. Einarsrud, “Hydrothermal Synthesis and Characterization of $KNbO_3$ Nanorods”, to be submitted.
123. I. Pribošič, D. Makovec, and M. Drofenik, “Formation of Nanoneedles and Nanoplatelets of $KNbO_3$ Perovskite during Templated Crystallization of the Precursor Gel”, *Chem. Mater.*, 2005, 17, 2953-2958.
124. Y. Hu, H. Gu, Z. Hu, W. Di, Y. Yuan, J. You, W. Cao, Y. Wang, and H. L. W. Chan, “Controllable Hydrothermal Synthesis of $KTa_{1-x}Nb_xO_3$ Nanostructures with Various Morphologies and Their Growth Mechanisms”, *Cryst. Growth. Des.*, 2008, 8, 832-837.
125. J. A. Nelson and M. J. Wagner, “Synthesis of Sodium Tantalate Nanorods by Alkalide Reduction”, *J. Am. Chem. Soc.*, 2003, 125, 332-333.
126. T.-J. Park, Y. Mao, and S. S. Wong, “Synthesis and characterization of multiferroic $BiFeO_3$ nanotubes”, *Chem. Commun.*, 2004, 2708-2709.
127. X. Y. Zhang, C. W. Lai, X. Zhao, D. Y. Wang, and J. Y. Dai, “Synthesis and ferroelectric properties of multiferroic $BiFeO_3$ nanotube arrays”, *Appl. Phys. Lett.*, 2005, 87, 143102.

128. X. Y. Zhang, J. Y. Dai, and C. W. Lai, "Synthesis and characterization of highly ordered $BiFeO_3$ multiferroic nanowire arrays", *Prog. Solid State Chem.*, 2005, 33, 147-151.
129. F. Gao, Y. Yuan, K. F. Wang, X. Y. Chen, F. Chen, J.-M. Liu, and Z. F. Ren, "Preparation and photoabsorption characterization of $BiFeO_3$ nanowires", *Appl. Phys. Lett.*, 2006, 89, 102506.
130. J. Wei, D. Xue, and Y. Xu, "Photoabsorption characterization and magnetic property of multiferroic $BiFeO_3$ nanotubes synthesized by a facile sol-gel template process", *Scripta Mater.*, 2008, 58, 45-48.
131. J. B. Liu, H. Wang, Y. D. Hou, M. K. Zhu, H. Yan, and M. Yoshimura, "Low-temperature preparation of $Na_{0.5}Bi_{0.5}TiO_3$ nanowhiskers by a sol-gel-hydrothermal method", *Nanotechnology*, 2004, 15, 777-780.
132. J. Yang, Y. Hou, C. Wang, M. Zhu, and H. Yan, "Relaxor behaviour of $(K_{0.5}Bi_{0.5})TiO_3$ ceramics derived from molten salt synthesized single-crystalline nanowires", *Appl. Phys. Lett.*, 2007, 91, 023118.
133. Y.-D. Hou, L. Hou, S.-Y. Huang, M.-K. Zhu, H. Wang, and H. Yan, "Comparative study of $K_{0.5}Bi_{0.5}TiO_3$ nanoparticles derived from sol-gel-hydrothermal and sol-gel routes", *Solid State Commun.*, 2006, 137, 658-661.
134. L. Hou, Y.-D. Hou, X.-M. Song, M.-K. Zhu, H. Wang, and H. Yan, "Sol-gel-hydrothermal synthesis and sintering of $K_{0.5}Bi_{0.5}TiO_3$ nanowires", *Mater. Res. Bull.*, 2006, 41, 1330-1336.
135. Y.-D. Hou, L. Hou, T.-T. Zhang, M.-K. Zhu, H. Wang, and H. Yan, "$(Na_{0.8}K_{0.2})_{0.5}Bi_{0.5}TiO_3$ Nanowires: Low-Temperature Sol-Gel-Hydrothermal Synthesis and Densification", *J. Am. Ceram. Soc.*, 2007, 90, 1738-1743.
136. Y. Hou, L. Hou, M. Zhu, and H. Yan, "Synthesis of $(K_{0.5}Bi_{0.5})_{0.4}Ba_{0.6}TiO_3$ nanowires and ceramics by sol-gel-hydrothermal method", *Appl. Phys. Lett.*, 2006, 89, 243114.
137. M. Liao, X. L. Zhong, J. B. Wang, H. L. Yan, J. P. He, Y. Qiao, and Y. C. Zhou, "Nd-substituted bismuth titanate ferroelectric nanofibers by electrospinning", *J. Cryst. Growth*, 2007, 304, 69-72.
138. B. I. Seo, U. A. Shaislamov, S. J. Lee, S.-W. Kim, I. S. Kim, S. K. Hong, and B. Yang, "Growth of ferroelectric BLT and Pt nanotubes for semiconductor memories", *J. Cryst. Growth*, 2006, 292, 315-319.
139. B. I. Seo, U. A. Shaislamov, S.-W. Kim, H.-K. Kim, B. Yang, and S. K. Hong, "$Bi_{3.25}La_{0.75}Ti_3O_{12}$ (BLT) nanotube capacitors for semiconductor memories", *Physica E*, 2007, 37, 274-278.
140. F. D. Morrison, L. Ramsay, and J. F. Scott, "High aspect ratio piezoelectric strontium-bismuth-tantalate nanotubes", *J. Phys.: Condens. Matter.*, 2003, 15, L527-L532.
141. Z. Hua, P. Yang, H. Huang, J. Wan, Z.-Z. Yu, S. Yang, M. Lu, B. Gu, and Y. Du, "Sol-gel template synthesis and characterization of magnetoelectric $CoFe_2O_4/Pb(Zr_{0.52}Ti_{0.48})O_3$ nanotubes", *Mater. Chem. Phys.*, 2008, 107, 541-546.
142. S. H. Xie, J. Y. Li, Y. Qiao, Y. Y. Liu, L. N. Lan, Y. C. Zhou, and S. T. Tan, "Multiferroic $CoFe_2O_4$-$Pb(Zr_{0.52}Ti_{0.48})O_3$ nanofibers by electrospinning", *Appl. Phys. Lett.*, 2008, 92, 062901.

143. S. H. Xie, J. Y. Li, Y. Y. Liu, L. N. Lan, G. Jin, and Y. C. Zhou, "Electrospinning and multiferroic properties of $NiFe_2O_4$-$Pb(Zr_{0.52}Ti_{0.48})O_3$ composite nanofibers", 2008, 104, 024115.
144. P. M. Rørvik, "Syntese og karakterisering av enkrystallinske nanostaver av $BaTiO_3$", Project work, NTNU, 2003.
145. P. M. Rørvik, "Framstilling av nanostrukturerte oksidmaterialer med perovskittstruktur", Master thesis, NTNU, 2004.
146. P. M. Rørvik, T. Lyngdal, R. Sæterli, A. T. J. van Helvoort, R. Holmestad, T. Grande, and M.-A. Einarsrud, "Influence of Volatile Chlorides on the Molten Salt Synthesis of Ternary Oxide Nanorods and Nanoparticles", *Inorg. Chem.*, 2008, 47, 3173-3181. (Paper I)
147. C.-Y. Xu, Q. Zhang, H. Zhang, L. Zhen, J. Tang, and L.-C. Qin, "Synthesis and Characterization of Single-Crystalline Alkali Titanate Nanowires", *J. Am. Chem. Soc.*, 2005, 127, 11584-11585.
148. J. Yu, S. Tang, R. Wang, Y. Shi, B. Nie, L. Zhai, X. Zhang, and Y. Du, "Synthesis of Single-Crystalline Barium Dititanate Nanobelts", *Cryst. Growth Des.*, 2008, 8, 1481-1483.
149. A. Gruverman and A. Kholkin, "Nanoscale ferroelectrics: processing, characterization and future trends", *Rep. Prog. Phys.*, 2006, 69, 2443-2474.
150. K. Zhu, T. B. Vinzant, N. R. Neale, and A. J. Frank, "Removing Structural Disorder from Oriented TiO_2 Nanotube Arrays: Reducing the Dimensionality of Transport and Recombination in Dye-Sensitized Solar Cells", *Nano Lett.*, 2007, 7, 3739-3746.
151. R. E. Cohen, "Origin of ferroelectricity in perovskite oxides", *Nature*, 1992, 358, 136-138.
152. Y. Kuroiwa, S. Aoyagi, A. Sawada, J. Harada, E. Nishibori, M. Takata, and M. Sakata, "Evidence for Pb-O Covalency in Tetragonal $PbTiO_3$", *Phys. Rev. Lett.*, 2001, 87, 217601.
153. E. Vasco, A. Magrez, L. Forró, and N. Setter, "Growth Kinetics of One-Dimensional $KNbO_3$ Nanostructures by Hydrothermal Processing Routes", *J. Phys. Chem. B*, 2005, 109, 14331-14334.
154. A. T. Chien, J. Sachleben, J. H. Kim, J. S. Speck, and F. F. Lange, "Synthesis and characterization of $PbTiO_3$ powders and heteroepitaxial thin films by hydrothermal synthesis", *J. Mater. Res.*, 1999, 14, 3303-3311.
155. F. F. Lange and G. K. L. Goh, "Hydrothermal epitaxial growth of perovskite films", *J. Ceram. Proc. Res.*, 2001, 2, 4-8.
156. D. F. K. Hennings, C. Metzmacher, and B. S. Schreinemacher, "Defect Chemistry and Microstructure of Hydrothermal Barium Titanate", *J. Am. Ceram. Soc.*, 2001, 84, 179-182.
157. M. E. Lines and A. M. Glass, "Principles and Applications of Ferroelectrics and Related Materials", Clarendon, Oxford, 1977, p. 8-15, 87-88, 102-105, 244-250, 620.
158. K. M. Rabe, M. Dawber, C. Lichtensteiger, C. H. Ahn, and J.-M. Triscone, "Modern Physics of Ferroelectrics: Essential Background", in "Physics of Ferroelectrics: A Modern Perspective", eds. K. M. Rabe, C. H. Ahn, and J.-M. Triscone, in the book series "Topics in Applied Physics", Springer, Berlin/Heidelberg, 2007, volume 105, p. 1-30.

159. A. S. Bhalla, R. Guo, and R. Roy, "The perovskite structure – a review of its role in ceramic science and technology", *Mat. Res. Innovat.*, 2000, 4, 3-26.
160. C. H. Ahn, K. M. Rabe, and J.-M. Triscone, "Ferroelectricity at the Nanoscale: Local Polarization in Oxide Thin Films and Heterostructures", *Science*, 2004, 303, 488-491.
161. B. Meyer and D. Vanderbilt, "*Ab initio* study of ferroelectric domain walls in $PbTiO_3$", *Phys. Rev. B*, 2002, 65, 104111.
162. D. Richter and S. Trolier-McKinstry, "Ferroelectrics", in "Nanoelectronics and Information Technology – Advanced Electronic Materials and Novel Devices", ed. R. Waser, 2nd ed., Wiley-VCH, Weinheim, 2005, p. 59-78.
163. D. W. Richerson, "Modern Ceramic Engineering", 2nd ed., Marcel Dekker, New York, 1992, p. 273-276.
164. C. Lichtensteiger, M. Dawber, and J.-M. Triscone, "Ferroelectric Size Effects", in "Physics of Ferroelectrics: A Modern Perspective", eds. K. M. Rabe, C. H. Ahn, and J.-M. Triscone, in the book series "Topics in Applied Physics", Springer, Berlin/Heidelberg, 2007, volume 105, pp. 305-338.
165. T. M. Shaw, S. Trolier-McKinstry, and P. C. McIntyre, "The properties of ferroelectric films at small dimensions", *Annu. Rev. Mater. Sci.*, 2000, 30, 263-298.
166. E. Erdem, H.-C. Semmelhack, R. Böttcher, H. Rumpf, J. Banys, A. Matthes, H.-J. Gläsel, D. Hirsch, and E. Hartmann, "Study of the tetragonal-to-cubic phase transition in $PbTiO_3$ nanopowders", *J. Phys.: Condens. Matter*, 2006, 18, 3861-3874.
167. E. K. Akdogan, C. J. Rawn, W. D. Porter, E. A. Payzant, and A. Safari, "Size effects in $PbTiO_3$ nanocrystals: Effect of particle size on spontaneous polarization and strains", *J. Appl. Phys.*, 2005, 97, 084305.
168. N. Nuraje, K. Su, A. Haboosheh, J. Samson, E. P. Manning, N. Yang, and H. Matsui, "Room Temperature Synthesis of Ferroelectric Barium Titanate Nanoparticles Using Peptide Nanorings as Templates", *Adv. Mater.*, 2006, 18, 807-811.
169. J. E. Spanier, A. M. Kolpak, J. J. Urban, I. Grinberg, L. Ouyang, W. S. Yun, A. M. Rappe, and H. Park, "Ferroelectric Phase Transition in Individual Single-Crystalline $BaTiO_3$ Nanowires", *Nano Lett.*, 2006, 6, 735-739.
170. D. D. Fong, G. B. Stephenson, S. K. Streiffer, J. A. Eastman, O. Auciello, P. H. Fuoss, and C. Thompson, "Ferroelectricity in Ultrathin Perovskite Films", *Science*, 2004, 304, 1650-1653.
171. J. Junguera and P. Ghosez, "Critical thickness for ferroelectricity in perovskite ultrathin films", *Nature*, 2003, 422, 506-509.
172. K. J. Choi, M. Biegalski, Y. L. Li, A. Sharan, J. Schubert, R. Uecker, P. Reiche, Y. B. Chen, X. Q. Pan, V. Gopalan, L.-Q. Chen, D. G. Schlom, and C. B. Eom, "Enhancement of Ferroelectricity in Strained $BaTiO_3$ Thin Films", *Science*, 2004, 306, 1005-1009.
173. H. N. Lee, H. M. Christen, M. F. Chisholm, C. M. Rouleau, and D. H. Lowndes, "Strong polarization enhancement in asymmetric three-component ferroelectric superlattices", *Nature*, 2005, 433, 395-399.
174. I. I. Naumov and H. Fu, "Spontaneous Polarization in One-Dimensional $Pb(ZrTi)O_3$ Nanowires", *Phys. Rev. Lett.*, 2005, 95, 247602.

175. G. Geneste, E. Bousquet, J. Junguera, and P. Ghosez, “Finite-size effects in $BaTiO_3$ Nanowires”, *Appl. Phys. Lett.*, 2006, 88, 112906.
176. J. Hong and D. Fang, “Size-dependent ferroelectric behaviors of $BaTiO_3$ nanowires”, *Appl. Phys. Lett.*, 2008, 92, 012906.
177. P. Khare and D. Sa, “Landau theory of ferroelectric transition in long cylindrical nanoparticles”, *Eur. Phys. J. B*, 2008, 63, 205-209.
178. Y. Zheng, C. H. Woo, and B. Wang, “Pulse-Loaded Ferroelectric Nanowire as an Alternating Current Source”, *Nano Lett.*, 2008, 8, 3131-3136.
179. A. N. Morozovska, E. A. Eliseev, and M. D. Glinchuk, “Ferroelectricity enhancement in confined nanorods: Direct variational method”, *Phys. Rev. B*, 2006, 73, 214106.
180. Y. Zheng, C. H. Woo, and B. Wang, “Surface tension and size effect in ferroelectric nanotubes”, *J. Phys.*: *Condens. Matter*, 2008, 20, 135216.
181. H. Fu and L. Bellaiche, “Ferroelectricity in Barium Titanate Quantum Dots and Wires”, *Phys. Rev. Lett.*, 2003, 91, 257601.
182. J. Wang and M. Kamlah, “Domain structures of ferroelectric nanotubes controlled by surface charge compensation”, *Appl. Phys. Lett.*, 2008, 93, 042906.
183. I. I. Naumov, L. Bellaiche, and H. Fu, “Unusual phase transitions in ferroelectric nanodisks and nanorods”, *Nature*, 2004, 432, 737-740.
184. I. Naumov and H. Fu, “Vortex-to-Polarization Phase Transformation Path in Ferroelectric $Pb(ZrTi)O_3$ Nanoparticles”, *Phys. Rev. Lett.*, 2007, 077603.
185. S. Prosandeev, I. Ponomareva, I. Naumov, I. Kornev, and L. Bellaiche, “Original properties of dipole vortices in zero-dimensional ferroelectrics”, *J. Phys.: Condens. Matter*, 2008, 20, 193201.
186. J. Wang, M. Kamlah, T.-Y. Zhang, Y. Li, and L.-Q. Chen, “Size-dependent polarization distribution in ferroelectric nanostructures: Phase field simulations”, *Appl. Phys. Lett.*, 2008, 92, 162905.
187. Z. Wang, A. P. Suryavanshi, and M.-F. Yu, “Ferroelectric and piezoelectric behaviours of individual single crystalline $BaTiO_3$ nanowire under direct axial electric biasing”, *Appl. Phys. Lett.*, 2006, 89, 082903.
188. S. V. Kalinin and D. A. Bonnell, “Electric Scanning Probe Imaging and Modification of Ferroelectric Surfaces”, in “Nanoscale Characterisation of Ferroelectric Materials”, eds. M. Alexe and A. Gruverman, Springer, Berlin, 2004, p. 1-43.
189. Z. Wang, J. Hu, and M.-F. Yu, “One-dimensional ferroelectric monodomain formation in single crystalline $BaTiO_3$ nanowire”, *Appl. Phys. Lett.*, 2006, 89, 263119.
190. W. S. Yun, J. J. Urban, Q. Gu, and H. Park, “Ferroelectric Properties of Individual Barium Titanate Nanowires Investigated by Scanned Probe Microscopy”, *Nano Lett.*, 2002, 2, 447-450.
191. P. M. Rørvik, C. Y. You, T. Tybell, T. Grande, and M.-A. Einarsrud, “Piezoresponse force microscopy studies of single $PbTiO_3$ nanorods”, unpublished. (Paper V)
192. Z. Wang, J. Hu, and M.-F. Yu, “Axial polarization switching in ferroelectric $BaTiO_3$ nanowire”, *Nanotechnology*, 2007, 18, 235203.

193. N. A. Spaldin, “Fundamental Size Limits in Ferroelectricity”, *Science*, 2004, 304, 1606-1607.
194. “International Technology Roadmap for Semiconductors”, 2007 Edition, “Front End Processes”, p. 53-57. (http://www.itrs.net/Links/2007ITRS/2007_Chapters/2007_FEP.pdf, accessed October 12th 2008)
195. A. Schilling, R. M. Bowman, G. Catalan, J. F. Scott, and J. M. Gregg, “Morphological Control of Polar Orientation in Single-Crystal Ferroelectric Nanowires”, *Nano Lett.*, 2007, 7, 3787-3791.
196. Z. L. Wang and J. Song, “Piezoelectric Nanogenerators Based on Zinc Oxide Nanowire Arrays”, *Science*, 2006, 312, 242-246.
197. Y. Qin, X. Wang, and Z. L. Wang, “Microfibre-nanowire hybrid structure for energy scavenging”, *Nature*, 2008, 451, 809-813.
198. M. Alexe, S. Senz, M. A. Schubert, D. Hesse, and U. Gösele, “Energy Harvesting Using Nanowires?”, *Adv. Mater.*, DOI: 10.1002/adma.200800272.
199. Z. Wang, J. Hu, A. P. Suryavanshi, K. Yum, and M.-F. Yu, “Voltage Generation from Individual $BaTiO_3$ Nanowires under Periodic Tensile Mechanical Load”, *Nano Lett.*, 2007, 7, 2966-2969.
200. S. Hirano, “Oxide Nanowire Arrays and Two-Dimensional Photonic Crystals for Control of Light”, *J. Ceram. Soc. Jpn.*, 2007, 115, 92-100.
201. G. L. Messing, S. Trolier-McKinstry, E. M. Sabolsky, C. Duran, S. Kwon, B. Brahmaroutu, P. Park, H. Yilmaz, P. W. Rehrig, K. B. Eitel, E. Suvaci, M. Seabaugh, and K. S. Oh, “Templated Grain Growth of Textured Piezoelectric Ceramics”, *Crit. Rev. Solid State*, 2004, 29, 45-96.
202. C. Xu, Harbin Institute of Technology, China, personal communication, March 1st 2008.
203. I. N. Anikin, I. I. Naumova, and G. V. Rumyantseva, “Solubility of titanium dioxide in molten salts and crystallization of rutile”, *Sov. Phys. Crystallogr.*, 1965, 10, 172-177.
204. V. L. Cherginets, “On studies of oxide solubilities in melts based on alkaline halides”, *Electrochim. Acta*, 1997, 42, 3619-3627.
205. A. Packter, “The Crystallisation of Alkaline-earth Metal Oxides from Metal Chloride Melts: Solubility-Temperature Phase Diagram Analyses and Preliminary Experimental Studies”, *Krist. Tech.*, 1980, 15, 413-420.
206. C. R. Peterson and E. B. Slamovich, “Effect of Processing Parameters on the Morphology of Hydrothermally Derived $PbTiO_3$ Powders”, *J. Am. Ceram. Soc.*, 1999, 82, 1702-1710.
207. J. Moon, M. L. Carasso, H. G. Krarup, J. A. Kerchner, and J. H. Adair, “Particle-shape control and formation mechanisms of hydrothermally derived lead titanate”, *J. Mater. Res.*, 1999, 14, 866-875.
208. P. M. Rørvik, R. Sæterli, T. Grande, and M.-A. Einarsrud, unpublished.
209. C. G. Hu, H. Liu, C. S. Lao, L. Y. Zhang, D. Davidovic, and Z. L. Wang, “Size-Manipulable Synthesis of Single-Crystalline $BaMnO_3$ and $BaTi_{1/2}Mn_{1/2}O_3$ Nanorods/Nanowires”, *J. Phys. Chem. B*, 2006, 110, 14050-14054.

210. H. Liu, C. Hu, and Z. L. Wang, “Composite-Hydroxide-Mediated Approach for the Synthesis of Nanostructures of Complex Functional-Oxides”, *Nano Lett.*, 2006, 6, 1535-1540.
211. V. Hoepfner, “Composite-hydroxide-mediated approach for the synthesis of nanostructured oxide materials”, Project work, NTNU, 2006.
212. Y. Saito, H. Takao, T. Tani, T. Nonoyama, K. Takatori, T. Homma, Y. Nagaya, and M. Nakamura, “Lead-free piezoceramics”, *Nature*, 2004, 432, 84-87.

Paper I

Is not included due to copyright

Paper II

Is not included due to copyright

Paper III

Is not included due to copyright

Paper IV

Paper IV

Template-assisted synthesis of $PbTiO_3$ nanotubes

Per Martin Rørvik,[1] Kiyoharu Tadanaga,[2] Masahiro Tatsumisago,[2] Tor Grande,[1] and Mari-Ann Einarsrud[1]

[1]Department of Materials Science and Engineering, Norwegian University of Science and Technology, 7491 Trondheim, Norway

[2]Department of Applied Chemistry, Graduate School of Engineering, Osaka Prefecture University, Sakai, Osaka 599-8531, Japan

Abstract

Nanotubes of ferroelectric lead titanate ($PbTiO_3$) have been made by a template-assisted method. An equimolar Pb-Ti sol was dropped onto porous alumina membranes and penetrated into the channels of the template. Single-phase $PbTiO_3$ perovskite nanotubes were obtained by annealing at 700 °C for 6 h. The nanotubes had diameters of 200 - 400 nm with a wall thickness of approximately 20 nm. Excess PbO or annealing in a Pb-containing atmosphere was not necessary in order to achieve single phase $PbTiO_3$ nanotubes. The influence of the heating procedure and the sol concentration is discussed.

Introduction

Template-assisted synthesis is a widely used method to produce one-dimensional (1D) nanostructures such as nanotubes and nanowires of a variety of materials.[1] For oxide materials, the most commonly used negative templates are porous anodic aluminium oxide (AAO) and track-etched polycarbonate membranes.[2] These templates have 1D pores or channels in which a sol or an aqueous solution containing the desired components can be incorporated. In following drying and annealing steps, the solvent evaporates and the material starts to crystallize and densify, forming nanostructures with dimensions constricted by the pore diameter and pore length of the template.

In this work we used commercial Whatman Anodisc AAO membranes to synthesize $PbTiO_3$ nanotubes. $PbTiO_3$ is a prototype ferroelectric material with a perovskite structure and with a Curie temperature of 490 °C. $PbTiO_3$ has previously been synthesized in AAO templates, producing nanotubes by sol-gel method[3-6] and nanowires by an aqueous solution method.[7] In addition, the closely related compound $PbZr_{1-x}Ti_xO_3$ (PZT) has also been synthesized as nanotubes and nanowires in AAO templates.[8-15] In this work we studied how the heating procedure, the sol concentration, and different nominal pore diameters of the Anodisc membranes influenced the morphology and phase composition of the nanotubes.

Experimental

Whatman Anodisc AAO membranes with a thickness of 60 µm were used as templates. Three types of membranes with different nominal pore diameters were used: 20 nm, 100 nm, and 200 nm. The diameter of the membrane was either 25 mm (200 nm membranes) or 47 mm (20 nm and 100 nm membranes). The pore diameters on the two sides of the membrane were different. For instance, the small pore side of the 200 nm Anodisc membranes had pore diameters ≤100 nm, while the large pore side had pore diameters of 200-250 nm (figure 1). The pore diameter across the membrane was therefore not homogeneous.

A Pb-Ti sol was made by dissolving lead(II) acetate trihydrate (Wako, >99.9 %) in acetic acid (Wako, >99.0 %), and titanium(IV) tetrabutoxide (Wako,

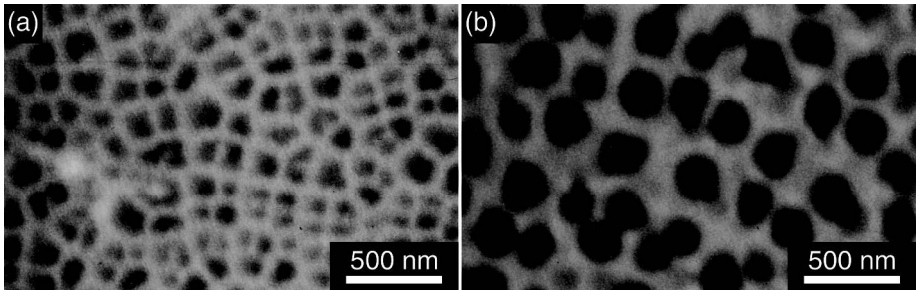

Figure 1. SEM images of Whatman Anodisc membranes (200 nm nominal pore diameter, 60 µm thick). (a) Small pore side. (b) Large pore side.

Table 1. Amount of reactants and sol concentration for the three different sols used.

Sol number	1	2	3
Cation concentration	0.43 mol/L	0.75 mol/L	1.35 mol/L
Lead(II) acetate trihydrate	10.0 mmol	10.0 mmol	10.0 mmol
Titanium(IV) tetrabutoxide	10.0 mmol	10.0 mmol	10.0 mmol
Acetic acid	2.0 mL	5.0 mL	10.0 mL
2-methoxyethanol	2.0 mL	5.0 mL	10.0 mL

>95.0 %) in 2-methoxyethanol (Wako, >98.0 %), and mixing these two solutions by stirring. Three sol concentrations were used: 0.43, 0.75 and 1.35 mol/L (n_{Pb}/V_{total}), see table 1. The Pb/Ti ratio was 1.00 for all the sols. The sol was dropped onto the large pore side of a membrane which had been taped at the small pore side. After 10 min, excess sol was removed by wiping with a paper or with a scalpel. The membranes infiltrated with the sol were dried in air for 30 min and thereafter heat-treated at 700 °C for 0.5 - 6 h. The membranes were either directly heated to 700 °C in a preheated furnace, or slowly heated at a rate of 1 °C/min from room temperature. The cooling rate was 3 °C/min for all the experiments. After the heat treatment, excess $PbTiO_3$ material was carefully scraped off using a scalpel. The membrane was dissolved by immersing in 4 mol/L NaOH for at least 1 h, followed by washing and centrifugation in water. Large-area arrays of nanotubes were obtained by coating the small pore side of the membrane with epoxy before the NaOH treatment, while free-standing nanotubes were obtained by sonication during the NaOH treatment. For comparison, the sols were also heat-treated, at 700 °C for 0.5 h with a 1 °C/min heating rate.

The phase composition of the products was studied by X-ray powder diffraction (XRD, Shimadzu LabX XRD-6000). The morphology of the products and the Anodisc membranes was studied by scanning electron microscopy (SEM, JEOL JSM-5300), and field emission scanning electron microscopy (FESEM, Hitachi S-4500). The samples were coated with gold or osmium before imaging.

Results

The diameters of nanotubes synthesized in 200 nm membranes were 200 - 400 nm, while the lengths varied from 2 μm to above 10 μm (figure 2). A side view of the nanotube array shows that the growth of nanotubes was inhomogeneous in the membrane (figure 2b), suggesting that the internal structure of the membrane was inhomogeneous. During the drying after dissolving the membrane the nanotubes typically bundled together (figure 2c). However, the nanotubes could detach from each other easily by sonication (figure 2d).

The X-ray diffractograms of the heat-treated products show that while the perovskite phase ($PbTiO_3$) was formed from the sol after annealing at 700 °C for 30 min with slow heating rate (figure 3a), the same heat treatment for the sol in the membrane resulted in the metastable fluorite phase (figure 3b),[16,17] which is non-ferroelectric and therefore unwanted. Prolonged heating increased the perovskite

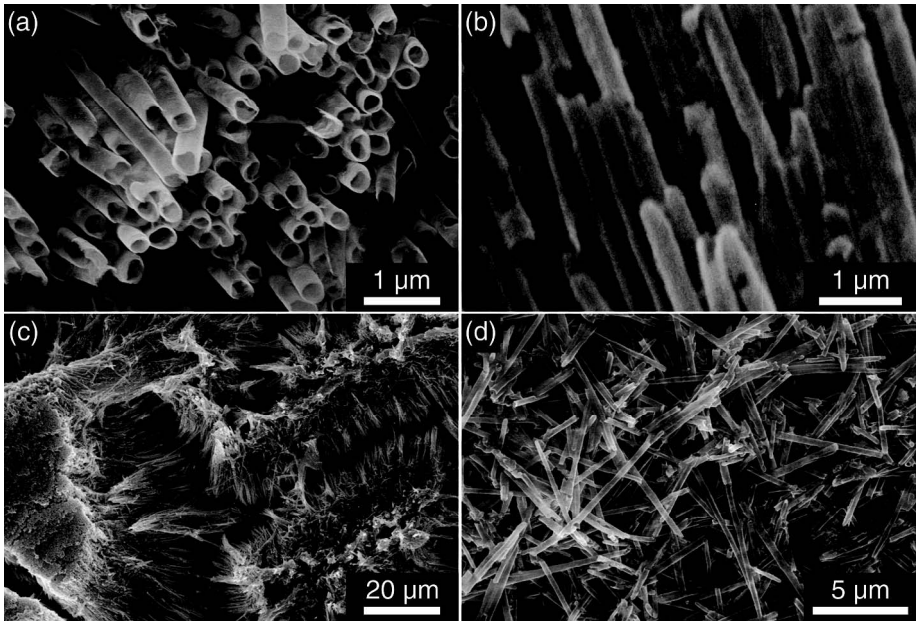

Figure 2. SEM and FESEM images of nanotubes synthesized in 200 nm membranes. (a) Nanotube ends. (b) Side view revealing growth inhomogeneties. (c) The nanotubes bundled during drying after dissolving the membrane. (d) Free-standing nanotubes after sonication.

content (figure 3c); however, it was more effective to insert the sol-infiltrated membrane directly into a furnace preheated to 700 °C (figure 3d-f). Initially, a small amount of the fluorite phase was formed also with the direct heating, but after 6 h at 700 °C the fluorite phase could not be detected by XRD (figure 3f).

Comparing figure 3f with figure 3a, the diffraction lines in figure 3f are much broader than the corresponding lines in figure 3a, and in addition the splitting of the (101) and (110) diffraction lines at 32 - 33° evident in figure 3a is far less pronounced in figure 3f. The difference between these two diffractograms is caused by line-broadening because of small crystallite size. Similar diffractograms to figure 3f have been shown for $PbTiO_3$ nanotubes that exhibited ferroelectric properties, implying a tetragonal structure.[6] The line broadening indicates that the perovskite crystallites formed in the membrane are much smaller than the crystallites formed during heat treatment of the sol. The template therefore has a confinement effect on the coalescence of the nanoparticles.

To study if the wall thickness of the nanotubes could be controlled by changing the sol concentration, three different sols (table 1) were used with otherwise identical synthesis conditions. However, the wall thickness estimated from FESEM images was 15 - 20 nm for all the three sol concentrations and no significant difference was observed (figure 4). Figure 4 also shows that the nanotubes were polycrystalline, consisting of grains with diameters ≤20 nm.

Anodisc membranes with 20 nm and 100 nm nominal pore diameters (according to the supplier) were tried used to make $PbTiO_3$ nanotubes with smaller diameter. However, the nanotube diameters were the same as when 200 nm

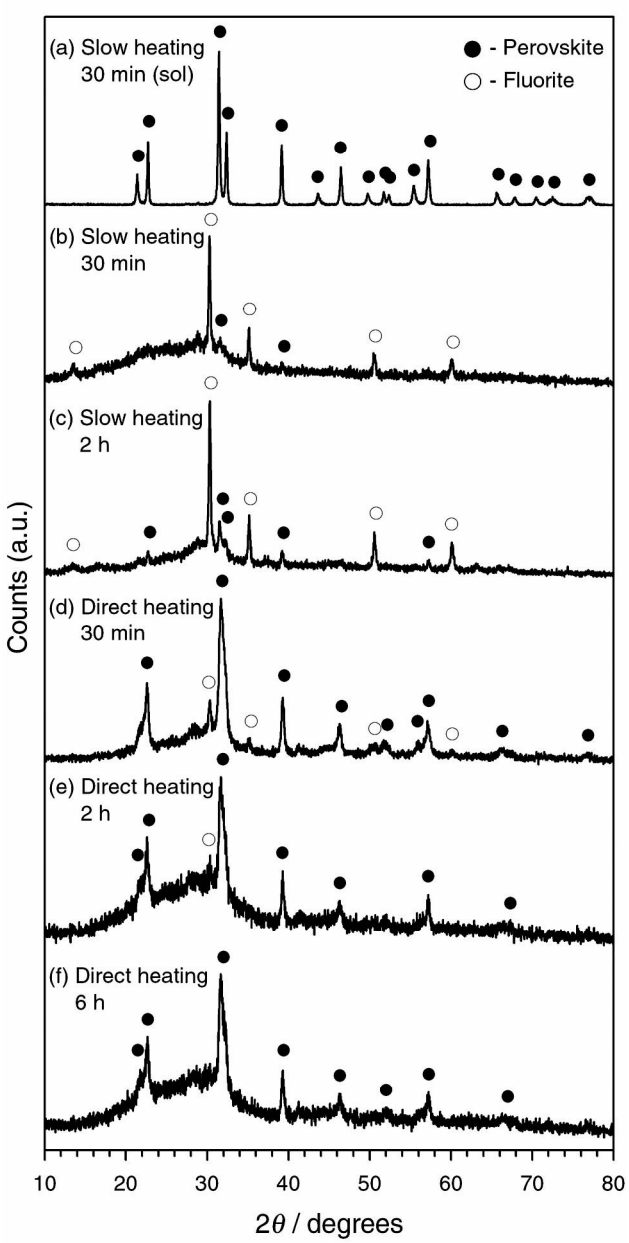

Figure 3. X-ray diffractograms of products synthesized with 0.75 mol/L sol after various heat treatments. (a) Sol annealed at 700 °C for 30 min with slow heating rate (1 °C/min). (b)-(f) Products synthesized in 200 nm membranes (the membranes were dissolved before XRD characterization). The products were annealed at 700 °C for the stated length of time, and were either slowly heated (1 °C/min) to 700 °C, or directly inserted into a preheated furnace at 700 °C. Line identities are based on the PDF standard patterns of tetragonal perovskite $PbTiO_3$ (6-452) and pyrochlore $Pb_2Ti_2O_6$ (24-142).

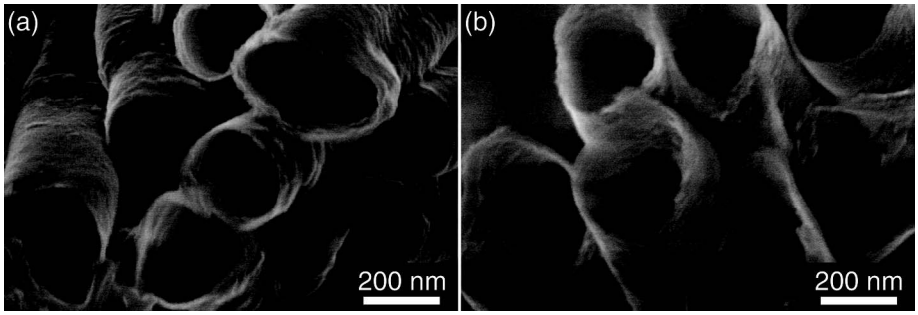

Figure 4. FESEM images of nanotubes synthesized in 200 nm membranes using sol concentrations of (a) 0.43 mol/L and (b) 1.35 mol/L.

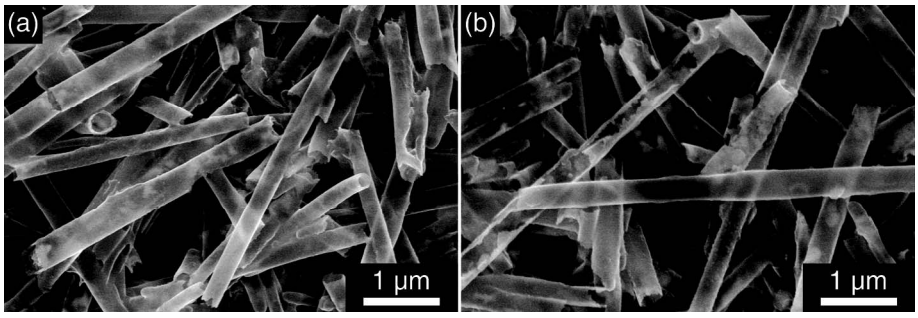

Figure 5. FESEM images of nanotubes synthesized in (a) 20 nm membrane and (b) 100 nm membrane.

Anodisc membranes were used; 200 - 400 nm (figure 5). SEM images of the small pore and large pore side of a 20 nm membrane (figure 6a and b) show that the small pore side has pore diameters of approximately 20 nm, while the large pore side has pore diameters of 200 - 300 nm, just as the 200 nm membrane (figure 1b). Cross-section SEM images of a 100 nm membrane show that it was only a thin layer (~1.5 µm) at the small pore side of the membrane that had the nominal pore diameter, while the rest of the membrane had larger pores (200 - 400 nm). The layer with small pore diameter in the 20 nm membranes was even thinner (<1 µm).

Discussion

The results show that template-assisted synthesis is an easy method to fabricate ceramic nanotubes. However, control of the micro/nanostructure and phase composition can be a challenge. For the $PbTiO_3$ system studied here, the effect of various heat treatment procedures on the resulting phase is clearly demonstrated in figure 3. The non-ferroelectric fluorite phase that was formed during slow heating of the membranes is often encountered as an unwanted intermediate phase during annealing of Pb-based ferroelectrics.[17-20] In the fluorite structure, neither the oxygen vacancies nor the cations are ordered, so during annealing, formation of the metastable fluorite phase may be kinetically favoured over the thermodynamically stable, but highly ordered perovskite phase, because of limited ion diffusion at

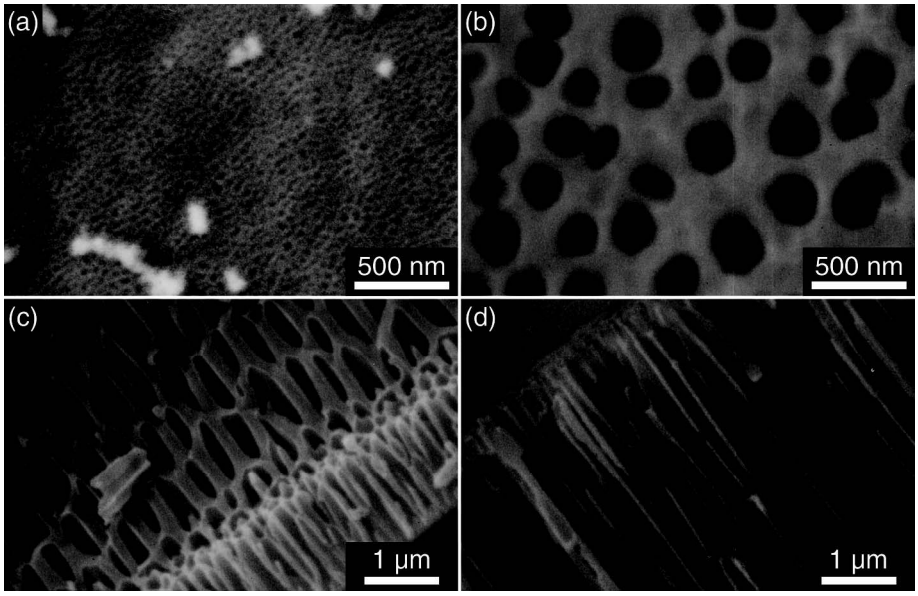

Figure 6. SEM images of the internal structure of Whatman Anodisc membranes. (a)-(b) Membrane with nominal pore diameter 20 nm imaged from the small pore side (a) and from the large pore side (b). (c)-(d) Cross-sections of a membrane with nominal pore diameter 100 nm imaged from the small pore side (c) and the large pore side (d).

lower temperatures.[17,18] The formation of the fluorite phase will also reduce the driving force associated with the nucleation of the perovskite phase.[18] Thus, when the fluorite phase is nucleated from the amorphous precursor, the further transformation into the perovskite phase is slow, although the perovskite phase is the thermodynamically stable phase. The difference in phase composition between the powders that were obtained by the slow heat treatment of the sol (figure 3a) and the sol in the membrane (figure 3b), indicates that the pore walls of the membrane influence the nucleation and growth process. As the fluorite phase was only observed in the diffractogram of the membrane-synthesized sample (figure 3b), it can be assumed that heterogeneous nucleation of the fluorite phase occurred at the pore walls, in a temperature range in which the fluorite phase is kinetically stable. In contrast, for the sol alone, homogeneous nucleation is more likely, and the homogeneous nucleation is likely to be initiated at a higher temperature than the heterogeneous nucleation. At this higher temperature, the perovskite phase may be the preferred phase, so that in absence of the membrane, the perovskite phase is formed because heterogeneous nucleation is less likely.

Further, the direct heating procedure, in which the membrane was inserted into a pre-heated furnace, promotes nucleation of the perovskite phase because the rapid thermal processing bypasses the temperature range where the fluorite phase is kinetically stable. A small fraction of the fluorite phase was formed also during the direct heating procedure; however, by prolonged annealing time at 700 °C (up to 6 h) the fluorite phase transformed into the perovskite phase (figure 3d-f). The fluorite phase has a much higher tolerance for Pb deficiency than the perovskite

phase,[18] so the complete transformation of the fluorite phase into the perovskite phase also shows that significant volatilization of Pb did not occur, although the precursor solution had a 1.00 Pb/Ti ratio and the nanotubes have a high surface/volume ratio. A standard approach to compensate for Pb loss during annealing of Pb-based ferroelectrics is addition of 5 - 25 mol% excess Pb to the precursor solution, or annealing in a Pb- or PbO-rich atmosphere.[18] In the previous reports of $PbTiO_3$ nanotubes made by sol-gel processing in AAO membranes, either a Pb/Ti ratio of 1.05 was used[4,6] or not specified,[3] or the annealing was performed in a Pb vapour-saturated atmosphere.[5] In contrast, this study shows that single-phase perovskite nanotubes can be obtained with an equimolar precursor solution, provided that a direct heating procedure is used during the annealing. Excessive lead is generally unwanted as it can diffuse into Pt electrodes and decrease the dielectric constant and the resistivity.[20]

The concentration of the sol did not significantly influence the morphology of the nanotubes (figure 4). This has also been reported by Hernandez-Sanchez *et al.*[4] Although the 1.35 mol/L sol was three times as concentrated as the 0.43 mol/L sol, the wall thicknesses estimated from the FESEM images were the same, 15 - 20 nm. It may be that the difference is too small to be observable by FESEM. More accurate estimation of the wall thickness can be obtained by using for example transmission electron microscopy. A possible explanation for the equal wall thickness is that the higher viscosity of the high concentration sol lowers the ability of the sol to penetrate the pores, especially for the long pores used here (60 μm), thus reducing the amount of material that is deposited in the pores. The wall thickness is most importantly affected by the pore diameter, as Zhao *et al.*[5] have shown that the wall thickness increased with the diameter of the nanotubes. From the results of Zhao *et al.*, a wall thickness of 10 – 15 % of the pore diameter is expected, which is consistent with the 20 nm wall thickness obtained in the 200 nm pore diameter membranes in the present study. To increase the wall thickness, successive coatings of the template can be used, but the fragile nature of the AAO membranes makes this difficult.[4] Increasing the immersion time can also be an alternative, as Zhang *et al.*[10] reported the synthesis of PZT nanowires in a 45 nm AAO membrane using a long sol immersion time of 5 h. However, to synthesize $PbTiO_3$ or PZT nanowires instead of nanotubes in AAO membranes, growth by a particle-directing method such as electrophoresis[21] or growth from aqueous salt solutions[7] is probably more suitable.

The commercial Whatman Anodisc membranes that were used in this work have most likely been produced by a one-step procedure, in which the aluminium film has only been anodized once. By a two-step procedure, a much better control of the pore diameter and pore distribution can be obtained, with a constant pore diameter throughout the membrane.[22] Therefore, to make nanotubes with diameters below 200 nm, it is necessary with a more careful preparation of the membrane templates.

Conclusions

$PbTiO_3$ nanotubes with diameters of 200 - 400 nm were successfully prepared by a template-assisted method. Direct heating at 700 °C for 6 h was shown to be

sufficient to obtain single-phase perovskite nanotubes from an equimolar precursor solution, avoiding the addition of excess lead or annealing in a Pb-rich atmosphere. Variation of the sol concentration did not significantly affect the wall thickness of the nanotubes. Large internal pores in the Anodisc membranes with nominal pore diameters of 20 nm and 100 nm prevented the formation of nanotubes with smaller diameters.

Acknowledgements

A research stay at Osaka Prefecture University for Per Martin Rørvik was financially supported by the International Section at the Norwegian University of Science and Technology (NTNU) and the Scandinavia-Japan Sasakawa Foundation. This work was additionally financially supported by the Strategic Area of Materials at NTNU.

References and footnotes

1. G. Cao and D. Liu, "Template-based synthesis of nanorod, nanowire, and nanotube arrays", *Adv. Colloid Interfac.*, 2008, 136, 45-64.
2. C. Bae, H. Yoo, S. Kim, K. Lee, J. Kim, M. M. Sung, and H. Shin, "Template-Directed Synthesis of Oxide Nanotubes: Fabrication, Characterization, and Applications", *Chem. Mater.*, 2008, 20, 756-767.
3. B. A. Hernandez, K.-S. Chang, E. R. Fischer, and P. K. Dorhout, "Sol-Gel Template Synthesis and Characterization of $BaTiO_3$ and $PbTiO_3$ Nanotubes", *Chem. Mater.*, 2002, 14, 480-482.
4. B. A. Hernandez-Sanchez, K.-S. Chang, M. T. Scancella, J. L. Burris, S. Kohli, E. R. Fischer, and P. K. Dorhout, "Examination of Size-Induced Ferroelectric Phase Transitions in Template Synthesized $PbTiO_3$ Nanotubes and Nanofibers", *Chem. Mater.*, 2005, 17, 5909-5919.
5. L. Zhao, M. Steinhart, J. Yu, and U. Gösele, "Lead titanate nano- and microtubes", *J. Mater. Res.*, 2006, 21, 685-690.
6. L. Liu, T. Ning, Y. Ren, Z. Sun, F. Wang, W. Zhou, S. Xie, L. Song, S. Luo, D. Liu, J. Shen, W. Ma, and Y. Zhou, "Synthesis, characterization, photoluminescence and ferroelectric properties of $PbTiO_3$ nanotube arrays", *Mat. Sci. Eng. B*, 2008, 149, 41-46.
7. M. C. Hsu, I. C. Leu, Y. M. Sun, and M. H. Hon, "Template synthesis and characterization of $PbTiO_3$ nanowire arrays from aqueous solution", *J. Solid State Chem.*, 2006, 179, 1421-1425.
8. Y. Luo, I. Szafraniak, N. D. Zakharov, V. Nagarajan, M. Steinhart, R. B. Wehrspohn, J. H. Wendorff, R. Ramesh, and M. Alexe, "Nanoshell tubes of ferroelectric lead zirconate titanate and barium titanate", *Appl. Phys. Lett.*, 2003, 83, 440-442.
9. F. D. Morrison, Y. Luo, I. Szafraniak, V. Nagarajan, R. B. Wehrspohn, M. Steinhart, J. H. Wendorff, N. D. Zakharov, E. D. Mishina, K. A. Vorotilov, A. S. Sigov, S. Nakabayashi, M. Alexe, R. Ramesh, and J. F. Scott, "Ferroelectric nanotubes", *Rev. Adv. Mater. Sci.*, 2003, 4, 114-122.

10. X. Y. Zhang, X. Zhao, C. W. Lai, J. Wang, X. G. Tang, and J. Y. Dai, "Synthesis and piezoresponse of highly ordered $Pb(Zr_{0.53}Ti_{0.47})O_3$ nanowire arrays", *Appl. Phys. Lett.*, 2004, 85, 4190-4192.
11. O. M. Zhigalina, E. D. Mishina, N. E. Sherstyuk, K. A. Vorotilov, V. A. Vasiljev, A. S. Sigov, O. I. Lebedev, Yu. V. Grigoriev, M. P. De Santo, R. Barberi, and Th. Rasing, "Crystallization of PZT in Porous Alumina Membrane Channels", *Ferroelectrics*, 2006, 336, 247-254.
12. M. Liu, X. Li, H. Imrane, Y. Chen, T. Goodrich, Z. Cai, K. S. Ziemer, J. Y. Huang, and N. X. Sun, "Synthesis of ordered arrays of multiferroic $NiFe_2O_4$-$Pb(Zr_{0.52}Ti_{0.48})O_3$ core-shell nanowires", *Appl. Phys. Lett.*, 2007, 90, 152501.
13. S. A. Yang, K. O. Jeong, J. Kim, Y. C. Choi, J. K. Han, and S. D. Bu, "Synthesis of PZT Nanotubes and Its Nanometer-Scale Shape Modification with an Electron-Beam Irradiation", *J. Korean Phys. Soc.*, 2007, 51, S174-S177.
14. J. Kim, S. A. Yang, Y. C. Choi, J. K. Han, K. O. Jeong, Y. J. Yun, D. J. Kim, S. M. Yang, D. Yoon, H. Cheong, K.-S. Chang, T. W. Noh, and S. D. Bu, "Ferroelectricity in Highly Ordered Arrays of Ultra-Thin-Walled $Pb(Zr,Ti)O_3$ Nanotubes Composed of Nanometer-Sized Perovskite Crystallites", *Nano Lett.*, 2008, 8, 1813-1818.
15. A. Nourmohammadi, M. A. Bahrevar, S. Schulze, and M. Hietschold, "Electrodeposition of lead zirconate titanate nanotubes", *J. Mater. Sci.*, 2008, 43, 4753-4759.
16. The oxygen-deficient fluorite and pyrochlore structures are closely related for the phases of interest here ($Pb_2Ti_2O_6$). The defining difference between the two phases is the presence (pyrochlore) or absence (fluorite) of cationic ordering.[17] Such ordering is beyond the scope of the present study, and we will therefore refer to the non-ferroelectric metastable phase as "fluorite".
17. A. D. Polli, F. F. Lange, and C. G. Levi, "Metastability of the Fluorite, Pyrochlore, and Perovskite Structures in the PbO-ZrO_2-TiO_2 System", *J. Am. Ceram. Soc.*, 2000, 83, 873-881.
18. M. J. Lefevre, J. S. Speck, R. W. Schwartz, D. Dimos, and S. J. Lockwood, "Microstructural development in sol-gel derived lead zirconate titanate thin films: The role of precursor stoichiometry and processing environment", *J. Mater. Res.*, 1996, 11, 2076-2084.
19. R. W. Schwartz, "Chemical Solution Deposition of Perovskite Thin Films", *Chem. Mater.*, 1997, 9, 2325-2340.
20. G. L. Brennecka, C. M. Parish, B. A. Tuttle, L. N. Brewer, and M. A. Rodriguez, "Reversibility of the Perovskite-to-Fluorite Phase Transformation in Lead-Based Thin and Ultrathin Films", *Adv. Mater.*, 2008, 20, 1407-1411.
21. S. J. Limmer, S. Seraji, M. J. Forbess, Y. Wu, T. P. Chou, C. Nguyen, and G. Cao, "Electrophoretic Growth of Lead Zirconate Titanate Nanorods", *Adv. Mater.*, 2001, 13, 1269-1272.
22. A. P. Li, F. Müller, A. Birner, K. Nielsch, and U. Gösele, "Polycrystalline nanopore arrays with hexagonal ordering on aluminum", *J. Vac. Sci. Technol. A*, 1999, 17, 1428-1431.

Paper V

Paper V

Piezoresponse force microscopy studies of single $PbTiO_3$ nanorods

Per Martin Rørvik,[1] Chang Chuan You,[2] Thomas Tybell,[2] Tor Grande,[1] and Mari-Ann Einarsrud[1]

[1]Department of Materials Science and Engineering, Norwegian University of Science and Technology, 7491 Trondheim, Norway

[2]Department of Electronics and Telecommunications, Norwegian University of Science and Technology, 7491 Trondheim, Norway

Abstract

The piezoelectric properties of single $PbTiO_3$ nanorods made by a hydrothermal method have been studied by piezoresponse force microscopy in both vertical and lateral mode. Piezoelectric activity and polarization switching was observed in the vertical mode, demonstrating the ferroelectric nature of the nanorods. The nanorods decomposed after repeated cycling of the dc bias at one spot on the nanorod, which resulted in parts of the nanorod disappearing and/or accumulation of particles on the surface of the nanorod.

Introduction

Lead titanate ($PbTiO_3$) is a prototype displacive ferroelectric material with the perovskite structure and with a Curie temperature (T_C) of 490 °C. $PbTiO_3$ has a high spontaneous polarization of 75 μC/cm^2.[1] The study of nanoscale properties of $PbTiO_3$, such as the critical size for ferroelectricity, has mainly been concentrated on zero-dimensional nanoparticles[2] and two-dimensional thin films,[3] while investigations of ferroelectricity in one-dimensional (1D) $PbTiO_3$ nanostructures, such as nanorods, nanowires and nanotubes, are scarce. A reason for this is the difficulty of preparing high quality 1D nanostructures of $PbTiO_3$, especially single-crystalline nanostructures, which are the most interesting for fundamental ferroelectric studies. Single-crystalline $PbTiO_3$ nanowires and nanorods with the perovskite structure have been successfully made by hydrothermal synthesis methods,[4-9] in which the synthesis takes place far below T_C, typically at 180 - 200 °C. These nanowires and nanorods have the polar [001] direction of the tetragonal perovskite structure oriented along the length direction, and are thus ideal for the study of ferroelectricity in 1D $PbTiO_3$.

For nanoscale characterization of ferroelectric and piezoelectric properties of materials, the most used and applicable technique is scanning probe microscopy (SPM), especially piezoresponse force microscopy (PFM).[10,11] The high spatial resolution, easy implementation, effective manipulation and control of nanoscale domains and local spectroscopy capabilities make PFM a well-suited tool for nanoscale ferroelectric studies. PFM is used both for imaging and for non-imaging spectroscopy studies.[10,11] In PFM, a conductive atomic force microscopy (AFM) probe tip is brought into contact with the sample top surface in contact mode. An ac bias is applied between the probe and the conductive sample back surface, which induces local oscillatory structural deformation because of the converse piezoelectric effect. This deformation is measured through a lock-in amplifier. PFM can be operated in two modes, vertical and lateral (figure 1). In the vertical PFM mode, the induced local vertical deformation is measured through the vertical

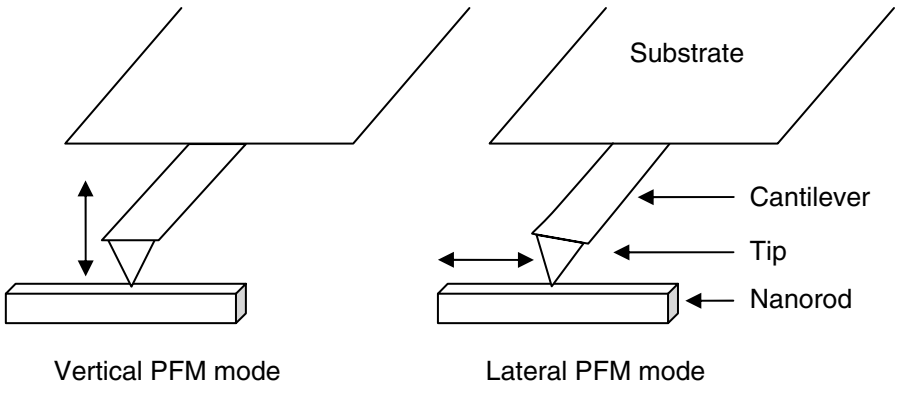

Figure 1. Schematic illustration of the vertical and lateral modes of PFM in the study of a single nanorod, with the three major components of the AFM probe.

deflection of the AFM cantilever and the out-of-plane polarization is studied, while in the lateral PFM mode, the local shear deformation of the sample is measured through the torsional twisting of the AFM cantilever and the in-plane polarization is studied.[10-12] Correct quantitative results from PFM studies are difficult to obtain and requires complex calibration, because the electrical field is not uniform, as a consequence of the geometry of the tip as an electrode.[11,13,14]

The study of ferroelectricity and piezoelectricity in single-crystalline 1D nanostructures of ferroelectric perovskites using SPM techniques have been reported by a few research groups. Yun *et al.*[15,16] and Bao *et al.*[17] have studied the radial ferroelectric response in $BaTiO_3$ nanowires using electrostatic force microscopy (EFM). Wang *et al.* have studied $BaTiO_3$ nanowires both with conventional PFM[12] and with an axial dc bias PFM setup.[18,19] Other 1D nanostructures that have been studied using conventional PFM are $PbZr_{1-x}Ti_xO_3$ (PZT) nanowires,[13] $KNbO_3$ and $KNb_{1-x}Ta_xO_3$ nanorods,[14] and $NaNbO_3$ nanorods.[20] The present study is thus the first PFM study of single-crystalline $PbTiO_3$ nanorods.

Experimental

The $PbTiO_3$ nanorods were synthesized by a hydrothermal method as previously reported.[7,8] Briefly, an amorphous $PbTiO_3$ precursor was hydrothermally treated at 180 °C for 48 h in the presence of a surfactant (sodium dodecylbenzenesulfonate). The dispersion volume was 50 mL and the surfactant/Pb molar ratio was 1.5:1. The product was washed in distilled water and ethanol, dried at 100 °C, and then annealed at 350 °C or 600 °C for 6 h. The annealing procedure was performed to remove protons (water) incorporated in the structure,[21] to remove adsorbed surfactant molecules, and to remove defects originating from the growth process. A dispersion of the product was made by adding 0.1 g of the product into 30 mL ethanol (96 %). The dispersion was sonicated by an ultrasonic probe for 5 min at 10 % amplitude (Branson Digital Sonifier). The larger particles in the dispersion (microspheres[7,8]) were removed by decanting after sedimentation for 1 h. The nanorod dispersion was dropped onto a gold film on a silicon substrate. To make the gold film, a layer of 10 nm Ti and thereafter a layer of 50 nm Au was electron beam evaporated (Pfeiffer Vacuum Classic 500) onto a 4 inch silicon wafer (V.S.I.). The wafer was cut into ~8 × 8 mm^2 substrates.

The ferroelectric and piezoelectric properties of individual $PbTiO_3$ nanorods dispersed on gold films were studied by PFM using a Veeco Multimode V AFM equipped with a NanoScope V controller and a signal access module. The probes used were platinum/iridium-coated Veeco SCM-PIT probes with nominal force constant of 2.8 N/m. Previous to the PFM study, the samples were studied with field emission scanning electron microscopy (FESEM, Zeiss Ultra 55) to locate single nanorods that were suitable for PFM study. Since the polar direction of the nanorods was along the length direction,[7-9,22] the torsional force afflicted onto the tip in lateral PFM mode was maximized by aligning the samples such that the nanorod length direction was perpendicular to the AFM cantilever length direction (figure 1). The surface of the sample was examined in tapping mode to locate the nanorods. For the spectroscopic PFM measurements, the tip was placed at the desired spot on the nanorod with zero scan size, and the mode was switched to

contact mode (tapping mode deflection). The piezoresponse amplitude and phase signals were measured while sweeping the dc bias between -10 V and +10 V, using an ac bias with amplitude of 1 - 5 V and frequency of typically 3 kHz. The PFM amplitude and phase signals were detected through an external lock-in amplifier (Stanford Research Systems SR830 DSP). The dc bias sweep time was 100 s for one cycle. 128 points were measured both on the approach line and the retract line. After the PFM study, the nanorods were re-examined by FESEM.

Results

Figure 2 shows the spectroscopic PFM studies from a spot on a nanorod that had been annealed at 600 °C. Cycle number 6 (lateral) and 7 (vertical) are shown. In the lateral direction, no hysteresis was observed. In the vertical direction, clear hysteresis loops were observed, both a "butterfly"-shaped amplitude loop, and a phase loop with hysteresis. The same response was achieved also after repeated

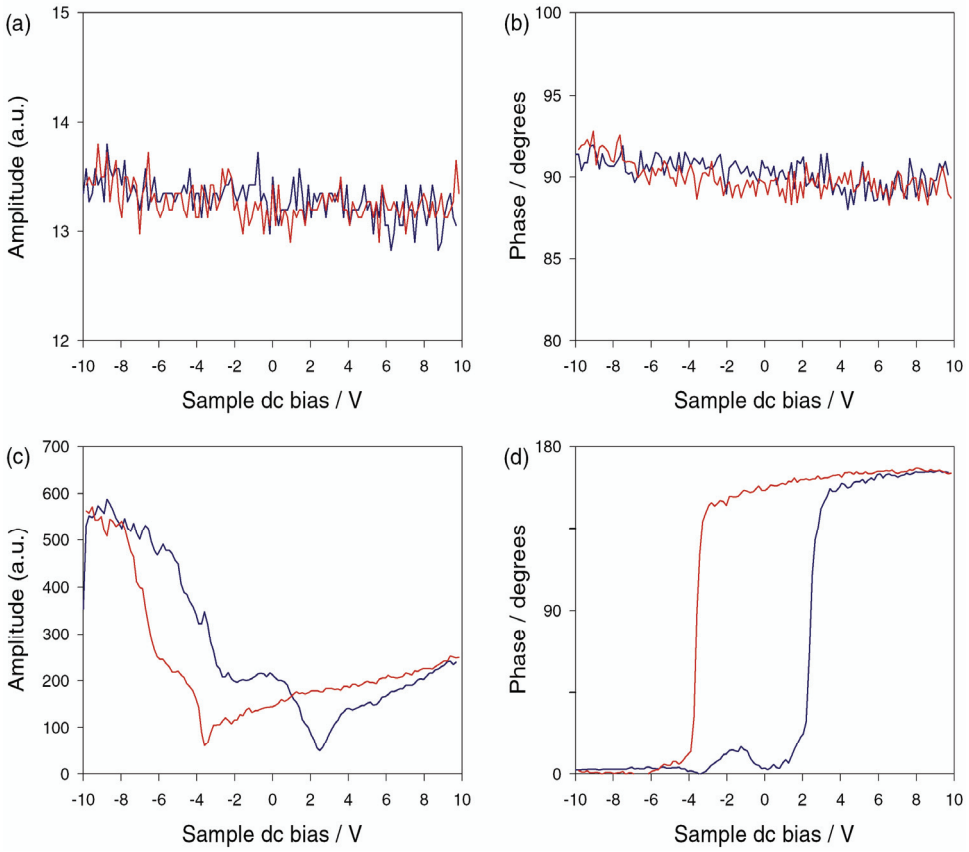

Figure 2. Spectroscopic PFM study of a single $PbTiO_3$ nanorod annealed at 600 °C. (a) Lateral PFM amplitude response. (b) Lateral PFM phase response. (c) Vertical PFM amplitude loop. (d) Vertical PFM phase loop. All measurements were performed on the same spot on the nanorod. The blue lines indicate the approach lines (from -10 V to +10 V) and the red lines the retract lines.

cycling at the same spot on the nanorod. In total 30 cycles were performed at this spot. The amplitude loop in figure 2c does not have a perfect butterfly shape, as the amplitude at the positive dc bias side is lower than that of the negative side. The exact cause of this is uncertain. The piezoelectric response in the vertical direction is contrary to what was expected, as the as-synthesized nanorods have been demonstrated to have the polar direction (the [001] direction in the tetragonal perovskite structure) along the length direction,[7-9,22] which should give piezoelectric response in the lateral direction. Nevertheless, the important facts are that the polarization of nanorods could be switched and that the nanorods showed piezoelectric activity.

In figure 3, FESEM images taken before and after the PFM study of the nanorod in figure 2, and topographic AFM images taken after the spectroscopic PFM measurements, are shown. Figure 3c shows an AFM image, taken directly after the spectroscopic measurements of figure 2 were recorded. In that image, the

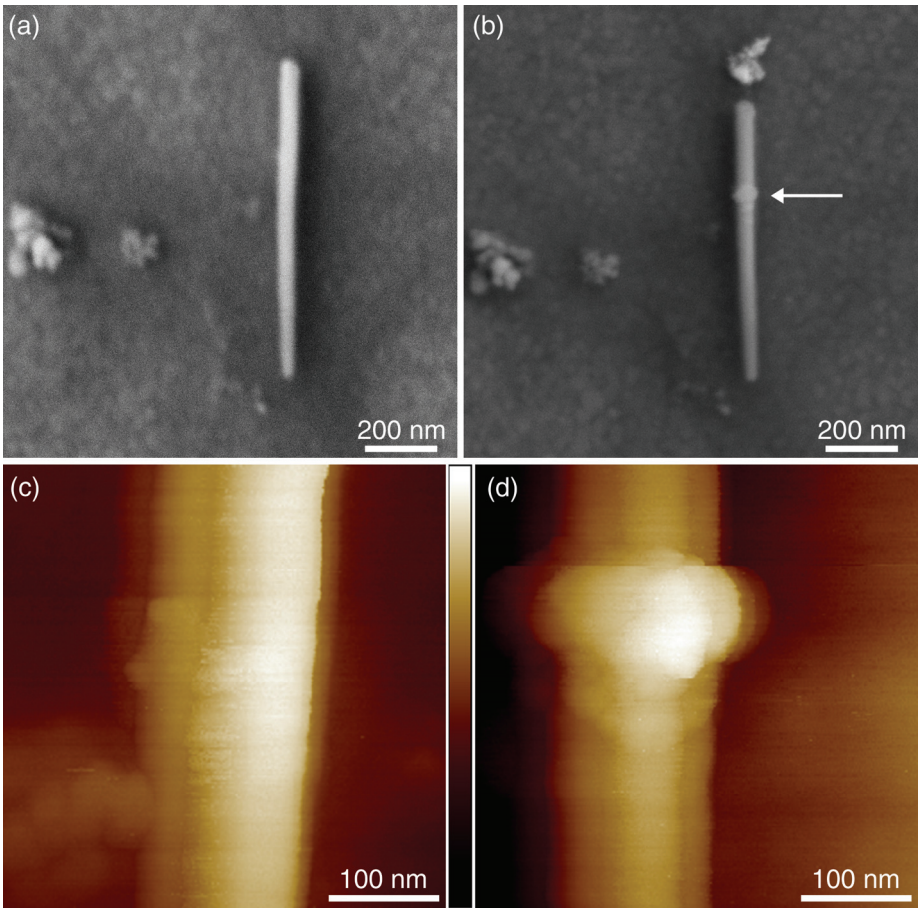

Figure 3. (a)-(b) FESEM images of a $PbTiO_3$ nanorod annealed at 600 °C, taken before (a) and after (b) the PFM study. (c)-(d) Topography AFM images from the same spot of the $PbTiO_3$ nanorod after 7 cycles (c) and after 30 cycles (d). The accumulation of particles in (d) is the same as indicated by the arrow in (b). The colour of the scale bar in between (c) and (d) indicates 0 - 150 nm height.

surface of the nanorod appears smooth, which demonstrates that the spectroscopic PFM measurements shown in figure 2 were measured on a smooth area of the nanorod. In comparison, figure 3d shows the same area of the nanorod, after 23 more cycles had been recorded from the same spot on the nanorod. In figure 3d it is evident that an accumulation of particles had taken place at the surface of the nanorod. The spectroscopic measurements that was taken just before the AFM image in figure 3d was recorded, which can then be assumed to have been measured at the accumulation of particles, actually also showed hysteresis in the vertical direction, but not in the lateral direction, just as shown in figure 2. This indicates that the nanorod was not completely decomposed beneath the accumulation of particles, as ferroelectric response was still observed, and/or that the accumulation of particles showed the same ferroelectric response as the nanorod.

A spot towards the top of the nanorod was also studied by PFM. The FESEM image taken after the PFM study (figure 3b) shows that at that spot the nanorod disintegrated completely. During the PFM study on both these spots, several cycles with the dc bias cycling between -10 V and +10 V were performed. However, as shown in figure 3c, the nanorod did not decompose at once. An additional observation from the FESEM and AFM images in figure 3, is that the diameter of the nanorods appears broader in the AFM images than in the FESEM images. This is caused by the geometry of the tip, and has also been observed by others.[13]

Nanorods that had been annealed at 350 °C were examined similarly to the nanorods that had been annealed at 600 °C. However, no clear hysteresis loops were observed in the spectroscopic PFM study, neither lateral nor vertical. Figure 4 shows FESEM and AFM images taken before and after the PFM study of a $PbTiO_3$ nanorod. In total 27 cycles were performed during the PFM study of the nanorod in figure 4. The response was either dielectric, or the hysteresis loops were very narrow or not saturated, or the response contained only low signal values (similar

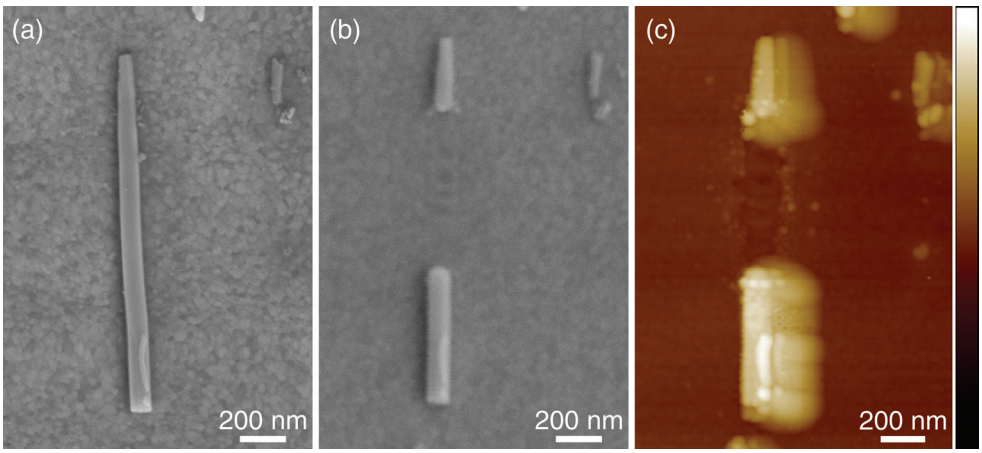

Figure 4. (a)-(b) FESEM images of a $PbTiO_3$ nanorod annealed at 350 °C, taken before (a) and after (b) the PFM study. (c) Topography AFM image of the $PbTiO_3$ nanorod, taken after the PFM study. The colour of the scale bar indicates 0 - 150 nm height.

to figure 2a and b). Decomposition or disintegration of the nanorods was also observed for the nanorods annealed at 350 °C. The absence of the middle part of the nanorod is evident in figure 4b and c; however, the positions of the remaining parts of the nanorod were the same as before the PFM study. During the PFM study, accumulation of particles was observed after several cycles, but the accumulated particles have evidently disappeared before the image in figure 4c was taken.

Discussion

The polarization switching and the hysteresis loops shown in figure 2, demonstrate the ferroelectric nature of the nanorods. The hysteresis in the vertical direction was contrary to what was expected, because the polar direction has been shown to be aligned along the length direction.[7-9,22] Hysteresis in the vertical direction of similar single-crystalline nanowires has also been observed by others. Yun *et al.* have shown vertical hysteresis in $BaTiO_3$ nanowires using the EFM technique.[15] However, the observation of ferroelectric behaviour in these $BaTiO_3$ nanowires is not without controversy. One of the possibilities is that the applied field resulted in the depletion of or accumulation of charge underneath the tip without actual ferroelectric switching.[10] Wang *et al*. observed hysteresis loop in the vertical direction of tapered PZT nanowires with the [001] direction along the length direction.[13] The response was explained by the geometry of the nanowires, with a tilt angle between the nanowire axis (polarization direction) and the horizontal substrate plane which lead to the manifestation of the out of plane polarization activity. Here, the nanorods were only very slightly tapered, so a tilt angle cannot explain the response, especially since the lateral PFM study did not give any piezoelectric response at all.

A more likely explanation for the vertical PFM response is that the domain structure of the nanorods changed after the annealing procedure, due to the transition from the paraelectric cubic phase to the ferroelectric tetragonal phase during cooling. Transmission electron microscopy investigations of annealed nanorods have not been performed in order to verify this theory. However, Schilling *et al*.[23] and Wang *et al*.[13] have shown that $BaTiO_3$ and PZT nanowires, respectively, can have 90° domain walls oriented 45° to the length direction of nanowires that have been annealed above T_C, resulting in possible polarization directions radial to the length direction. The nanorods presented here were synthesized far below T_C, directly into the tetragonal structure, and the domain structure in the as-synthesized nanorods may therefore not be the most stable domain structure.

Although hysteresis was observed for the nanorods that had been annealed at 600 °C, the PFM study of the nanorods that had been annealed at 350 °C did not show any hysteresis. Because of the lower annealing temperature, the incorporated protons may not have been removed to a sufficient degree, which can reduce the piezoelectric response of the nanorods, as the protons adversely affect the dielectric properties of the perovskites.[21] Other structural defects and adsorbed surfactant molecules will also be removed to a larger degree at 600 °C, than at 350 °C. However, one important conclusion that can be drawn from the lack of hysteresis loops for the nanorods annealed at 350 °C, is that the observed hysteresis loops in

figure 2c and d were not caused by depletion of or accumulation of charge underneath the tip caused by the applied field,[10] as such a charge depletion or accumulation would give the same response regardless of the annealing temperature of the nanorods.

In some of the PFM measurements that were done, especially of the 350 °C nanorods, very narrow hysteresis loops with unsaturated poling were obtained in the lateral direction. This indicates that the dc bias used was insufficient to saturate the polarization of the nanorods. In the present setup, the maximum dc bias was ±10 V, limited by the internal voltage supply. To increase the dc bias an external voltage supply would be necessary. These observations coincide with similar PFM studies of other nanowires. For instance, Wang *et al.*[12] used ±15 V in their study of $BaTiO_3$ nanowires, Wang *et al*.[13] used ±40 V in their study of PZT nanowires, and Suyal *et al*.[14] used ±50 V in their study of $KNbO_3$ nanorods.

The decomposition of the nanorods that took place after repeated cycling of the dc bias at the same spot of the nanorods is probably caused by the electric field, and not by the contact force of the tip. The decomposition happened after a number of cycles (figure 3c and d), which indicate that it was the repeated cycling of the polarization or at least the inflicted electric field, that caused the decomposition. The non-uniformity of the field in the conventional PFM setup used here may possibly enhance the decomposition, because of increased strain in the nanorod. An axial dc bias setup, as reported by Wang *et al*.,[18,19] gives a homogeneous polarization of the nanorod and is expected to be a better setup. An axial dc bias setup will anyway result in a better defined field, so that quantitative results will be easier obtained.

The decomposition of the nanorods may also be enhanced by the remaining defects in the structure, possibly originating from the growth by self-assembly of nanocrystals.[7-9] As both the nanorods that were annealed at 350 °C and at 600 °C decomposed, the heating/cooling of the nanorods across T_C, with rearrangement of domains and resulting strains, cannot explain the decomposition. For the use of these nanorods in applications, the decomposition after repeated cycling is of course unwanted, so methods to avoid such decomposition should be investigated.

Conclusions

Single-crystalline $PbTiO_3$ nanorods were studied by piezoresponse force microscopy. Piezoelectric activity was observed perpendicular to the length direction of the nanorods that had been annealed at 600 °C, and it was shown that the polarization could be switched. The ferroelectric nature of the nanorods was thus demonstrated. The nanorods decomposed after repeated cycling of the dc bias at one spot on the nanorod, which resulted in parts of the nanorod disappearing and/or accumulation of particles on the top of the nanorod.

Acknowledgements

The authors wish to thank Ørnulf Nordseth for help with the electron beam evaporation of the gold film. This work was financially supported by the Strategic Area of Materials at the Norwegian University of Science and Technology, and the Research Council of Norway (NANOMAT, Grant no. 158518/431).

References

1. K. M. Rabe, M. Dawber, C. Lichtensteiger, C. H. Ahn, and J.-M. Triscone, "Modern Physics of Ferroelectrics: Essential Background", in "Physics of Ferroelectrics: A Modern Perspective", eds. K. M. Rabe, C. H. Ahn, and J.-M. Triscone, in the book series "Topics in Applied Physics", Springer, Berlin/Heidelberg, 2007, volume 105, p. 1-30.
2. E. Erdem, H.-C. Semmelhack, R. Böttcher, H. Rumpf, J. Banys, A. Matthes, H.-J. Gläsel, D. Hirsch, and E. Hartmann, "Study of the tetragonal-to-cubic phase transition in $PbTiO_3$ nanopowders", *J. Phys.: Condens. Matter*, 2006, 18, 3861-3874.
3. D. D. Fong, G. B. Stephenson, S. K. Streiffer, J. A. Eastman, O. Auciello, P. H. Fuoss, and C. Thompson, "Ferroelectricity in Ultrathin Perovskite Films", *Science*, 2004, 304, 1650-1653.
4. Y. Hu, H. Gu, X. Sun, J. You, and J. Wang, "Photoluminescence and Raman scattering studies on $PbTiO_3$ nanowires fabricated by hydrothermal method at low temperature", *Appl. Phys. Lett.*, 2006, 88, 193120.
5. H. Gu, Y. Hu, J. You, Z. Hu, Y. Yuan, and T. Zhang, "Characterization of single-crystalline $PbTiO_3$ nanowire growth via surfactant-free hydrothermal method", *J. Appl. Phys.*, 2007, 101, 024319.
6. H. Gu, Y. Hu, H. Wang, X. Yang, Z. Hu, Y. Yuan, and J. You, "Fabrication of lead titanate single crystalline nanowires by hydrothermal method and their characterization", *J. Sol-Gel Sci. Techn.*, 2007, 42, 293-297.
7. G. Wang, R. Sæterli, P. M. Rørvik, A. van Helvoort, R. Holmestad, T. Grande, and M.-A. Einarsrud, "Hierarchical Nanostructures of $PbTiO_3$ Through Mesocrystal Formation", *J. Nanosci. Nanotechnol.*, 2007, 7, 2538-2541. (Appendix I)
8. G. Wang, R. Sæterli, P. M. Rørvik, A. T. J. van Helvoort, R. Holmestad, T. Grande, and M.-A. Einarsrud, "Self-Assembled Growth of $PbTiO_3$ Nanoparticles into Microspheres and Bur-like Structures", *Chem. Mater.*, 2007, 19, 2213-2221. (Appendix II)
9. P. M. Rørvik, Å. Almli, A. T. J. van Helvoort, R. Holmestad, T. Tybell, T. Grande, and M.-A. Einarsrud, "$PbTiO_3$ nanorod arrays grown by self-assembly of nanocrystals", *Nanotechnology*, 2008, 19, 225605. (Paper II)
10. A. Gruverman and A. Kholkin, "Nanoscale ferroelectrics: processing, characterization and future trends", *Rep. Prog. Phys.*, 2006, 69, 2443-2474.

11. S. V. Kalinin, A. Rar, and S. Jesse, “A Decade of Piezoresponse Force Microscopy: Progress, Challenges and Oppurtunities”, *IEEE T. Ultrason. Ferr.*, 2006, 53, 2226-2252.
12. Z. Wang, J. Hu, and M.-F. Yu, “One-dimensional ferroelectric monodomain formation in single crystalline $BaTiO_3$ nanowire”, *Appl. Phys. Lett.*, 2006, 89, 263119.
13. J. Wang, C. S. Sandu, E. Colla, Y. Wang, W. Ma, R. Gysel, H. J. Trodahl, N. Setter, and M. Kuball, “Ferroelectric domains and piezoelectricity in monocrystalline $Pb(Zr,Ti)O_3$ nanowires”, *Appl. Phys. Lett.*, 2007, 90, 133107.
14. G. Suyal, E. Colla, R. Gysel, M. Cantoni, and N. Setter, “Piezoelectric Response and Polarization Switching in Small Anisotropic Perovskite Particles”, *Nano. Lett.*, 2004, 4, 1339-1342.
15. W. S. Yun, J. J. Urban, Q. Gu, and H. Park, “Ferroelectric Properties of Individual Barium Titanate Nanowires Investigated by Scanned Probe Microscopy”, *Nano Lett.*, 2002, 2, 447-450.
16. J. E. Spanier, A. M. Kolpak, J. J. Urban, I. Grinberg, L. Ouyang, W. S. Yun, A. M. Rappe, and H. Park, “Ferroelectric Phase Transition in Individual Single-Crystalline $BaTiO_3$ Nanowires”, *Nano Lett.*, 2006, 6, 735-739.
17. N. Bao, L. Shen, G. Srinivasan, K. Yanagisawa, and A. Gupta, “Shape-Controlled Monocrystalline Ferroelectric Barium Titanate Nanostructures: From Nanotubes and Nanowires to Ordered Nanostructures”, *J. Phys. Chem. C*, 2008, 112, 8634-8642.
18. Z. Wang, A. P. Suryavanshi, and M.-F. Yu, “Ferroelectric and piezoelectric behaviours of individual single crystalline $BaTiO_3$ nanowire under direct axial electric biasing”, *Appl. Phys. Lett.*, 2006, 89, 082903.
19. Z. Wang, J. Hu, and M.-F. Yu, “Axial polarization switching in ferroelectric $BaTiO_3$ nanowire”, *Nanotechnology*, 2007, 18, 235203.
20. T.-Y. Ke, H.-A. Chen, H.-S. Sheu, J.-W. Yeh, H.-N. Lin, C.-Y. Lee, and H.-T. Chiu, “Sodium Niobate Nanowire and Its Piezoelectricity”, *J. Phys. Chem. C*, 2008, 112, 8827-8831.
21. F. F. Lange and G. K. L. Goh, “Hydrothermal epitaxial growth of perovskite films”, *J. Ceram. Proc. Res.*, 2001, 2, 4-8.
22. R. Sæterli, A. T. J. van Helvoort, G. Wang, P. M. Rørvik, B. S. Tanem, T. Grande, M.-A. Einarsrud, and R. Holmestad, “Detailed TEM characterization of $PbTiO_3$ nanorods”, *J. Phys.: Conf. Ser.*, 2008, 126, 012010. (Appendix III)
23. A. Schilling, R. M. Bowman, G. Catalan, J. F. Scott, and J. M. Gregg, “Morphological Control of Polar Orientation in Single-Crystal Ferroelectric Nanowires”, *Nano Lett.*, 2007, 7, 3787-3791.

Paper VI

Paper VI

Electron beam induced deposition of platinum for contacting nanorods

Per Martin Rørvik,[1] Thomas Tybell,[2] Tor Grande,[1] and Mari-Ann Einarsrud[1]

[1]Department of Materials Science and Engineering, Norwegian University of Science and Technology, 7491 Trondheim, Norway

[2]Department of Electronics and Telecommunications, Norwegian University of Science and Technology, 7491 Trondheim, Norway

Abstract

Electron beam induced deposition has been used to deposit platinum from a (trimethyl)methylcyclopentadienylplatinum(IV) molecular precursor. A home-made apparatus was constructed for the purpose and was mounted onto a JEOL JSM-840 scanning electron microscope. Calculations based on apparatus geometry and molecular flow were used to estimate the deposition time and the height of the deposits. The location and height of the deposits were controlled so that single nanorods could be successfully contacted at the ends of the nanorods.

Introduction

Electron beam induced deposition (EBID) is a process by which a solid material can be deposited onto a solid substrate by means of an electron-mediated decomposition of a precursor molecule. Typically, the precursor is a vapour, but EBID may also be performed using a liquid or viscous solid condensed on the substrate. An ideal EBID process can be visualized as shown in figure 1, where an electron beam dissociates a precursor species resulting in a solid deposit on the substrate and a volatile by-product, which subsequently desorbs from the surface.[1]

Controlled EBID must be performed in a vacuum environment to reduce electron scattering and deposit contamination. The most common EBID setup uses a modified scanning electron microscope (SEM), and an organometallic molecule as precursor. Perhaps the most well-studied EBID deposition material is tungsten, but many other metals have also been deposited. The recent review by Randolph *et al.*[1] gives a comprehensive introduction to EBID and the associated electron beam induced etching process.

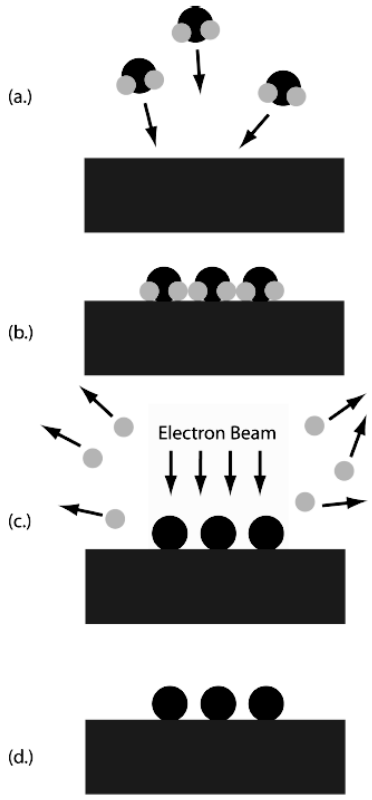

Figure 1. Schematic illustration of an ideal EBID process. A precursor vapour is introduced to a substrate (a) and absorbs to the surface (b). The substrate is exposed to an electron beam in the region of the incident vapour plume, inducing a dissociation reaction (c) and resulting in a solid deposit and a volatile by-product (d). The figure is adopted from Randolph *et al.*[1]

The purpose of this study was to develop a method to contact the ends of single $PbTiO_3$ nanorods onto gold electrodes. This contacting was necessary for the successful characterization of the piezoelectric properties of the nanorods by piezoresponse force microscopy, using an axial dc bias setup.

Experimental

The EBID apparatus used in this work was constructed for depositing platinum from a solid precursor material. The bottom part of an energy dispersive X-ray spectrometer detector was rebuilt with a precursor container, specified tube diameters and a nozzle. The EBID apparatus was mounted on a JEOL JSM-840 SEM (see figure 2).

The inner tube could be taken out of the EBID apparatus separately to refill precursor material into the container. The refilling was done in a glove bag filled with argon gas (5.0 quality). Some relevant parameters for the apparatus as used in this work are given in table 1.

The tube opening of both the inner and outer tube was located off-centre, thus, the gas flow could be opened and shut by rotating the outer tube. The nozzle was placed so that there was a 1 mm distance between the substrate surface and the bottom of the nozzle tip. The working distance of the microscope was 10 - 11 mm. The nozzle angle was fixed at 31° to reduce the working distance as much as possible without having the nozzle colliding with the polepiece. A photograph of the inside of the microscope chamber is shown in figure 3.

An organometallic platinum compound, (trimethyl)methylcyclopentadienyl-platinum(IV) (Aldrich, 98 %, 2 g glass container with plastic lid), was used as the

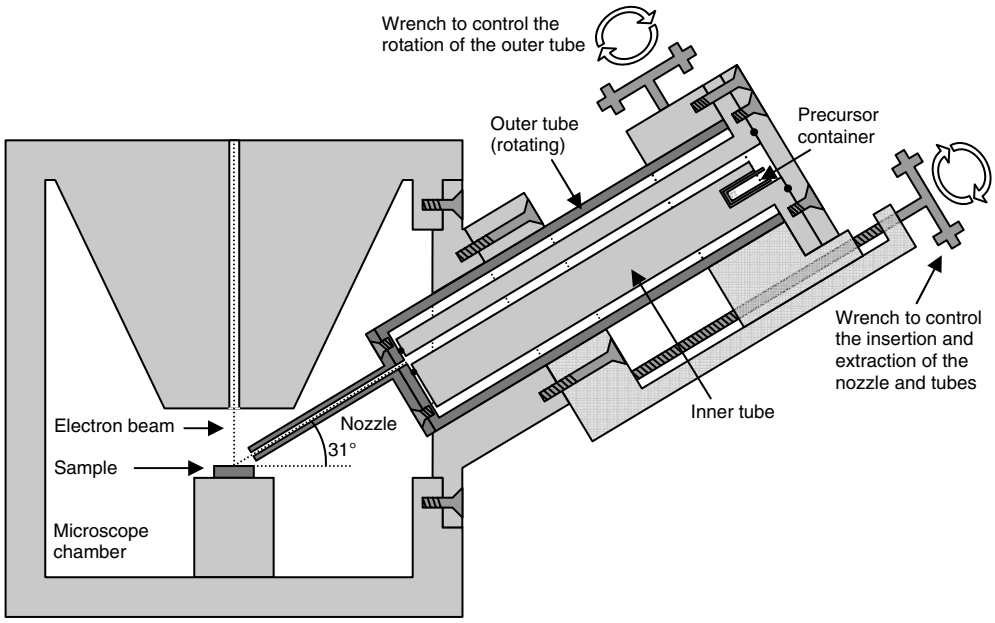

Figure 2. Schematic cross-section illustration of the EBID apparatus mounted on the SEM.

Table 1. EBID apparatus data

Quantity	Value
Inner diameter nozzle, d	0.060 cm
Outer diameter nozzle	0.115 cm
Length nozzle, l	5.0 cm
Inner diameter, inner tube	0.3 cm
Volume of void in the inner tube (gas opening, precursor container and compartment), V	~1.2 cm^3
Nozzle angle, α	31°
Clearance between substrate and nozzle, a	1 mm
Working distance	10 - 11 mm

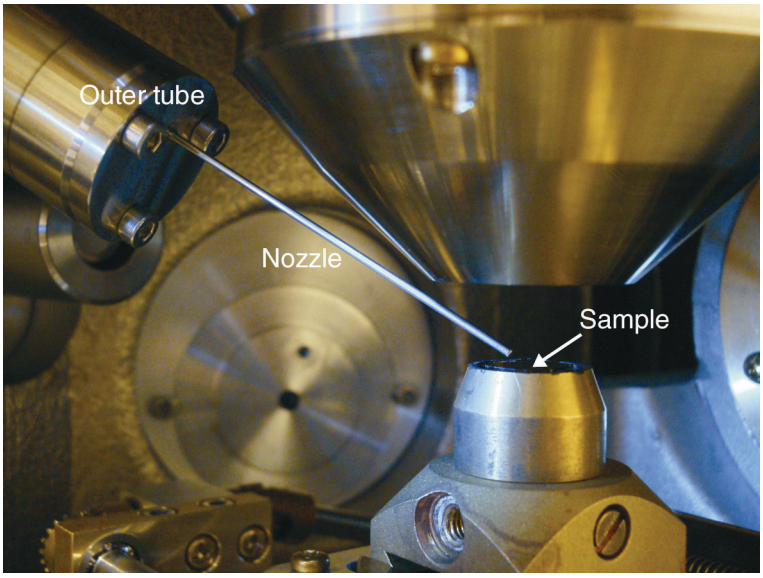

Figure 3. Photograph of the inside of the microscope chamber with the EBID apparatus in operating position.

precursor. Relevant data for this precursor is given in table 2. The precursor is sensitive to oxidizing conditions, so the precursor container was only opened in argon atmosphere inside a glove bag.

Table 2. Data for (trimethyl)methylcyclopentadienylplatinum(IV)

Quantity	Value	Reference
CAS number	94442-22-5	
Molar mass, M	319.32 g/mol	
Vapour pressure	0.0706 mbar at 23 °C	3
Melting point	29.5 - 30.0 °C	3

For the depositions, an accelerating voltage of 25 kV, a probe current of 1×10^{-9} A, and an emission current of approximately 125 μA were used. Approximately 50 mg precursor was used for each deposition session. The scanned sample area was reduced to typically 150 × 200 nm, and the outer tube was thereafter rotated to open for gas flow through the nozzle. The deposition time was varied from 10 to 60 min. After the desired length of time, the outer tube was rotated to stop the gas flow. During the deposition, the position of the scanned area was monitored and adjusted manually for drift in the system.

The morphology of the deposits was studied using a Hitachi S-3400N SEM. The element composition of the deposits was studied using energy-dispersive X-ray spectroscopy (EDS) in the Hitachi SEM.

For the contacting of nanorods, a silicon substrate with patterned gold structures was used. A droplet of a dispersion of $PbTiO_3$ nanorods in ethanol was placed on the substrate. After the ethanol had evaporated, nanorods that were placed between two gold electrodes were located by SEM. The deposition was carried out as described above, with the scanned area at the end of the nanorod. The deposition time was 10 min for the nanorod end deposits.

Calculations of EBID system design

The following calculations were helpful for the design and use of the EBID system. A schematic drawing of the EBID system that is relevant for the molecular flow calculations is given in figure 4.

The mean free path (λ) of molecules in a gas is given by:[3]

$$\lambda = \frac{k \cdot T}{\sqrt{2} \cdot \sigma \cdot p} \tag{1}$$

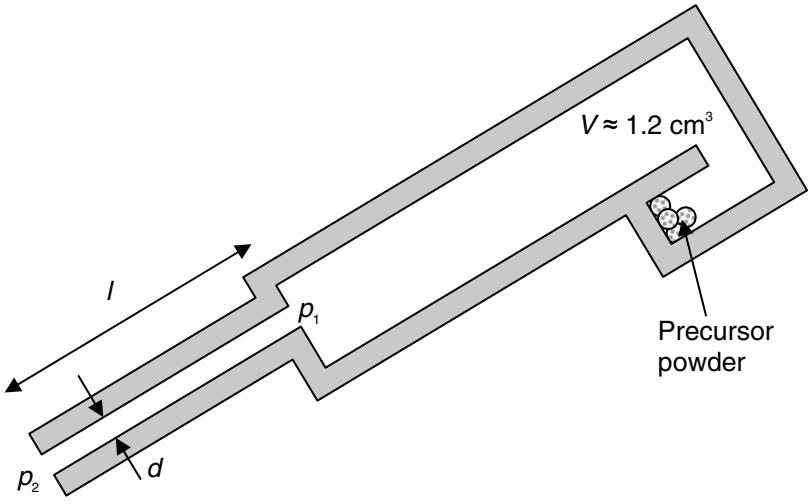

Figure 4. Schematic illustration of the EBID system with the nozzle and the void, with the relevant parameters for the molecular flow calculations.

where k is Boltzmann's constant, T temperature, σ collision cross-section and p pressure. In a tube or nozzle, if the mean free path is significantly shorter than the diameter viscous flow will dominate (molecule-molecule interactions). If the mean free path is significantly longer than the dimensions of the tube or nozzle, then molecular flow will dominate (molecule-wall interactions). Here, the inner diameter of the inner tube (3 mm) was significantly larger than the inner diameter of the nozzle (0.6 mm), therefore, the nozzle was the diffusion limiting part of the system. The inner tube and the precursor container were therefore considered as a void containing the precursor gas molecules, and the flow calculations were based on the nozzle geometry.

The Knudsen equation can be used to calculate the conductance (C) for both the viscous and molecular flow regimes and the transition between them:[4]

$$C = 135\frac{d^4}{l}\bar{p} + 12.1\frac{d^3}{l}\cdot\frac{1+192d\cdot\bar{p}}{1+237d\cdot\bar{p}} \text{ [L/s]} \quad (2)$$

$$\bar{p} = \frac{p_1 + p_2}{2} \quad (3)$$

Here d is the inner nozzle diameter in cm, l the nozzle length in cm ($l \geq 10\ d$), p_1 the pressure at the beginning of the nozzle (in mbar) and p_2 the pressure at the end of the nozzle (in mbar) (valid for air at 20 °C). The conductance in a nozzle connected to a closed container, as here, will decrease over time, as p_1 decreases. The exact determination of the conductance as a function of time in this situation will thus lead to solving a differential equation. However, after a certain time enough gas molecules will have diffused through the nozzle to reduce the pressure in the container to a level such that the molecular flow regime is reached. The conductance below the limit for molecular flow ($d\cdot\bar{p} < 10^{-2}$ mbar cm) can be derived from equation 2 and is described by:[4]

$$C = 12.1\cdot\frac{d^3}{l} \text{ [L/s]} \quad (4)$$

The conductance in the molecular flow regime is thus independent of the pressure difference. From the nozzle dimensions in table 1, this conductance was calculated as 0.523 cm^3/s.

As the volume of the void in the inner tube and precursor container is ~1.2 cm^3 (table 1), the molecular flow regime will be reached within seconds of opening the valve. The argon gas initially present will quickly diffuse through the nozzle. The pressure at the beginning of the tube, p_1, will therefore become equal to the vapour pressure of the precursor, 0.0706 mbar (table 2). The ideal deposition time available for a given mass of precursor material, t_{max}, can thus be calculated:

$$t_{max} = \frac{m\cdot R\cdot T}{M\cdot C\cdot p_1} \quad (5)$$

Here m is the mass of solid precursor material, R the gas constant, and M the molar mass of the precursor. For instance, 50 mg of precursor will result in a deposition time of 29.2 h.

The area at which the precursor is deposited on the substrate surface (A) can be determined by a conic section calculation. It is a function of the inner and outer radius of the nozzle (r_i and r_o), the clearance to the substrate a, the nozzle angle α and the spread angle β (figure 5) as follows:[1,5,6]

$$A(r_i, r_o, a, \alpha, \beta) = \pi \left(\frac{r_o}{\tan\alpha} + \frac{a}{\sin\alpha} + \frac{r_i}{\tan\beta} \right)^2 \cdot \left(\sin^2\beta\right) \cdot C \cdot D \tag{6}$$

$$C = \frac{\sin\alpha \cdot \cos\beta}{\cos^2\beta - \cos^2\alpha} \tag{7}$$

$$D = \sqrt{\left(\frac{\sin\alpha \cdot \cos\beta}{\cos^2\beta - \cos^2\alpha} \right)^2 - \left(\frac{\cos\alpha}{\cos\beta + \sin\alpha} + \frac{\sin\beta \cdot \cos\alpha}{\cos^2\beta - \cos^2\alpha} \right)^2} \tag{8}$$

Kohlmann *et al.*[5] state that spread angles less than about 30° cannot be realized, assuming a homogeneous gas distribution. Using the relevant parameters from table 1 and a spread angle of 30°, the gas covered area A becomes 1475 mm^2. However, this high value is a result of the small difference between the nozzle angle (31°) and the spread angle (30°), which gives a very large spreading of the gas. In comparison, spread angles of 20° or 10° will result in gas-covered areas of 33.5 and 7.7 mm^2, respectively.

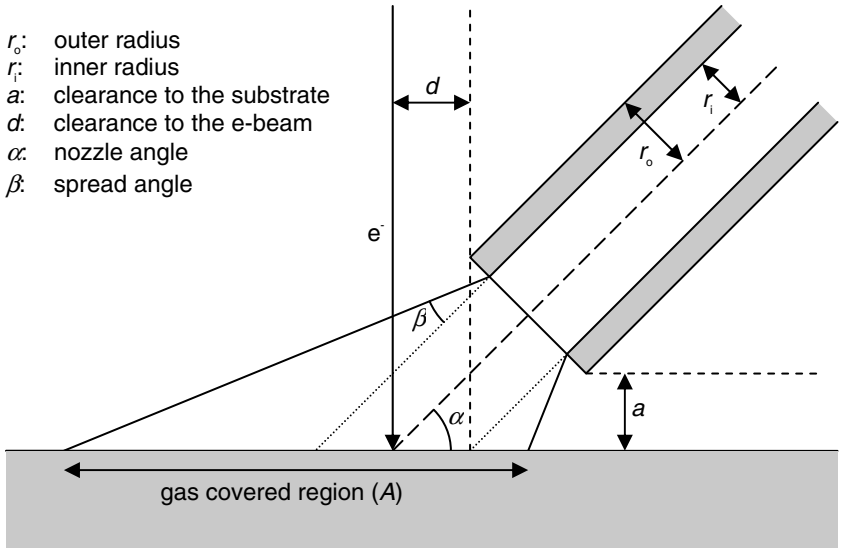

Figure 5. Schematic illustration of the nozzle parameters affecting the gas covered area, A. The figure is adapted from Kohlmann *et al.*[5]

Assuming evenly distributed precursor molecules in the area A, the time to deposit a platinum structure of height h, t_{dep}, is given by:

$$t_{dep} = \frac{\delta \cdot h \cdot A \cdot R \cdot T}{p_1 \cdot M_{Pt} \cdot C} \tag{9}$$

where δ and M_{Pt} are the density and molar mass of platinum, respectively. As an example, a 200 nm high platinum structure can be deposited in 8.2 min using a spread angle of 20°.

There are several uncertainties included here; the spread angle is probably too small, but in comparison the gas will be inhomogeneously distributed in the gas-covered area, resulting in more precursor molecules closer to the nozzle opening. In addition, diffusion of molecules along the substrate is not accounted for, and it is assumed that pure platinum is formed, while in reality a platinum-carbon composite will be formed. It is also assumed that the electron beam provides sufficient amounts of electrons to reduce the platinum in the deposited precursor molecules. However, the indicated t_{dep} shows that a reasonable time scale is achieved, with sufficient time to control the deposition, while still ensuring a conveniently rapid process.

Results

Examples of the deposits on silicon substrates are shown in figure 6. The height of the 10 min deposit was 200 - 300 nm, which is consistent with the calculations above, while the area was approximately 300 × 350 nm. The height of the deposits increased with increasing deposition time (figure 6b), as long as the drift in the system was corrected for during the deposition. The 60 min deposit thus reached a height of above 1 μm, with a cross-section area of approximately 500 × 500 nm, slightly larger than that of the 10 min deposit.

In addition to platinum, the deposits contained carbon (figure 6c and d). The deposit was thus composed of a platinum-carbon composite. In figure 6d some lead and titanium reflections were observed, which originate from $PbTiO_3$ nanorods that were dispersed on the sample surface.

In figure 7 an example of contacts on a single nanorod is shown. The ends of the nanorod were successfully contacted to the gold electrodes, with good control of the location of the deposits. The varying height of the deposits was a result of the drift correction, the height of the nanorod, and also a slightly inhomogeneous deposition within the scanned area.

If the precursor was exposed to air before deposition, deposits did form, but only carbon peaks were observed in the EDS spectrum of the deposits, without any visible platinum peaks. This indicates that the precursor easily decomposed into non-volatile platinum-containing species, in addition to carbonaceous species.

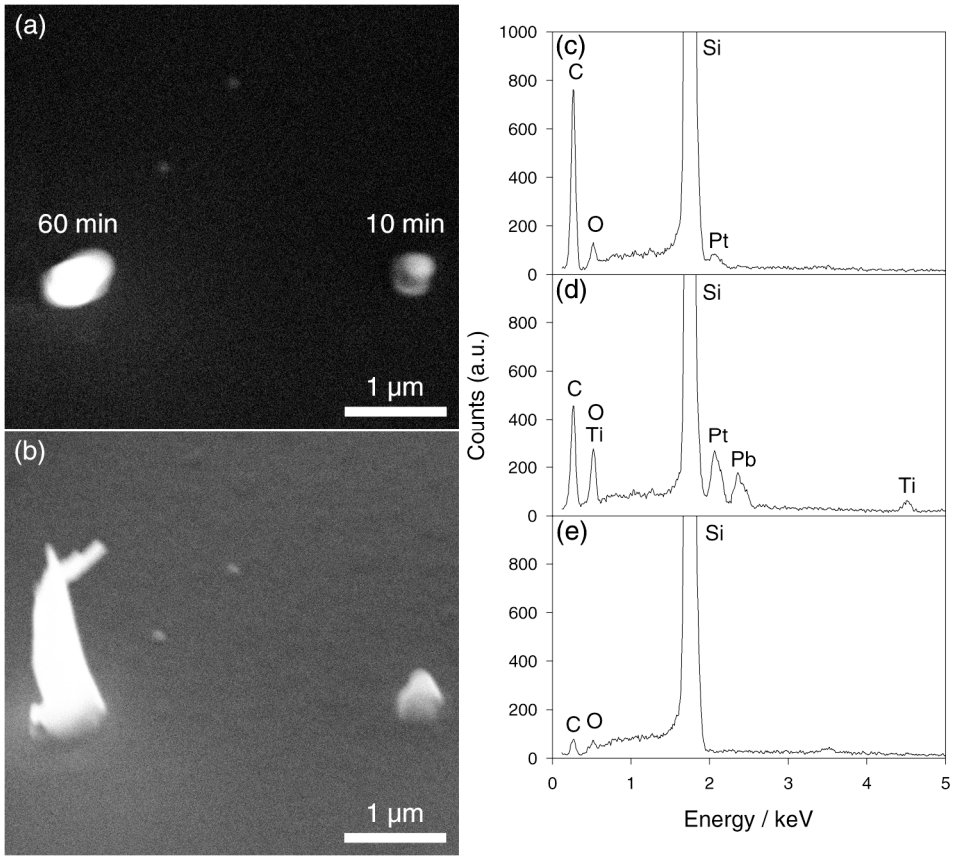

Figure 6. (a)-(b) SEM images of platinum deposits on a silicon substrate made using 10 min and 60 min depositon time. (a) Top-view. (b) 43° tilted view. (c)-(e) EDS spectra of (c) the 10 min deposit, (d) the 60 min deposit, and (e) the silicon substrate.

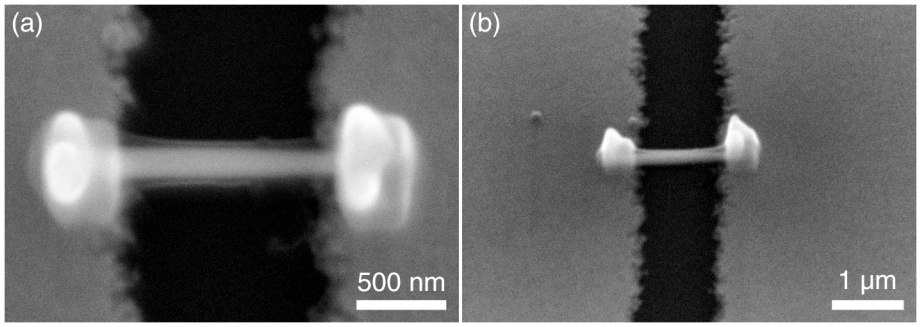

Figure 7. SEM images of platinum deposits at the ends of a $PbTiO_3$ nanorod located between to gold electrodes on top of a silicon substrate. The deposition time was 10 min for each nanorod end deposit. (a) Top-view. (b) 43° tilted view.

Discussion

The results show that the EBID apparatus worked according to plan, depositing a platinum-carbon composite at the desired positions on the sample. The ends of single nanorods could be contacted to the gold electrodes with a satisfactory precision of the deposit position. In addition, the height of the deposits could be controlled, enabling deposit heights from 100 nm to above 1 μm.

The consistency between the calculations and results regarding deposit height show that the calculations are reasonable. The gas flow, deposition time and deposition height were successfully estimated, which helped the design and the use of the system. The uncertainties in the calculations limit the calculation results to estimates, thus, to increase the control of the morphology and position of the deposits, calibrations based on actual results would be necessary.

The sensitivity of the precursor to oxidizing conditions necessitates careful handling of the precursor container. The container was only opened in argon atmosphere inside a glove bag to avoid exposure to air. However, for even better control of the precursor purity it would be better to use smaller containers with just enough precursor material for one deposition session (50 - 100 mg).

EBID is a technique that is applicable and useful within many areas of nano-technology, especially for depositing metallic structures on a substrate. The resolution of the deposits was sufficient for the present purpose, but for other purposes increased control of the resolution can be necessary. This can be achieved by mounting the EBID apparatus onto a field emission SEM instead of a regular SEM. In addition, more advanced nanostructures can be obtained by using automated control of the movement of either the electron beam or the sample stage.

Conclusions

Electron beam induced deposition of a platinum-carbon composite from a molecular precursor has been demonstrated in this work. A home-made EBID apparatus was constructed for the deposition and is described in detail. The height and the position of the deposits were successfully controlled. Geometry-based calculations were helpful to design the EBID apparatus and to estimate the deposition time and the deposit height. The deposits were used to make electric contacts between the ends of single nanorods and gold electrodes on a silicon substrate.

Acknowledgements

The rebuilding and modification of the EBID apparatus was done by Ketil Joner at the Mechanics workshop at the Faculty of Natural Sciences and Technology at the Norwegian University of Science and Tecnology (NTNU). Jarle Hjelen and Tor Nilsen, Department of Materials Science and Engineering, NTNU, are acknowledged for their help and generosity regarding design of the EBID apparatus and use of the JEOL SEM. This work was financially supported by the

Strategic Area of Materials at NTNU, and the Research Council of Norway (NANOMAT, Grant no. 158518/431).

References

1. S. J. Randolph, J. D. Fowlkes, and P. D. Rack, "Focused, Nanoscale Electron-Beam-Induced Deposition and Etching", *Crit. Rev. Solid State*, 2006, 31, 55-89.
2. Z. Xue, M. J. Strouse, D. K. Shuh, C. B. Knobler, H. D. Kaesz, R. F. Hicks, and R. S. Williams, "Characterisation of (Methylcyclopentadienyl)-trimethylplatinum and Low-Temperature Organometallic Chemical Vapor Deposition of Platinum Metal", *J. Am. Chem. Soc.*, 1989, 111, 8779-8784.
3. P. W. Atkins, "Physical Chemistry", 6th ed., Oxford University Press, 1999, p. 30.
4. W. Umrath, "Fundamentals of Vacuum Technology", Leybold Vacuum, Cologne, 1998, p. 15-18.
5. K. T. Kohlmann, M. Thiemann, and W. H. Brünger, "E-beam induced x-ray mask repair with optimized gas nozzle geometry", *Microelectron. Eng.*, 1991, 13, 279-282.
6. Be aware that the equations in Randolph *et al.*[1] contain a few errors compared to the same equations in Kohlmann *et al.*[5]

Appendix I

Is not included due to copyright

Appendix II

Is not included due to copyright

Appendix III

Detailed TEM characterization of $PbTiO_3$ nanorods

R Sæterli[1*], ATJ van Helvoort[1], G Wang[2], PM Rørvik[2], BS Tanem[3], T Grande[2], M-A Einarsrud[2] and R Holmestad[1]

1 Department of Physics, NTNU, N-7491 Trondheim, Norway

2 Department of Materials Science and Engineering, NTNU, N-7491 Trondheim, Norway

3 SINTEF Materials and Chemistry, N-7491 Trondheim, Norway

* Corresponding author: ragnhild.saterli@ntnu.no

Abstract. 1D functional oxides at nm-scale are interesting for fundamental reasons and promising for future applications. Here, ferroelectric $PbTiO_3$ nanorods, produced through a hydrothermal process, have been studied in detail by transmission electron microscopy. The length (up to one μm) and the diameter (30-100 nm) as well as the growth direction ([001]) of the nanorods could easily be determined using conventional imaging and electron diffraction techniques. However, variations along the length of the rods were clearly visible in the bright field images. Steps on the outer surfaces of the rods could be identified using energy filtered transmission electron microscopy and spectrum imaging thickness maps. The thickness variation parallel to the electron beam affected the bright field contrast and energy dispersive spectroscopy of the nanorods. From cross-sectional specimens, it was determined that the outer surfaces of the rods were dominantly {110} type, leading to a rectangular cross-section. The cross section diameter of the rods was reduced by the introduction of {100} surfaces. In addition, the cross-sectioned specimen revealed the presence of internal channels in the growth direction, especially in the bottom part of the rods. Such a detailed structural description of the nanorods was necessary to study the possible ferroelectric domain structure and to reveal the growth mechanism of the rods.

1. Introduction

Ferroelectric materials such as the tetragonal perovskite lead titanate ($PbTiO_3$, unit cell parameters a = b = 3.90 Å and c = 4.15 Å) are highly interesting to the electronics industry in for example non-volatile memory devices. The ferroelectricity of $PbTiO_3$ arises due to an overlap of the lead and oxygen shells, resulting in a net polarization along the c ([001]) direction. In order to implement $PbTiO_3$ and similar materials into devices, an understanding of the properties of the materials at the nanoscale is vital. It is for example well known, although not completely understood, that $PbTiO_3$ becomes less ferroelectric and less tetragonal as the size of the material decreases. The introduction of reduced dimensionality such as in thin films or nanorods may therefore affect the ferroelectric properties of the material. At the nanometer scale, surface and internal defects may also alter the ferroelectricity by introducing screening charges and pinning centers for domain walls. Hence, the understanding of the connection between size, dimensionality, structure and ferroelectricity is important for the use of the material in future applications.

2. Experimental details

$PbTiO_3$ specimens were prepared through a relatively simple hydrothermal synthesis route using Pb-Ti-citrate sol as precursor and the surfactant sodium dodecylbenzene sulfonate (SDBS). More details on the synthesis can be found elsewhere [1,2]. The resulting powder products were prepared for transmission electron microscopy (TEM) studies by two different sample preparation methods. Some of the powder was dispersed in ethanol and ultrasonically dispersed in order to separate the rods. The ethanol with the powder was then dripped on to a holey carbon grid before left to dry, resulting in a side-view of the nanorods as they land flat on the carbon film. The second technique was to embed the powder in epoxy before microtoming to slices of a thickness of approximately 50 nm, measured by the ratio of inelastic to elastic scattering by the use of electron energy-loss spectrometry (EELS). This second sample preparation technique resulted in a cross-section view of the rods.

The specimens were studied in a Philips CM30 and a JEOL2010F microscope, both operated at 200 kV. The CM30 was used for bright field (BF) and dark field (DF) imaging as well as selected area electron diffraction (SAED). The 2010F was fitted with a GIF2000 spectrometer for energy filtered imaging (EFTEM) and spectrum imaging (SI) thickness mapping, and was in addition used for high resolution electron microscopy (HREM) and energy dispersive x-ray spectroscopy (EDS, Oxford INCA).

3. Results

The powder sample consisted of microspheres with rods pointing out from the surface, as seen in figure 1a. Both microspheres and rods were found by EDS and SAED to be pure tetragonal $PbTiO_3$.

The growth direction of the nanorods was determined by HREM imaging and SAED of the side-view specimen to be the *c* direction, parallel to the polarization direction. HREM and SAED results of a typical rod are shown in figure 1. The diameters of the rods varied between 30 and 100 nm, with a decrease in diameter towards the end furthest away from the microsphere. The rods were up to one micrometer long.

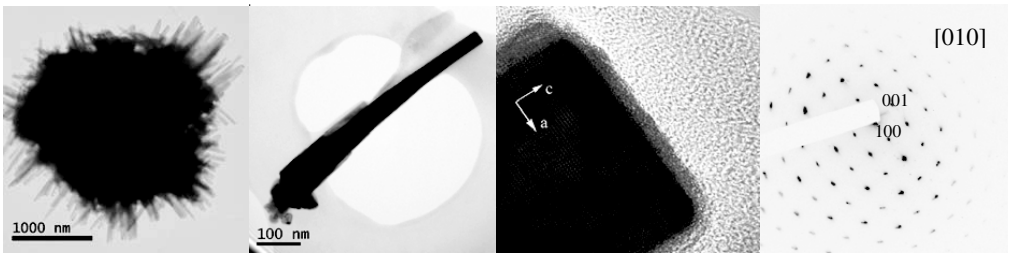

(a) (b) (c) (d)

Figure 1: (a) BF image of microsphere. (b) BF image of rod with (c) HREM image of the tip and (d) SAED pattern showing a growth direction of [001].

The outer surfaces of the rods were determined through HREM imaging of the cross-section specimen, as shown in figure 2 after tilting to the [001] orientation. Figures 2a-c show typical cross-sections, revealing that the surfaces are situated dominantly on {110} planes. {100} planes are the second most common surface planes, often seen to cut the corners of the {110} surfaces, as pointed out with black arrows in figure 2b. Examples were found where the surfaces were not situated along any major crystallographic planes, one of which is given in figure 2d. The cross-sections of the rods showed that a majority of the rods contain tunnels that extend through the thickness of the cross-section specimen, in the *c* direction of the rods. These internal defects seem to outline building blocks of approximately 10 by 10 nm which the rods were composed of. This is clearly visible in the cross-section depicted in figure 2c. These building blocks aligned and assembled perfectly in the *c* direction of the rods, while they were in several cases found to grow together with a small mismatch (less than one degree) in the lattice directions perpendicular to the growth direction. Cross-sections with

rectangular outer surfaces had in general less internal defects such as tunnels and rotational mismatch between building blocks than irregular shaped cross-sections.

As the specimen was cut at arbitrary places along the rods during cross-section sample preparation, EFTEM thickness mapping and SI line scans at different positions along the rods were used to determine the shape evolution from the thinner end (tip) to the end connected to the microsphere (bottom) end of the rods. It was found that the shape of the rods was more regular at the tip, while the bottom usually has a more irregular cross-section shape. The shape development of one rod is shown in figure 3. The thickness plots in figure 3b may indicate that the rod was square at the tip, while the bottom had a more complex shape. The difference between the two lower graphs may be interpreted as due to the introduction of {100} surfaces.

Figure 4 shows the BF image and EDS line scan measurements on a rod with a tunnel, illustrating how the BF contrast and intensity of the EDS signal varied with the cross-section shape of the rod.

In order to examine the possible 180° domain structure of the rods by TEM, a series of dark field experiments, as described in reference [4], were performed, in which no clear domain structure could be revealed.

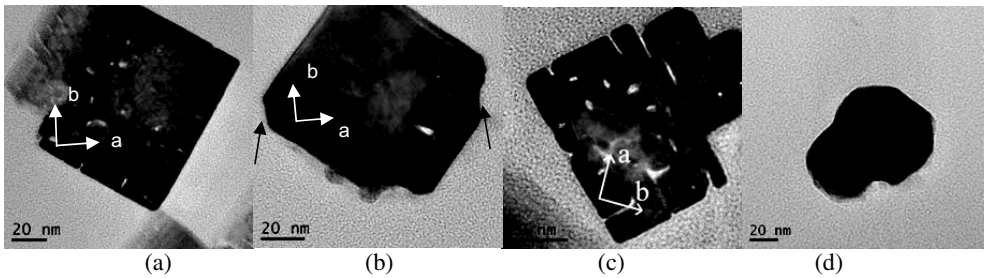

(a) (b) (c) (d)

Figure 2: [001]-oriented HREM images of cross-sections of rods. (a) – (c): The surfaces are predominantly along the {110} crystallographic planes, while in (d) a more irregular shape is found. The black arrows in figure (b) point to {100} surfaces.

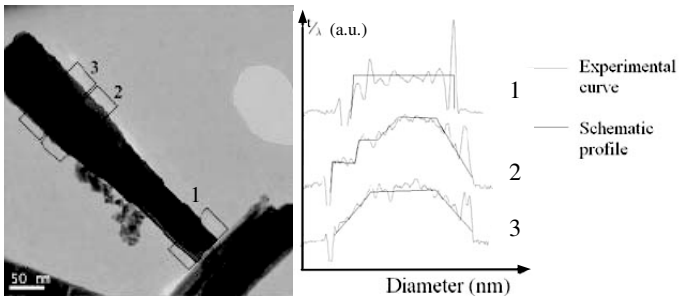

(a) (b)

Figure 3: (a) BF image and (b) thickness profiles of a rod, showing how the shape varies from the tip of the rod (1) to the bottom (3).

4. Discussion

It is clear that the growth mechanism for these rods is not dominated by the classical atom-by-atom picture. Rather, a mesocrystal growth explanation [3] is proposed. According to this theory, nanocrystals agglomerated into microspheres as a first step of the process, while other nanocrystals ripened to achieve well-defined surface planes and assembled to form the rods in a second step. It was found that the surfactant was vital for this second step to occur [2], and it was believed that polarization present in the building blocks was an important reason for the one-dimensional growth.

The tunnels and holes in the *c* direction arose as the building blocks grew together with a small rotation mismatch or due to deviations from a perfectly rectangular shape. These deviations became fewer toward the tip of the rods, which could be ascribed to a ripening of these building blocks before they were attached to the rod.

The reason for the inconclusive DF experiments was the irregular shape of the rods, with the varying thickness and surface steps as well as the tunnels and rotation of building blocks all gave unwanted diffraction and thickness contrast which masked any contrast from 180˚ domains. A further complication arose as domains were visible only when viewed edge-on, that is, when the wall is parallel to the electron beam. In addition, the ferroelectricity and domain structure itself could be expected to vary from needle to needle due to domain wall pinning to the tunnels and the internal defects possibly creating screening charges. Further domain structure experiments are in progress and will be performed on more homogeneous rods.

The two sample preparation methods used in this study combined gave a full 3D picture of the nanorods. This was essential for the understanding of the structure of the rods and the interpretation of DF and BF image contrast as well as variations in the EDS signal. Similar 3D information was also available from more advanced techniques such as EFTEM (more noisy) thickness mapping or SI (less noisy).

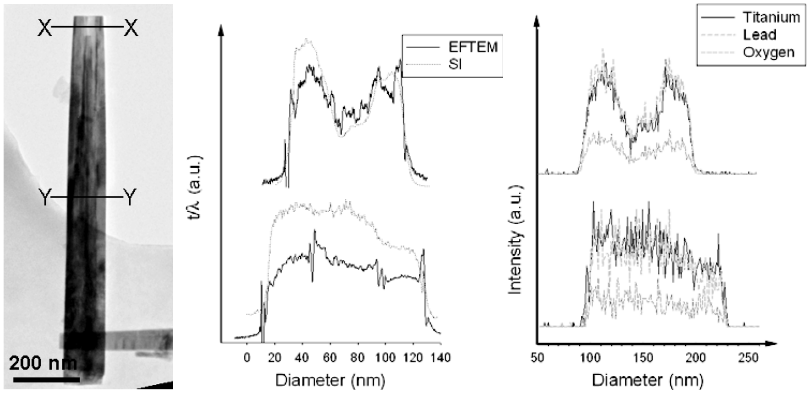

(a) (b) (c)

Figure 4: (a) BF image of rod. (b) SI (grey) and EFTEM (black) thickness profiles and (c) EDS linescan signal of two places along the rod (X-X (top) and Y-Y (bottom) in figure a), showing a clear correlation between the EDS signal and the shape of the rod.

5. Conclusion

Detailed TEM characterization of $PbTiO_3$ nanorods has been performed to reveal the shape, the growth direction and the internal structure of the rods. This was achieved by two different sample preparation methods providing a side-view as well as a cross-section view of the rods which, combined with thickness mapping techniques, provided a 3D view. The defects in the rods, such as tunnels, rotation of building blocks creating internal defects and surface steps, affected both BF and DF contrast and the EDS measurements and must be fully characterized before attempting to resolve the ferroelectric domain structure of the rods.

References

[1] G. Wang et al. J. Nanosci. Nanotechnol. 7, 2538 (2007).
[2] G. Wang et al. Chem. Mater. 19, 2213 (2007).
[3] See for example H. Cölfen and M. Antonietti. Angew. Chem. Int. Ed. 44, 5576 (2005).
[4] M Tanaka. Acta cryst. A 31, 59 (1975).

Appendix IV

Appendix IV

Fabrication of sample device and proposed setup for piezoresponse force microscopy study of single nanorods using an axial dc bias setup

Background

As discussed in chapter 3.2.3. in the introduction, there exist some limitations in the conventional piezoelectric force microscopy (PFM) setup (figure 1a) for in-plane study. Because of the concern for electric breakdown and the localized nature of the electric field, whenever a high bias is needed for in-plane polarization switching or a sample segment needs to be uniformly polarized, the conventional PFM setup is incapable. Wang *et al.*[1] have reported a setup where the dc bias is applied along the length direction of a nanorod (figure 1b). The ac bias is still applied through the atomic force microscopy (AFM) probe tip, but the dc bias used to switch the in-plane polarization of the nanorod is applied directly between the two ends of the nanorod. This provides in-plane polarization control while

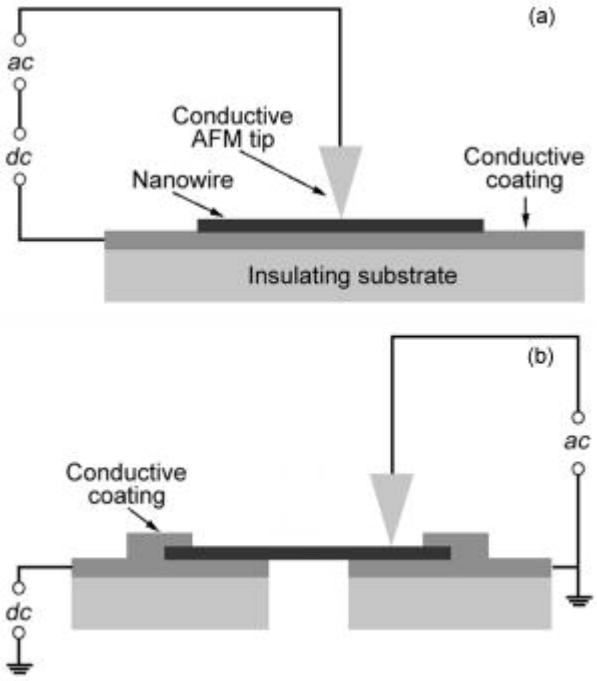

Figure 1. Schematic illustration of (a) the biasing condition in conventional PFM of nanorods, and (b) the axial dc biasing setup in the study of Wang *et al.*[1] The figure is adapted from Wang *et al.*[1]

simultaneously allowing the study of ferroelectric hysteresis and shear piezoresponse of a nanorod with PFM.

We were interested in using this technique to study the ferroelectric and piezoelectric properties of single $PbTiO_3$ nanorods. However, because of experimental challenges and insufficient time, a sample device was not completed within the time limit for this thesis, so the PFM studies using an axial dc bias setup will be a topic for future work. Here we describe the efforts that were done to fabricate a sample device and the ideas for the setup that were developed.

Fabrication of sample device

An electrode pattern of gold on silicon was made as follows. A layer of 10 nm Ti and thereafter a layer of 50 nm Au were electron beam evaporated (Pfeiffer Vacuum Classic 500) onto a 4 inch silicon wafer (V.S.I.). The Ti layer was important for the adherence of the Au layer. The wafer was cut into ~8 × 8 mm^2 substrates. The substrates were washed in isopropanol in an ultrasonic bath for 1 min to remove small particles directly before a resist layer of polymethyl methacrylate (PMMA, 4 % in anisole, MicroChem) was spin coated onto the substrate at 4000 rpm for 50 s. The substrates were thereafter soft baked on a hotplate at 180 °C for 90 s. An approximately ~500 µm wide line was made in the resist layer across the middle of the substrate by a diamond knife, exposing the gold film. To make an electrode pattern, parts of the resist layer located close to the line were then exposed to an electron beam at 20 kV with typical area dose 170 µC/cm^2 in a scanning electron microscope (SEM, Zeiss DSM 940), using a Raith ELPHY Plus nanolithography system and software. The exposed area was 400 × 400 μm^2. A typical electrode pattern is shown in figure 2. The pattern was

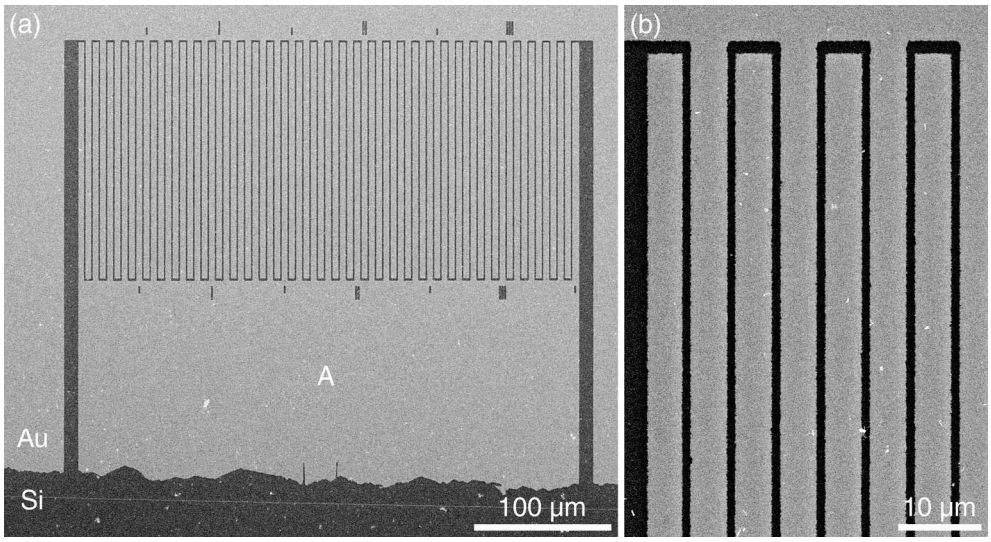

Figure 2. SEM images of a typical gold electrode pattern on a silicon substrate. The area marked with A in (a) was used for the wire bonding. The image in (b) shows an enlarged view of the upper left part of the finger structures in (a).

composed of an array of electrode finger structures (upper half in figure 2a) and an area without any structures (lower half in figure 2a) which was used for the wire bonding. The finger structures were 5 µm wide and 180 µm long. The gap between two finger structures was 0.5 - 1 µm. The exposed resist was developed for 30 s in a 1:3 methylisobutylketone:isopropanol solution (MicroChem). The substrate was then rinsed for 120 s in isopropanol, blown dry with nitrogen gas, and hard baked on a hot plate at 100 °C for 90 s. The exposed gold layer was removed by immersing the substrate in aqua regia (1:3 HNO_3:HCl by volume) for 3 × 15 s with water rinsing after each immersion. The remaining resist layer was removed by immersing the substrate in acetone in an ultrasonic bath for 5 min. The exposed Ti layer was then removed by immersing the substrate in a 1:1:20 HF:H_2O_2:H_2O solution for 1 min.

A dispersion of $PbTiO_3$ nanorods was made by adding 0.1 g of the product from the hydrothermal synthesis[2,3] into 30 mL ethanol (96 %). The dispersion was sonicated by an ultrasonic probe for 5 min at 10 % amplitude (Branson Digital Sonifier). The larger particles in the dispersion (microspheres[2,3]) were removed by decanting after sedimentation for 1 h. The nanorod dispersion was dropped onto the gold electrode pattern on a silicon substrate.

The samples were studied with scanning electron microscopy (SEM, Hitachi S-3400N) to locate single nanorods that stretched over the gap between two finger electrode structures. Suitable nanorods were electrically contacted to the gold electrode finger structures by depositing platinum/carbon composite upper electrodes at the ends of the nanorods by electron beam induced deposition of (trimethyl)methylcyclopentadienylplatinum(IV) (Aldrich, >98 %) using a homebuilt EBID apparatus in a JEOL JSM-840 SEM.[4] Figure 3 shows SEM images of a $PbTiO_3$ nanorod lying across a gap between two electrode finger structures, with platinum deposits at the ends of the nanorod.

The part of the electrode pattern without finger structures (marked with an A in figure 2a) was contacted to the other half of the gold film (across the 500 µm wide line dividing the gold film) by wire bonding with a 25 µm diameter gold wire. However, the thin gold film (50 nm) made the wire bonding difficult. A gold film of 100 nm or up to 200 nm would be better for the wire bonding process. However,

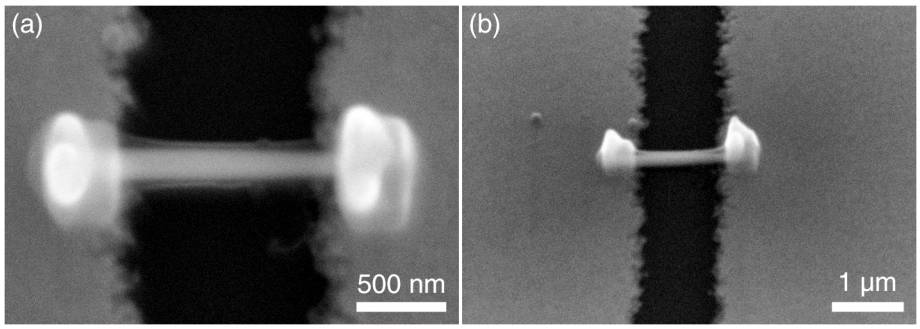

Figure 3. SEM images of platinum deposits at the ends of a $PbTiO_3$ nanorod located between to gold electrode finger structures on top of a silicon substrate. (a) Top-view. (b) 43° tilted view.

the etching step may then become more problematic because of uneven etching at long etching times.

As the wire bonding has relatively low accuracy and can easily destroy or short-circuit the electrode finger structures, a method to fabricate a sample device without using wire bonding would be beneficial. For instance, using electron beam lithography also to make the line dividing the gold film into two electrode parts, would make it possible to fabricate the finger structures directly between the two main electrodes, avoiding wire bonding and securing good electric contact. This concept is shown in figure 4.

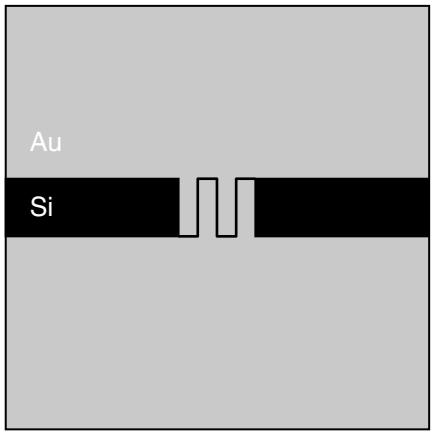

Figure 4. Schematic illustration of a possible electrode structure if electron beam lithography is used to make the dividing line between the two main electrodes.

Proposed setup for PFM using an axial dc bias setup in the AFM

To use the sample device for PFM study with an axial dc bias setup, each gold electrode side of the finger structure has to be electrically contacted to an external dc bias source. A proposed setup is shown in figure 5. One electrode is contacted to the conducting AFM sample holder with silver paste. The AFM sample holder is contacted to the dc bias source via an electric wire fastened to the AFM sample holder by a metallic screw. The other electrode is connected to the dc bias source via a metallic spring which is connected to an electric wire. To prevent electric contact between the metallic spring and the AFM sample holder, a Teflon spacer and a Teflon screw are used to fasten the spring and the wire. This setup secures good electric contact between the electrodes and the dc bias source, and prevents electric contact between the electrodes.

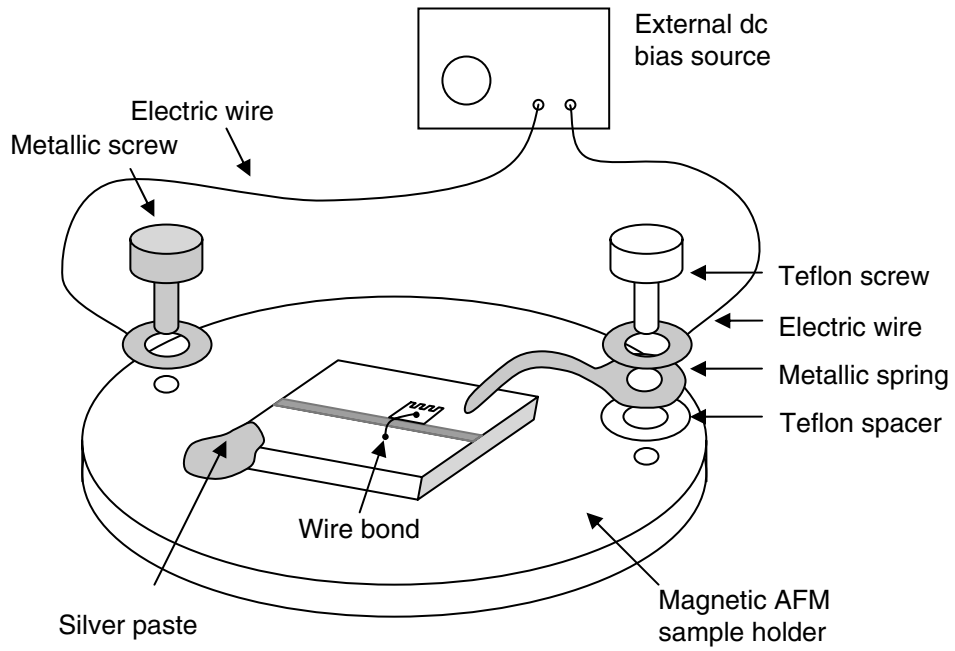

Figure 5. Proposed setup for studying piezoelectricity and ferroelectricity in single nanorods with PFM using an axial dc bias setup.

References

1. Z. Wang, A. P. Suryavanshi, and M.-F. Yu, "Ferroelectric and piezoelectric behaviours of individual single crystalline $BaTiO_3$ nanowire under direct axial electric biasing", *Appl. Phys. Lett.*, 2006, 89, 082903.
2. G. Wang, R. Sæterli, P. M. Rørvik, A. van Helvoort, R. Holmestad, T. Grande, and M.-A. Einarsrud, "Hierarchical Nanostructures of $PbTiO_3$ Through Mesocrystal Formation", *J. Nanosci. Nanotechnol.*, 2007, 7, 2538-2541. (Appendix I)
3. G. Wang, R. Sæterli, P. M. Rørvik, A. T. J. van Helvoort, R. Holmestad, T. Grande, and M.-A. Einarsrud, "Self-Assembled Growth of $PbTiO_3$ Nanoparticles into Microspheres and Bur-like Structures", *Chem. Mater.*, 2007, 19, 2213-2221. (Appendix II)
4. P. M. Rørvik, T. Tybell, T. Grande, and M.-A. Einarsrud, "Electron beam induced deposition of platinum for contacting nanorods", unpublished. (Paper VI)